Next generation synthetic fibers UHPFRC for sustainable structural applications

Thèse N° 7362

Présentée le 4 novembre 2019

à la Faculté de l'environnement naturel, architectural et construit
Laboratoire de maintenance, construction et sécurité des ouvrages
Programme doctoral en génie civil et environnement

pour l'obtention du grade de Docteur ès Sciences

par

Amir HAJIESMAEILI

Acceptée sur proposition du jury

Prof. C. J. D. Fivet, président du jury
Dr. E. Denarié, directeur de thèse
Prof. P. Serna Ros, rapporteur
Prof. C. Oesterlee, rapporteuse
Dr P.-E. Bourban, rapporteur

2019

EPFL
ÉCOLE POLYTECHNIQUE
FÉDÉRALE DE LAUSANNE

To my loved ones

Sogol,
Nahid & Mohammad kazem

بیرون ز تو نیست هر چه در عالم هست

در خود بطلب هر آنچه خواهی، که توئی

مولانا، جلال الدین محمد بلخی

You are the universe in ecstatic motion
Find what you are looking for, in yourself
                                    Rumi

Foreword

Ultra-High-Performance Fiber Reinforced Concretes (UHPFRC) are now well established in many countries, for new structural applications. Thanks to major research and dissemination efforts in Switzerland over the last 20 years under the impulse of our laboratory, they also proved in practice to be an excellent solution to improve existing structures, alone or associated to rebars for reinforcement applications. Simultaneously, the major trends of development in the UHPFRC field became: (1) focus on tensile response and achievement of a robust tensile strain hardening response usable for design, (2) massive replacement of clinker by Supplementary Cementitious Materials to achieve more sustainable mixes. Structural UHPFRC only reinforced by synthetic fibers, with an elastic limit above 7 MPa remained however a challenge. In this context, the Swiss National Research program "Energy Turnaround" (NRP 70) provided a strong incentive to develop next generation structural UHPFRC mixes with decreased embodied energy, using synthetic fibers and low-clinker matrices.

UHPFRC formulations currently used for structural applications such as the rehabilitation or construction of new structures are reinforced with discontinuous steel fibers. This type of fibers represents a particularly high environmental cost of production in UHPFRC materials. To date, no replacement solution with synthetic fibers achieves a level of tensile performances equivalent to that obtained with steel fibers, especially regarding the elastic limit. In parallel, in order to make the most effective use of UHPFRC at service state, their transport properties must also be studied under tensile loading, in the vicinity of their elastic limit and after, under the action of the transport phenomena acting in practical applications.

Amir Hajiesmaeili was able to develop new structural UHPFRC mixes using state of the art UHMW PE fibers, and low clinker matrices. These mixes are particularly well adapted for cast-on site applications, thanks to their very significantly decreased eigenstresses under restrained shrinkage. His works also shed a new light on the effect of tensile loading on the transport properties of UHPFRC subjected to capillary absorption of water, with direct implications for design at serviceability.

He demonstrated throughout his thesis his ability to conduct research in multidisciplinary domains with a creative and critical vision. In the name of the whole MCS team, I thank him for his constant and deep dedication to his research topic as well as for his professional skills, openness of mind, enthusiasm and scientific curiosity.

Lausanne, July 2019   Dr. Emmanuel Denarié

Acknowledgement

Furthermore, many thanks to all my friends all over the world who are my biggest support and deserves my greatest gratitude, for making my life more fun, enjoyable, and exciting. My special thanks to Ali, Mortez, Nastaran, Soheil & Mehrnaz, Soroush, Mohammadreza, and Ali & Narges in Lausanne, Agha Farhad, Alireza & Mina, Sina, Omid, Kaseb, Nojoumi & Nooshin, and Aryan in Iran, and Ehsan, Amir Masoud, and Hossein in US and many others with whom I shared many great memories.

Last but not least, nobody has been more important to me in the pursuit of this journey than the members of my family. I would like to thank my parents, whose love and support are with me in whatever I pursue. They are the ultimate role models. Moreover, my sincere gratitude goes to my family in-law for their endless kindness and support. Most importantly, I wish to thank my lovey wife, Sogol who provides me unending inspiration. Her love, support and patience over this past year helped me over the finish line.

Lausanne, July 2019   Amir Hajiesmaeili

x

Summary

The ever-increasing demand for rehabilitation of existing structures and construction of new ones, along with environmental issues of the construction sites represent a heavy burden for society in terms of economy and environment. Meanwhile, Ultra-High Performance Fiber Reinforced Concrete (UHPFRC) has proved its potential to be one of the solutions to contain the explosion of the maintenance costs (economy and environment), because of its extremely low permeability and outstanding mechanical properties, and has successfully gained the ground through numerous applications. Even though using UHPFRC already significantly contributes to decreasing the environmental impact of rehabilitation construction sites by up to 50% when compared to using conventional concretes, further optimization of their mix design with replacement of high environmental cost components like steel fibers and clinker, would be another step towards sustainability.

The main objective of this study was to further improve the already established concept of UHPFRC in two main directions: firstly, to develop new strain hardening UHPFRC mixes with reduced environmental impact by replacing the steel fibers with synthetic ones and by replacing 50% vol. clinker with cheap and widely available Supplementary Cementitious Materials (SCM), and secondly, to investigate the mechanical properties, delayed response, protective function, and environmental impact of the newly developed material for structural applications.

An advanced packing density model was developed to optimize the powder mix that consisted of six different powders: cement, two types of limestone fillers of different gradings, silica fume, quartz powder, and quartz sand. An extensive experimental campaign with a focus on the tensile behavior was carried out to investigate the factors influencing the mechanical properties of the UHPFRC mixes and validate their performances. The achieved new UHPFRC mix named *PE-UHPFRC* has on average a tensile elastic limit of 7.7 MPa, a tensile strength of 11.7 MPa, a tensile deformation capacity of more than 3.5%, and a compressive strength of 120 MPa, well adapted for cast on-site applications of rehabilitation, or strengthening associated to rebar.

The delayed response of PE-UHPFRC was investigated with a focus on autogenous deformations and associated eigenstresses under full restraint conditions, using a Temperature Stress Testing Machine (TSTM), with 20 °C curing conditions. The results showed more than 70% reduction in the eigenstresses in a 50 mm thick PE-UHPFRC layer

when compared to those observed in conventional UHPFRC with steel fibers, which is highly beneficial for rehabilitation applications.

An original capillary absorption setup was developed to investigate the protective properties of the PE-UHPFRC under tensile loading, at different strain levels ranging from 0.15 to 20‰. Before reaching the tensile elastic limit, the capillary absorption coefficient was extremely low, at 24 g/m²√h, however, a sudden increase in the capillary absorption was observed after the elastic limit under tensile load. Furthermore, the crack characteristics were studied at different strain levels using Digital Image Correlation (DIC) and it was found that the average crack width remained below 0.1 mm throughout the tensile response.

Finally, the environmental benefits of PE-UHPFRC combined with rebar were characterized at the structural level, for the strengthening of a bridge with a span of 34 m, and compared with those of: (1) a strengthening with conventional UHPFRC with steel fibers combined with rebar, and (2) the demolition of the existing bridge and reconstruction of a post-tensioned reinforced concrete one. The Life Cycle Analysis (LCA) considered three indicators: Global Warming Potential (GWP), Cumulative Energy Demand (CED) and Ecological Scarcity (UBP). The LCA results showed on average 55% and 34% decrease in the environmental impact for the strengthening method with R-PE-UHPFRC compared with the reconstruction with post-tensioned reinforced concrete and strengthening with conventional R-UHPFRC, respectively for all the indicators.

Keywords: UHPFRC; PE-UHPFRC; Sustainability; UHMW-PE fibers; Limestone filler; Tensile response; Strain Hardening; CIPM; Packing; Autogenous shrinkage; Eigenstresses; Capillary absorption; Crack characteristics; DIC; TSTM; LCA; Embodied Energy

Résumé

La demande sans cesse croissante de réhabilitation des structures existantes et de construction de nouvelles structures, ainsi que les problèmes environnementaux des chantiers de construction représentent un lourd fardeau pour la société en termes d'économie et d'environnement. Dans le même temps, le Béton Fibré Ultra Performant (BFUP) a prouvé son potentiel comme l'une des solutions pour contenir l'explosion des coûts de maintenance (économie et environnement), en raison de sa perméabilité extrêmement faible et de ses propriétés mécaniques exceptionnelles, et a su gagner du terrain grâce à de nombreuses applications. Même si l'utilisation du BFUP contribue déjà de manière significative à réduire l'impact environnemental des chantiers de réhabilitation jusqu'à 50 % par rapport à l'utilisation de bétons conventionnels, une optimisation supplémentaire de leur formulation avec le remplacement des composants à coût environnemental élevé, comme les fibres d'acier et le clinker, serait une étape de plus en faveur du développement durable.

L'objectif principal de cette étude était de poursuivre l'amélioration du concept déjà établi du BFUP selon deux directions principales : premièrement, développer de nouveaux mélanges de BFUP écrouissants ayant un impact environnemental réduit en remplaçant les fibres d'acier par des fibres synthétiques et en remplaçant 50 % en volume de clinker par des additions minérales bon marché et largement disponibles; deuxièmement, étudier les propriétés mécaniques, les fonctions de protection, le comportement différé et les impacts environnementaux du nouveau matériau développé, en vue d'applications structurales.

Un modèle de compacité existant a été généralisé pour optimiser le mélange de poudres qui se composait de six poudres différentes dont : du ciment, deux types de fillers calcaires de granulométries différentes, de la fumée de silice, de la poudre de quartz et du sable de quartz. Une vaste campagne expérimentale axée sur le comportement en traction a été menée pour étudier les facteurs influençant les propriétés mécaniques des mélanges de BFUP et valider leurs performances. Le nouveau BFUP obtenu appelé BFUP-PE présente, en moyenne, une limite élastique à la traction de 7,7 MPa, une résistance à la traction de 11,7 MPa, une capacité de déformation à la traction de plus de 3,5 % et une résistance à la compression de 120 MPa, bien adaptées aux applications coulées en place de réhabilitation ou de renforcement avec des barres d'armature.

Le comportement différé du BFUP-PE a été étudié en mettant l'accent sur les déformations endogènes et les autocontraintes associées, sous entrave totale, à l'aide d'une machine d'essai contraintes-température (TSTM), dans des conditions de cure à 20 °C. Les résultats ont

montré une réduction de plus de 70 % des autocontraintes dans une couche de BFUP-PE de 50 mm d'épaisseur par rapport à celles observées avec des BFUP classiques, avec des fibres d'acier. En outre, le rapport entre les autocontraintes sous entrave totale et la limite élastique de traction a été considérablement réduit par rapport à celui des mélanges de BFUP avec des fibres d'acier, ce qui a permis d'augmenter sensiblement l'efficacité du matériau pour les charges utiles et les charges permanentes.

Un dispositif d'absorption capillaire original a été développé pour étudier les propriétés de protection du BFUP-PE sous charges de traction, à différents niveaux de déformation allant de 0,15 à 20 ‰. Avant d'atteindre la limite élastique de traction, le coefficient d'absorption capillaire était extrêmement faible, à 24 g/m2√h, cependant, une augmentation soudaine et significative de l'absorption capillaire a été observée après la limite élastique sous charge de traction. De plus, les caractéristiques des fissures ont été étudiées à différents niveaux de déformation à l'aide de la corrélation numérique d'images (CID) et il a été constaté que l'ouverture moyenne des fissures restait inférieure à 0,1 mm tout au long de la réponse en traction.

Enfin, les avantages environnementaux du BFUP-PE ont été caractérisés au niveau structural, pour le renforcement d'un pont d'une portée de 34 m, en combinaison avec des barres d'armature, et comparés à ceux : (1) d'un renforcement avec du BFUP conventionnel avec des fibres d'acier combinées à des barres d'armature, et (2) de la démolition du pont existant et la reconstruction d'un pont en béton précontraint. L'analyse du cycle de vie (ACV) a pris en compte trois indicateurs : Potentiel de Réchauffement de la Planète (PRP), Demande Énergétique Cumulée (DEC) et pénurie écologique (UBP). Les résultats de l'ACV ont montré une diminution moyenne de 55% et 34% de l'impact environnemental de la solution utilisant le BFUP-PE armé par rapport à la reconstruction avec du béton précontraint et au renforcement avec du BFUP armé conventionnel, respectivement pour tous les indicateurs.

Mots-clés : BFUP ; BFUP-PE ; Durabilité ; Fibres ; UHMW-PE ; Filler calcaire ; Comportement en traction ; Écrouissage ; CIPM ; Compacité ; Absorption capillaire ; Caractéristiques de fissuration ; CID ; Autocontraintes ; TSTM ; ACV ; énergie Grise

Table of Contents

List of figures

Chapter 1 – Introduction

Chapter 2 – Development of Next Generation UHPFRC with synthetic fibers, for structural applications

Chapter 3 – Tensile response of PE-UHPFRC under imposed shrinkage deformations

Chapter 4 – Capillary flow in UHPFRC with synthetic fibers, under high tensile stresses

Chapter 5 – Life Cycle Analysis of Strengthening Existing RC Structures with PE-UHPFRC

List of tables

Chapter 4 – Capillary flow in UHPFRC with synthetic fibers, under high tensile stresses

Chapter 5 – Life Cycle Analysis of Strengthening Existing RC Structures with PE-UHPFRC

xxx

Glossary

Abbreviations

AP	Acidification Potential
CED	Cumulative Energy Demand
CIPM	Compaction-Interaction Packing Model
CPF	Controlled Permeability Formliner
CPM	Compressible Packing Model
CRC	Compact Reinforced Composite
DIC	Digital Image Correlation
DSP	Densified Systems containing homogeneously arranged, ultra-fine Particles
ECC	Engineered Cementitious Composites
EE	Embodied Energy
FRC	Fiber Reinforced Concrete
GF-UHPFRC	Glass Fiber UHPFRC
GGBFS	Ground Granulated Blast Furnace Slag
GGBS	Granulated Blast Furnace Slag
GWP	Global Warming Potential
HIFCOM	High-performance Impermeable Fiber reinforced COMposite
HPFRCCs	High-Performance Fiber Reinforced Cementitious Composites
HRWRA	High-Range Water-Reducing Admixture
HSHDC	High-Strength, High-Ductility Concrete
HS-SHCC	High-Strength Strain Hardening Cement-based Composite
ITZ	Interfacial Transition Zone
LCA	Life Cycle Analysis, Life Cycle Assessment

LVDT	Linear Variable Differential Transformer
NP	Eutrophication Potential
ODP	Ozone Depletion in the stratosphere
PE-UHPFRC	UHPFRC with PE fibers (mix PE21 in the present thesis)
POCP	Photochemical Ozone Creation Potential
PSD	Particle Size Distribution
PVA	Polyvinyl Alcohol
RC	Reinforced Concrete
RPC	Reactive Powder Concrete
SCC	Self-Compacting Concrete
SCM	Supplementary Cementitious Materials
SEM	Scanning Electron Microscopy
SHCC	Strain Hardening Cement-based Composite
SIFCON	Slurry InFiltrated Concretes
S-LF-UHPFRC	UHPFRC with steel fibers and 50% mass clinker replacement with limestone fillers
SP	Superplasticizers
SSM	Solid Suspension Model
S-UHPFRC	Steel fiber UHPFRC
TSTM	Temperature Stress Testing Machine
UBP	Ecological Scarcity
UHMW-PE	Ultra-High Molecular Weight Polyethylene
UHPC	Ultra-High Performance Concrete
UHPFRC	Ultra-High Performance Fiber Reinforced Concrete
UHP-SHCC	Ultra-High Performance-Strain Hardening Cementitious Composites
VRF	Vibration Resonance Frequency

Symbols

Latin upper-case letters

C_a	compaction-interaction constant within the loosening effect
C_b	compaction-interaction constant within the wall effect
K	compaction index depending on the compaction energy applied to the mixture.
M_p	mass of the powder
M_w	mass of the water
S	constant referred as the Sorptivity

Latin lower-case letters

a_{ij}	loosening effect
b_{ij}	wall effect
d_c	transition diameter in the CIPM below which compaction-interaction is taken into account
d_i	diameter of size class i
d_j	diameter of size class j
d_{max}	*maximal diameter*
i	cumulative absorption
p_k	volume fraction of material k
r_i	volume fraction of size class i
$r_{k,i}$	volume fraction of material k in class i
t	time
$w_{0,a}$	function for maximum range of loosening effect
$w_{0,b}$	function for maximum range of wall effect
w_a	constant denoting the maximum range of loosening effect

w_b constant denoting the maximum range of wall effect

w_c crack width

Greek upper-case letters

Φ actual packing density

Greek lower-case letters

α experimental packing density of the component

$α_i$ experimentally determined packing density of class i for a prescribed packing process and K value

β virtual packing density of the component

β_i virtual packing density of grain size class i

$\beta_{k,i}$ virtual packing density of material k in size class i

ρ density of the powder mix in kg/m^3

Chapter 1

Introduction

1. Context

The construction, operation, and maintenance of the built environment account for 36% of the global energy consumption and nearly 40% of total direct and indirect CO_2 emissions worldwide [1]. These demands are increasing due to population growth on one hand and the premature deterioration of the built environment on the other hand. In this regard, containing the energy consumption by developing novel technologies is the subject of an extensive number of researches including NRP70 [2] in Switzerland. This has promoted the necessity of developing advanced materials and construction techniques with long durability among others in order to be able to control the ever-increasing economic and environmental costs of the building sector and meet the needs of the present without compromising the ability of future generations to meet their own needs [3] that is the concept of sustainable development.

Enhancing the effectiveness, sustainability, and durability of concrete as one of the most widely used construction material has led to the formulation of Fiber Reinforced Concretes (FRC), Self-Compacting Concretes (SCC), and High-performance Fiber-Reinforced cementitious composites (HPFRCCs), such as: Slurry InFiltrated Concretes (SIFCON), Engineered Cementitious Composites (ECC), Strain Hardening Cement-based Composites (SHCC), High-Strength Strain Hardening Cement-based Composites (HS-SHCC), High-Strength, High-Ductility Concretes (HSHDC) and Ultra-High Performance Fiber Reinforced Concrete (UHPFRC), with different viewpoints and approaches to improve the performances.

UHPFRC are cementitious materials with a very dense matrix, reinforced with discontinuous fibers, which typically have a compressive strength of 150-200 MPa, a tensile strength of 7-15 MPa, a strain hardening domain of 1-2 ‰, and a very low water capillary

absorption, typically 5 times smaller than that of concretes prescribed for severe exposure classes (XD3/XF4). UHPFRC are by far the most widely used at an industrial scale among HPFRCCs. These materials not only enhanced both mechanical resistance and durability properties of concretes by more than a factor of 4 but also opened up the application of advanced techniques in rehabilitation and strengthening of existing structures as well as the construction of new structures with freedom of shapes unknown in the past.

The idea of rehabilitation and strengthening of existing bridges with UHPFRC was proposed by Brühwiler in 1999. This conceptual vision is illustrated in Fig. 1, with an extension to underground structures. Strain hardening UHPFRC are used only where they are needed, as a thin overlay (25 to 50 mm thickness) in zones of severe mechanical and environmental exposure where the material properties are best exploited, alone or associated to rebar for strengthening [4]. This type of intervention minimizes the traffic interruptions and disturbances due to construction sites and reduces their environmental impact by up to 50% [5], reduces the construction time by a factor of 3, and provides an efficient one-time intervention rather than having multiple interventions during the service life of the structure. This concept of intervention was extended in 2013 to marine signalization structures by Denarié et al [6,7] and has been successfully implemented for rehabilitation and strengthening of structures and infrastructures for over 15 years in Switzerland, France, and Slovenia [8–10], and more recently in Japan [11], Austria [12], USA [13], and Germany [14].
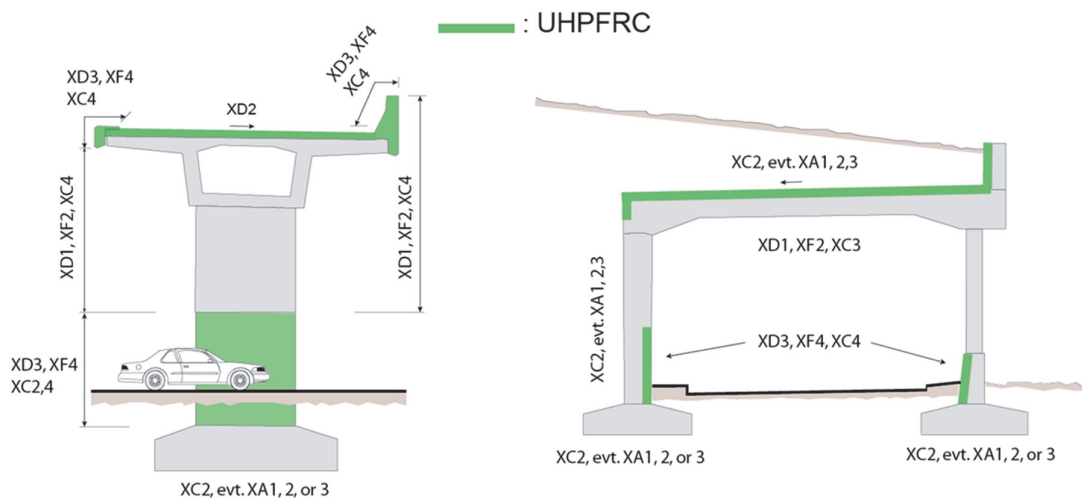
Fig. 1_ General concept of application of UHPFRC for the rehabilitation of strengthening of structures, after [15]

Fig. 2 shows the use of R-UHPFRC for the strengthening of the Chillon viaducts in Switzerland, which is still the largest application of this kind worldwide, with 2400 m3 cast on site UHPFRC (Ductal® NaG3 FM TX, with steel fibers) combined with rebar [10]. The UHPFRC mix was optimized for application by means of a specially developed machine, on slopes up to 7 %.

Fig. 2_ Strengthening of the Chillon viaducts with R-UHPFRC (photos from [16])

2. Motivation and scope

2.1 Overview

Although UHPFRC have enhanced the built environment by their outstanding mechanical and durability properties, which lead to reducing the environmental impact compared with conventional methods, there is still room for further improvement of these materials. Fig. 3 shows the contribution of components for the production of UHPFRC, to the impact categories of global warming (GWP), ozone depletion in the stratosphere (ODP), summer smog, i.e. photochemical ozone creation (POCP), acidification (AP) and eutrophication (NP) [17]. According to this figure, considering that more than 95% of the Global Warming Potential (GWP) impact of current UHPFRC is from the steel fibers and clinker contributions (48% and 47% respectively), replacing the steel fibers with synthetic ones and replacing clinker with Supplementary Cementitious Materials (SCM) can reduce significantly the environmental costs of these materials and make them even more sustainable.
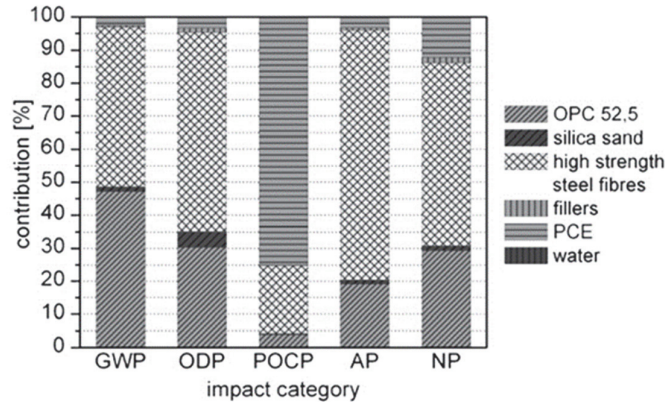
Fig. 3_ contribution of components to the different impact categories for the production of UHPFRC [17]

Furthermore, one of the most important characteristics of UHPFRC is to increase the lifetime of structures by their exceptional protective properties. However, although different measurements on undamaged UHPFRC specimens show a considerable improvement in the protective function of these materials compared to that of ordinary and high strength concretes, only a few notable studies were carried out on the effects of damage on transport properties of UHPFRC.

Taking into account the aforementioned domains with improvement potential, this study was realized under the National Research Program "Energy Turnaround (NRP 70)" of the Swiss National Science Foundation with the goal of developing innovative solutions for securing a sustainable energy policy in Switzerland [2]. This thesis addresses the development of a new UHPFRC mix by focusing on reducing the environmental impact of the fibrous mix and the matrix, along with considering the challenges of determination of reliable mechanical properties to validate recipes. The first step of the study is at the material level towards the full replacement of steel fibers with synthetic ones and partial replacement of clinker with SCM. In the second step, the experimental and analytical investigations focus on the tensile response under imposed shrinkage strains, the protective function of the newly developed material, and its contribution to the decrease of environmental impact. The following sections briefly illustrate the major challenges and driving forces of the study.

2.2 Improvement of the fibrous mix

UHPFRC mixes for structural applications are currently exclusively based on steel fibers. The resistance and deformability of UHPFRC highly depend on the properties of the fibrous mix that are mainly geometry, dosage, aspect ratio, and orientation of the fibers.

Upon the required performances, UHPFRC mixes generally contain between 1.5% to 5% and in the most extreme cases, 9 % volume steel fibers. Steel fibers have a superior balance of stiffness, strength, and bond with a cementitious matrix that make them one of the best choices for internal reinforcement of high-performance cementitious materials like UHPFRC (and also FRC). However, steel fibers are one of the most environmentally costly components of UHPFRC with a share of 48% in their environmental impact. Furthermore, the robustness of the strain hardening response of the UHPFRC mixes, which is one of the most important characteristics of this material, is often not guaranteed especially in case of low steel fiber dosages, below 3 % volume. Placing methods, workability of the mix, narrow spacing of the rebars, or confined condition of the complex formworks can highly affect the fiber orientation and the strain hardening character of the material [18,19].

Additionally, the superficial corrosion of the steel fibers reduces the attractiveness of this material from an architectural point of view. These corrosion spots are only on the surface of the material and do not affect the mechanical and durability properties of the structure. However, in certain cases, the aesthetic and architectural considerations may enforce the use of very expensive stainless steel fibers with limited dosages due to the budget constraints. Consequently, the limited volume of fibers in the mix increases the chances of microcracking in the structures. The Republic bridge and the roof of the TGV station in Montpellier, France are two examples which had the requirement of using stainless steel fibers from an architectural point of view (Fig. 4).

(a) (b)

Fig. 4_ Republic bridge [20] (a) and the roof of the TGV station [21] (b) in Montpellier, France

Considering the aforementioned issues, it is beneficial to further optimize the fibrous mix of UHPFRC in order to reduce the environmental impact and increase the robustness of the mixes by replacing steel fiber with an alternative synthetic fiber.

However, currently, synthetic fibers reinforced cementitious materials cannot face the challenges for structural applications and more precisely for the principal load-bearing elements, mostly because of their insufficient mechanical properties. Attempts to employ synthetic fibers to achieve strain hardening can be traced back to works of Li et al. in 1992 [22] which led to the development of Engineered Cementitious Composites (ECC) [23] with discontinuous Polyethylene fibers, a tensile strength around 4.5 MPa, and 5% strain hardening capacity. Kunieda et al. [24] and Kamal [25] tried to develop a material with the advantages of both UHPFRC and Strain Hardening Cementitious Composites (SHCC) with high strength and high modulus (88GPa) PE fibers. They achieved UHP-SHCC materials with a dense matrix, significant strain hardening capacity (close to 1%) and relatively high compressive strength (83 MPa) compared to normal SHCC (20.2 MPa). However, the dense network of synthetic fibers that hindered efficient de-airing at fresh state, significantly decreased the tensile elastic limit to 4.5 MPa. More recently, Rigaud et al. [26], Ranade et al. [27] and Curosu et al. [28] developed mixes with different types of synthetic fibers (glass, UHMW-PE, aramid, and PBO) and curing methods. The compressive strength of the synthetic fiber reinforced cementitious materials was improved and reached close to 150 MPa, however, the tensile elastic limit remained below 6 MPa in all those studies. According to Table 1, among the choices for alternatives to steel fibers, Ultra High Molecular Weight Polyethylene (UHMW-PE) fibers are the most promising option according to their mechanical properties (modulus of elasticity and strength), bond with cementitious matrix and their durability in an alkaline environment.

Table 1_ Properties and consideration of the alternative options for steel fibers in cementitious composites

Fiber type	E Modulus (GPa)	Tensile Strength (MPa)	Consideration
Carbon	250	4400	Poor bond with matrix, brittle, damage while mixing
Basalt	89	4840	Brittle, damage while mixing
Glass	80	3450	Durability issues in alkaline environment
PP	5	400-600	Low mechanical properties
PVA	35-45	1600	Low E modulus
PBO	180-270	5800	Durability issues with UV rays
Aramid	74	3400	Durability issues in alkaline environment
UHMW-PE	86-155	2800-4100	Sensitivity to high temperatures

Fig. 5 illustrates the fundamental difference between (a) steel fibers (macro 10/0.2 mm used in strain hardening UHPFRC mixes) and (b) chopped UHMW-PE fibers (6/0.012 mm). Chopped UHMW-PE fibers come in agglomerates of individual fibrils of 12 μm diameter that are dispersed at mixing. The number of individual fibers per m^3 UHPFRC is approximately 30 x higher for mixes with PE fibers compared to that for mixes with steel fibers, for similar tensile performances. PE fibers can be more uniformly and finely distributed than steel ones.

(a)   (b)
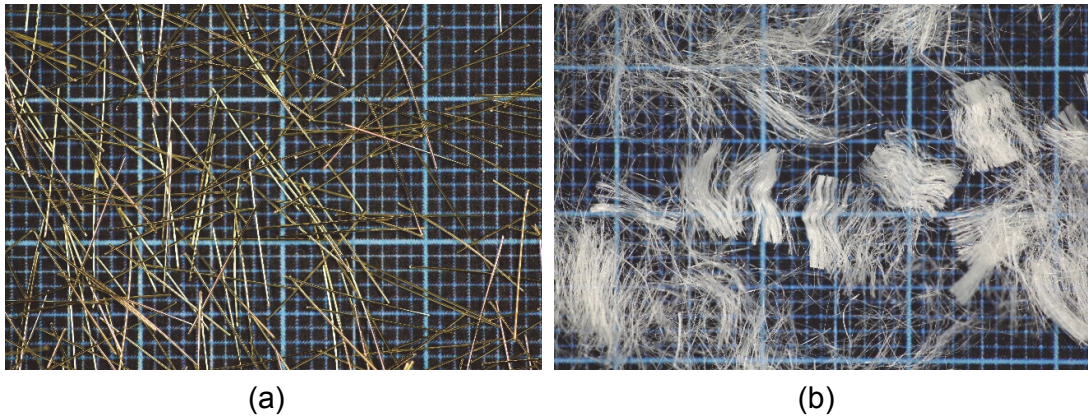
Fig. 5_ difference between (a) 10/0.2 mm steel fibers, and (b) 6/0.012 mm chopped UHMW PE fibers

Synthetic fibers are currently used in UHPFRC for non-structural applications, mostly facade elements with more or less complex shapes. Insufficient mechanical properties, lack of robust hardening and long-term durability concerns are the main reasons for not employing synthetic fiber reinforced cementitious materials in structural applications. **Thus, fundamental research is needed to develop a structural UHPFRC mix with synthetic fibers with required mechanical properties (e.g. tensile elastic limit above 7 MPa) as well as robust tensile hardening behavior without special treatment and curing procedures.**

2.3 Massive replacement of clinker with SCM

The low degree of hydration of cement in cementitious materials with a low water/cement ratio like UHPFRC mixes (close to 30 to 50 % at 28 days) on one hand and the high environmental cost of clinker on the other hand have motivated researchers to investigate the possibility of replacing clinker with SCM in the material mix design. A thought-out use of SCM with different particle size distributions in mix design can enhance the packing

density of the dry mix, the mechanical and durability properties of the material and also act as a mineral superplasticizer to improve the workability by decreasing the voids filling water. Furthermore, using SCM in the mix may lead to a reduction in the autogenous shrinkage [29] and an increase in the viscoelastic response of the mix [30] and consequently a reduction in the eigenstress development, which is beneficial for rehabilitation and strengthening applications with UHPFRC.

Limestone fillers, fly ash, silica fume, metakaolin, quartz powders, Ground Granulated Blast Furnace Slag (GGBFS), and Burnt Oil Shale (BOS) are the main SCMs that have been used as supplementary cementitious materials in high-performance cementitious materials. Denarié et al. [31] proposed UHPFRC formulations based on the massive use of limestone filler to replace clinker that were successfully applied on sites in Slovenia and Switzerland [32]. Additionally, Huang et al. [33] reported better workability and higher compressive strength for up to 54% replacement of clinker with limestone filler in UHPC mixes. Yu et al. [34] showed that the replacement of 30% clinker with GGBFS does not change the compressive strength of UHPFRC. Moreover, MCS/EPFL developed jointly with HOLCIM [18] High-performance Impermeable Fiber reinforced COMposite (HIFCOM) a type of UHPFRC using CEM III/B, in which 66-80% of the clinker was replaced with GGBFS. HOLCIM also developed a thixotropic UHPFRC mix using a cement combined with BOS [35]. Due to the increased availability of scrap steel from recycling in the steel industry especially in Europe, the availability of GGBFS, which is a by-product of the iron/steel manufacturing industries, has markedly decreased and currently more than 90% of the GGBFS is already used as an SCM in cement-based mixes [36]. However, limestone fillers are widely available in large quantities in different regions of the world [37] and thus, it is currently the most promising SCM for UHPFRC, due to their availability and very small production energy.

SCMs can replace a massive part of clinker in UHPFRC mixes in order to make this material more sustainable and environmentally friendly. However, **further research is needed to develop accurate and efficient tools for modeling and optimization of the packing density of dry powder mixes with multiple components and grain sizes in order to optimize the workability and mechanical properties of UHPFRC mixes with SCM.**

2.4 Mechanical Testing methods

Determination of reliable mechanical properties of UHPFRC and comparing the performances of recipes according to the existing literature are challenging due to the lack of unified testing methods especially for the characterization of the tensile behavior. Uniaxial tensile tests can easily be severely biased by bending effects due to eccentricities and inappropriate boundary conditions, and by fiber orientation which may lead to misleading conclusions or irrelevant claims of progress. Kanakubo [38] showed that the testing methods and boundary conditions of support highly affect the apparent tensile behavior of fiber reinforced cementitious materials. As a matter of fact, there are more than 20 configurations for uniaxial tensile tests of UHPFRC reported in the literature [39]. The inverse analysis of 3 or 4-point bending test results is used to investigate the tensile properties of UHPFRC [40–43], mainly in order to avoid the difficulties of uniaxial tensile tests, and the results are promising for UHPFRC with a hardening domain of 1-5‰ [43]. However, the accuracy of this method to predict the tensile strength and deformability in case of cementitious materials with a very high tensile deformation capacity (several %) decreases due to the large deflections under loading. Furthermore, although it is less critical than tensile, the compressive testing of the UHPFRC, in which the size and geometry of specimens play an important role, encounters similar issues and reporting the compressive strength of small cubes [33,44] may lead to overestimation of material properties.

As such, relevant testing setups and specimen geometries are needed and special attention should be given in order to overcome the challenges of reliable determination of mechanical properties representative of practical applications.

2.5 Protective function

The protective function is one of the most important properties of UHPFRC materials, especially in rehabilitation or strengthening applications. In order to investigate this function, different measurements methods for evaluating the transport properties, such as capillary absorption, gas penetration, and liquid penetration were carried out on undamaged UHPFRC specimens [45–47], which all show a considerable improvement compared to ordinary and high strength concretes.

However, although at service state the structural elements experience different levels of mechanical loading under both autogenous (eigenstresses) and exogenous actions (climate conditions, live loads, deadweight, accidental actions, fire, etc.) which may cause damage,

9

there are only few notable studies that were carried out on the effects of damage on transport properties of UHPFRC [48–52]. The results show that the permeability of liquids under pressure (Darcy) is very much linked to the crack features and cracking patterns and regardless of the material type (SHCC, normal concrete, and UHPFRC), the permeability to liquids under pressure starts increasing at a much faster rate with increasing crack width after 0.05 to 0.1 mm [53–55]. However, the capillary water absorption in UHPFRC specimens was found to increase drastically by increasing the stress in the specimens. Wang et al. [51] found that the absorbed water mass increased by a factor of two when the specimens were loaded up to 50 % of their compressive strength. Moreover, it was shown that capillary absorption is significantly increased if the material is subjected to tensile stresses higher than 50 % of its tensile strength [52]. Even though the crack width plays an important role in the capillary absorption of cementitious materials, its effects have been underestimated in the aforementioned studies as the capillary absorption was determined after unloading the specimens. A similar trend was observed for ECC and SHCC [56,57].

As such, fundamental research is needed to investigate the effect of strain/stress level and the associated crack properties on the protective function of UHPFRC while it is under tensile loading and subjected to the capillary absorption of liquids, to provide a basis to define suitable limit states of deformation /stress level at serviceability.

3. Objectives

The main objectives of the thesis were to develop a new Strain Hardening UHPFRC mix with replacement of steel fibers with UHMW-PE ones and replacement of 50% vol. clinker with limestone filler, and to investigate the protective function, delayed response under tensile loading, and environmental impact of the newly developed material. The specific objectives of the thesis were:

1. To review the existing knowledge on synthetic fiber reinforced cementitious materials, use of SCM in cementitious matrices, tensile behavior influencing factors, transport properties and delayed response of fiber reinforced cementitious materials.

2. To develop the necessary tools for characterization and optimization of the matrix e.g. tools for the characterization of the matrix porosity and for calculating and measuring the packing density of the mix and individual components.

3. To develop a new structural UHPFRC mix with full replacement of the steel fibers with synthetic fibers and replacement of 50% vol. clinker with limestone filler.

4. To investigate the mechanical properties of the newly developed UHPFRC with a focus on tensile properties of specimens with geometry and size representative of practical applications.

5. To investigate the evolution of autogenous deformations and development of eigenstresses in a layer of the newly developed material under full restraint condition.

6. To investigate the cracking behavior and the effect of the tensile strain level on the protective function of the material while the specimen is under loading, using capillary absorption of water as the reference parameter.

7. To investigate the environmental impact of the newly developed material in a practical application of strengthening of a bridge, and compare it with that of solutions with conventional UHPFRC with steel fibers or demolition and reconstruction with post-tensioned reinforced concrete.

4. Overview

The structure of this thesis and its contents are presented in Fig. 6. The work is presented as a compilation of four journal papers that have been submitted to international peer-reviewed journals.

Chapter 1:
Introduction

- Context
- Motivation
- Objectives

Chapter 2:
Development of Next Generation UHPFRC with synthetic fibers

- Development of generalized CIPM packing model
- Investigation of mechanical properties with focus on tensile response
- Development of PE-UHPFRC mix with 50% clinker replacement and UHMW-PE fibers

Chapter 3:
Tensile response of UHPFRC under imposed shrinkage

- Development of elastic modulus
- Investigation of autogenous deformations and eigenstresses development in PE-UHPFRC layer under full and partial restraint conditions
- Tensile response of PE-UHPFRC under fully restrained Shrinkage deformations

Chapter 4:
Protective function of PE-UHPFRC, under tensile loading

- Development of an original capillary absorption setup under loading
- Investigation of sorptivity at different strain level (0.15-2%), under load and after unloading
- Investigation of crack characteristics at different strain level
- Discussion on SLS of PE-UHPFRC

Chapter 5:
Rehabilitation/strengthening of structures using PE-UHPFRC

- LCA of PE-UHPFRC at structural level compared with conventional UHPFRC and normal concrete
- LCA Investigations in three categories: GWP, CED, and UPB

Chapter 6:
Conclusions and Outlook

- Response to the research objectives
- Perspectives and future works

Fig. 6_ Structure of the thesis

Chapter 2 (Paper I) presents the development of the UHPFRC mix with 50% vol. replacement of the clinker with limestone fillers and full replacement of steel fibers with UHMW-PE ones, named PE-UHPFRC. The mechanical properties of the newly developed mix are investigated with a focus on tensile response.

Chapter 3 (Paper II) studies the tensile response of PE-UHPFRC under imposed shrinkage deformation compared with that of conventional UHPFRC. The development of the

dynamic elastic modulus from an early age is investigated for PE-UHPFRC and compared to that of UHPFRC mixes with steel fibers.

Chapter 4 (Paper III) investigates the capillary absorption and crack characteristics of PE-UHPFRC under different tensile strain levels ranging from 0.15% to 2%. The original setup used for the investigation of capillary absorption under loading is presented.

Chapter 5 (Paper IV) investigates the environmental impact of the strengthening of a bridge using R-PE-UHPFRC, conventional R-UHPFRC, or replacement by a new post-tensioned reinforced concrete bridge.

Finally, chapter 6 summarizes the most important conclusions of the works and suggests a perspective for future works.

References

1.   Abergel, T., Dean, B. & Dulac, J. *Towards a zero-emission, efficient, and resilient buildings and construction sector: Global Status Report 2017*. UN Environment and International Energy Agency: Paris, France (2017).

2.   *National Research Programme 'Energy Turnaround' (NRP 70)*. (2013).

3.   Brundtland, G. H., Khalid, M., Agnelli, S. & Al-Athel, S. *Our common future*. in *Report of the World Commission on Environment and Development* (1987).

4.   Denarie, E. & Brühwiler, E. *Structural Rehabilitations with Ultra-High Performance Fibre Reinforced Concretes (UHPFRC)/Strukturelle Instandsetzung von Betonbrücken mit Ultra-hochleistungsfähigem Faserfeinkornbeton (UHFB)*. Restoration of Buildings and Monuments 12, 93–108 (2006).

5.   Habert, G., Denarié, E., Šajna, A. & Rossi, P. *Lowering the global warming impact of bridge rehabilitations by using Ultra High Performance Fibre Reinforced Concretes*. Cement and Concrete Composites 38, 1–11 (2013).

6.   Denarié, E. *UHPFRC for the cast-in place reinforcement of offshore maritime signalization structures*. in *HAC2018| V Congreso Iberoamericano de Hormigón Autocompactante y Hormigones Especiales* (eds. Serna Ros, P., Marti Vargas, J. R. & Llano Torre, A.) 17–30 (2018).

7.   Denarié, E., Jacomo, D., Fady, N. & Corvez, D. *Rejuvenation of maritime signalisation structures with UHPFRC*. in *2nd International Symposium on Ultra-High Performance Fibre-Reinforced Concrete (UHPFRC)* 157–166 (RILEM Pro087, 2013).

8.   Denarié, E. & Brühwiler, E. *Cast-on site UHPFRC for improvement of existing structures–achievements over the last 10 years in practice and research*. 7th

workshop on High Performance Fiber Reinforced Cement Composites, 1-3, June 2015, Stuttgart, Germany (2015).

9. Brühwiler, E. & Denarié, E. *Rehabilitation and strengthening of concrete structures using ultra-high performance fibre reinforced concrete*. Structural Engineering International 23, 450–457 (2013).

10. Brühwiler, E. & Bastien Masse, M. *Strengthening the Chillon viaducts deck slabs with reinforced UHPFRC. IABSE Conference Geneva 2015 'Structural Engineering: Providing Solutions to Global Challenges'* 1171–1178 (2015).

11. Kosaka, Y., Imai, T., Kunieda, M., Mitamura, H., & Matsui, S. *Development of ultra-high performance fibre reinforced cement composites for rehabilitation of bridge deck*. in *International conference on regeneration and conservation of concrete structures (RCCS)* (2015).

12. Hadl, P., della Pietra, R., Hoang, K. H., Pilch, E. & Tue, N. V. *Application of UHPC as road bridge topping within the adaptation of an existing conventional bridge to an integral abutment bridge in Austria*. BETON-UND STAHLBETONBAU 110, 162–170 (2015).

13. Haber, Z. B., Munoz, J. F. & Graybeal, B. A. *Field testing of an ultra-high performance concrete overlay (No. FHWA-HRT-17-096)*. in *Federal Highway Administration Office of Infrastructure Research and Development* (2017).

14. Pelke, E., Jaborek, A., Berger, D. & Brühwiler, E. *Überführungsbauwerk der L3378 bei Fulda-Lehnerz: Erster Einsatz von UHFB in Deutschland im Straßenbrückenbau, Teil 1: Projektentwicklung und Baudurchführung*. Beton-und Stahlbetonbau 113, 831–841 (2018).

15. Denarié, E. *SAMARIS D25b-Guidance for the use of UHPFRC for rehabilitation of concrete highway structures*. (2006).

16. Brühwiler, E. & Shen, X. *Strengthening of existing structures using R-UHPFRC: principles and conceptual design*. in *2nd ACF Symposium– Innovations for Sustainable Concrete Infrastructures* (2017).

17. Stengel, T. & Schießl, P. *Sustainable construction with UHPC–from life cycle inventory data collection to environmental impact assessment*. in *Proceedings of the 2nd international symposium on ultra high performance concrete. Kassel University Press, Kassel* 461–468 (2008).

18. Oesterlee, C. *Structural Response of Reinforced UHPFRC and RC Composite Members*. Doctoral thesis (2010).

19. Behloul, M. *Analyse et modélisation du comportement d'un matériau à matrice cimentaire fibrée à ultra hautes performances: bétons de poudres réactives, du matériau à la structure*. Doctoral thesis (1996).

20. *Pont de la République*. (2011). Available at: http://rudyricciotti.com/projet/pont-de-la-republique#!/rudyricciotti.com/wp.

21. *TGV-Bahnhof Montpellier*. (2018). Available at: https://www.baunetzwissen.de/beton/objekte/oeffentlicher-raum/tgv-bahnhof-

montpellier-5380749.

22. Li, V. C. & Wu, H.-C. *Conditions for pseudo strain-hardening in fiber reinforced brittle matrix composites*. Applied Mechanics Reviews 45, 390–398 (1992).

23. Li, V. C. *From micromechanics to structural engineering-the design of cementitous composites for civil engineering applications*. Structural Eng./Earthquake Eng. 10, 37–48 (1993).

24. Kunieda, M., Denarié, E., Brühwiler, E. & Nakamura, H. *Challenges for strain hardening cementitious composites–deformability versus matrix density*. in *HPFRCC5* (2007).

25. Kamal, A. *Material development of UHP-SHCC for repair applications and its evaluation*. Doctoral thesis (2008).

26. Rigaud, S., Chanvillard, G. & Chen, J. *Characterization of bending and tensile behavior of Ultra-High Performance Concrete containing glass fibers*. in *High Performance Fiber Reinforced Cement Composites 6* 373–380 (Springer, 2012).

27. Ranade, R., Li, V. C., Stults, M. D., Heard, W. F. & Rushing, T. S. *Composite Properties of High-Strength, High-Ductility Concrete*. ACI Materials Journal 110, (2013).

28. Curosu, I., Liebscher, M., Mechtcherine, V., Bellmann, C. & Michel, S. *Tensile behavior of high-strength strain-hardening cement-based composites (HS-SHCC) made with high-performance polyethylene, aramid and PBO fibers*. Cement and Concrete Research 98, 71–81 (2017).

29. Kang, S.-H., Jeong, Y., Tan, K. H. & Moon, J. *High-volume use of limestone in ultra-high performance fiber-reinforced concrete for reducing cement content and autogenous shrinkage*. Construction and Building Materials 213, 292–305 (2019).

30. Hafiz, M. A., Hajiesmaeili, A. & Denarié, E. *Tensile response of low clinker UHPFRC subjected to fully restrained shrinkage*. Cement and Concrete Research (2019).

31. Denarié, E. & Houst, Y. *Cement matrices for high performance fibre reinforced cementitious composites (HPFRCCs), in particular ultra high performance fibre reinforced concretes (UHPFRCs)*. *European patent* (2009).

32. Denarié, E., Kazemi Kamyab, M., Brühwiler, E., Haddad, B. G. & Nendaz, S. *Béton fibré ultra performant pour la maintenance, un nouvel élan*. *tracés n°12* 20–23 (2011).

33. Huang, W., Kazemi-Kamyab, H., Sun, W. & Scrivener, K. *Effect of cement substitution by limestone on the hydration and microstructural development of ultra-high performance concrete (UHPC)*. Cement and Concrete Composites 77, 86–101 (2017).

34. Yu, R., Spiesz, P. & Brouwers, H. J. H. *Development of an eco-friendly Ultra-High Performance Concrete (UHPC) with efficient cement and mineral admixtures uses*. Cement and Concrete Composites 55, 383–394 (2015).

35. *https://www.holcimpartner.ch/fr/know-how/reference/la-centrale-hydraulique-berne-suisse*. (2019).

36. *Cement Sustainability Initiative, Getting the Numbers Right: Project Emissions Report 2014*. WBCSD (2016).

37. Scrivener, K. L., John, V. M. & Gartner, E. M. *Eco-efficient cements: Potential economically viable solutions for a low-CO2 cement-based materials industry*. Cement and Concrete Research 114, 2–26 (2018).

38. Kanakubo, T. *Tensile Characteristics Evaluation Method for Ductile Fiber-Reinforced Cementitious Composites*. Journal of Advanced Concrete Technology 4, 3–17 (2006).

39. Wille, K., El-Tawil, S. & Naaman, A. E. *Properties of strain hardening ultra high performance fiber reinforced concrete (UHP-FRC) under direct tensile loading*. Cement and Concrete Composites 48, 53–66 (2014).

40. Chanvillard, G. & Corvez, D. *Explicit back analysis method for quick determination of direct tensile strength of plate structural members*. in *RILEM-fib-AFGC Int. Symposium on Ultra-High Performance Fibre-Reinforced Concrete, UHPFRC 2013* (2013).

41. Baby, F., Graybeal, B., Marchand, P. & Toutlemonde, F. *UHPFRC tensile behavior characterization: inverse analysis of four-point bending test results*. Materials and structures 46, 1337–1354 (2013).

42. López, J. Á., Serna, P., Navarro-Gregori, J. & Camacho, E. *An inverse analysis method based on deflection to curvature transformation to determine the tensile properties of UHPFRC*. Materials and Structures 48, 3703–3718 (2015).

43. Denarié, E., Sofia, L. & Brühwiler, E. *Characterization of the tensile response of strain hardening UHPFRC-Chillon viaducts*. in *AFGC-ACI-fib-RILEM Int. Symposium on Ultra-High Performance Fibre-Reinforced Concrete, UHPFRC 2017* 242–250 (2017).

44. Wille, K., Naaman, A. E. & Parra-Montesinos, G. J. *Ultra-High Performance Concrete with Compressive Strength Exceeding 150 MPa (22 ksi): A Simpler Way*. ACI materials journal 108, (2011).

45. Dobias, D., Pernicova, R. & Mandlik, T. *Water Transport Properties and Depth of Chloride Penetration in Ultra High Performance Concrete*. in *Key Engineering Materials* 711, 137–142 (Trans Tech Publ, 2016).

46. Wang, W. *et al. Durability of an Ultra High Performance Fiber Reinforced Concrete (UHPFRC) under progressive aging*. Cement and Concrete Research 55, 1–13 (2014).

47. Roux, N., Andrade, C. & Sanjuan M, A. *Experimental Study of Durability of Reactive Powder Concretes*. Journal of Materials in Civil Engineering 8, 1–6 (1996).

48. Charron, J.-P., Denarié, E. & Brühwiler, E. *Transport properties of water and glycol in an ultra high performance fiber reinforced concrete (UHPFRC) under high tensile deformation*. Cement and Concrete Research 38, 689–698 (2008).

49. Wang, R., Gao, X., Li, Q. & Yang, Y. *Influence of splitting load on transport properties of ultra-high performance concrete*. Construction and Building Materials 171, 708–718 (2018).

50. Ma, Z., Zhao, T. & Yao, X. *Influence of Applied Loads on the Permeability Behavior of Ultra High Performance Concrete with Steel Fibers*. Journal of Advanced Concrete Technology 14, 770–781 (2016).

51. Wang, P., Yao, X., Wittmann, F. H., Zhang, P. & Zhao, T. *Influence of Imposed Compressive Stress and Subsequent Self-healing on Capillary Absorption and Chloride Penetration into UHPFRCC*. in *Seventh International RILEM Workshop on High Performance Fiber Reinforced Cement Composites (HPFRCC7)* 243–250 (2015).

52. Wittmann, F. H., Yao, X., Wang, P., Zhang, P. & Zhao, T. *Influence of an imposed tensile stress and subsequent self-healing on capillary absorption and chloride penetration into HPFRCC*. in *Seventh International RILEM Workshop on High Performance Fiber Reinforced Cement Composites (HPFRCC7)* 251–258 (2015).

53. Lepech, M. & Li, V. C. *Water permeability of cracked cementitious composites. Proceedings ICF11, 11th International Conference on Fracture* (2002).

54. Charron, J.-P., Denarié, E. & Brühwiler, E. *Permeability of ultra high performance fiber reinforced concretes (UHPFRC) under high stresses*. Materials and Structures 40, 269–277 (2007).

55. Lepech, M. D. & Li, V. C. *Water permeability of engineered cementitious composites*. Cement and Concrete Composites 31, 744–753 (2009).

56. Wittmann, F. H., Wang, P., Zhang, P., Zhao, T. & Beltzung, F. *Capillary absorption and chloride penetration into neat and water repellent SHCC under imposed strain*. in *2nd International RILEM Conference on Strain Hardening Cementitious Composites (SHCC2-Rio)* 165–172 (RILEM Publications SARL Rio de Janeiro, 2011).

57. Şahmaran, M. & Li, V. C. *Influence of microcracking on water absorption and sorptivity of ECC*. Materials and structures 42, 593–603 (2009).

Chapter 2

Paper 1

Development of Next Generation UHPFRC with synthetic fibers, for structural applications

1 – corresponding author - conducted all the experiments presented in the paper along with the writing of the full article

2 – thesis supervisor

Abstract

The already established concept of Ultra High-Performance Fiber Reinforced Concrete (UHPFRC) was further improved by developing and validating a new mix with 70% reduction in Embodied Energy (EE), an elastic limit above 7 MPa, and a robust strain hardening response. Steel fibers were replaced by ultra-high molecular weight polyethylene (UHMW-PE) ones and 50% volume of clinker was replaced by Supplementary Cementitious Materials (SCM). An optimized test set-up was used to guarantee a realistic determination of the tensile behavior, on specimens with a size representative of practical applications. Three types of matrixes optimized using a generalized Compaction-Interaction Packing Model (CIPM), three types of fibers, and two types of admixtures were investigated. The new UHPFRC mix with synthetic fibers is well adapted for structural applications owing to its high tensile elastic limit above 7 MPa, its tensile strength of more than 11 MPa, and its robust tensile hardening domain of 3.5% (average values).

Keywords: UHPFRC; Sustainability; UHMW-PE fibers; Tensile response; Strain Hardening; Embodied Energy; CIPM

1. Introduction

The ever-increasing demand for the rehabilitation of existing structures and the construction of new ones, along with environmental issues of construction sites, are heavy burdens for society in terms of economy and environment. Meanwhile, UHPFRC has proved its potential to be one of the solutions to contain the explosion of the maintenance costs (Economy and Environment), because of its extremely low permeability associated with outstanding mechanical properties. Considering all the direct and indirect expenses, UHPFRC already helps to decrease the environmental impact of construction sites by up to 50%, when compared to conventional concretes for rehabilitation purposes [1]. Bearing in mind that more than 95% of the Global Warming Potential (GWP) impact of current UHPFRC is from the steel fibers and clinker contributions (48% and 47% respectively) [2,3], the objective of this study was to improve the already established concept of UHPFRC by replacing the steel fibers with synthetic ones and replacing clinker with SCM, which would have a very positive effect on reducing the environmental costs of this material.

UHPFRC with steel fibers are commonly used in structural applications, associated with rebar and/or pre-stressing. However, no UHPFRC mixes based exclusively on synthetic fibers exist for structural applications and more precisely for the principal load-bearing elements. Synthetic fibers reinforced cementitious materials cannot currently face the challenges for structural applications mostly because of their insufficient mechanical properties. Based on French standard on UHPFRC [4], the compressive strength and the tensile elastic limit should be higher or equal to 130 MPa and 6 MPa (5% fractile), respectively for non-steel fiber UHPFRC. Swiss recommendations for UHPFRC [5] do not distinguish between steel and synthetic fibers and put the limit of 120 MPa (5% fractile) and 7 MPa (mean value) for compressive strength and the tensile elastic limit, respectively. Glass fiber-reinforced UHPFRC (GF-UHPFRC) are so far the best regarding the mechanical performance among UHPFRC with synthetic fibers, but sensitivity of glass fibers in alkaline environments is a concern for their long-term durability.

Toward developing a structural UHPFRC mix with synthetic fibers, matrix density, fibrous mix and the bond between matrix and fibers are the factors governing the mechanical and durability properties. Moreover, defining appropriate methods to determine the required properties is of great importance especially in the case of tensile response, as the testing methods and boundary conditions highly affect the tensile behavior [6] and the tensile test can easily be severely biased by bending effects due to eccentricities and/or inappropriate

boundary conditions. Fig. 1 summarize the factors influencing the apparent tensile behavior of a fiber reinforced cementitious material.
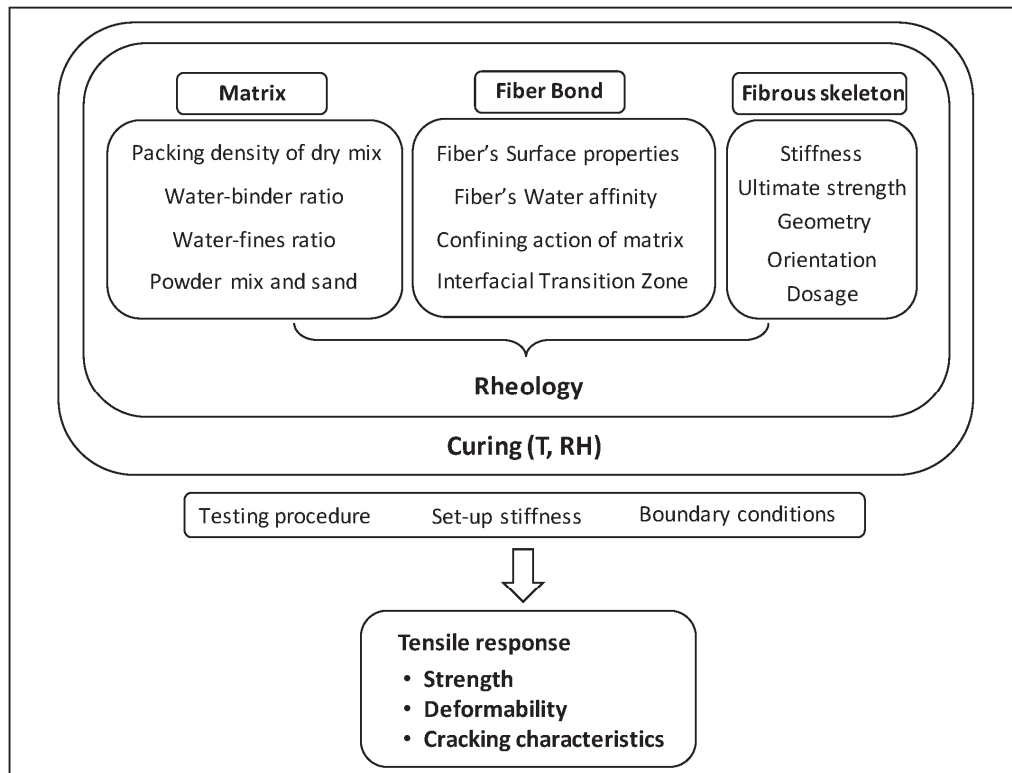
Fig. 1_ Influencing factors on apparent tensile behavior of a fiber reinforced cementitious material

This paper reports on the methodology and the obtained results on development of a new UHPFRC mix with synthetic fibers adapted for structural applications, which reduces the environmental impact of conventional UHPFRC mixes by replacing the steel fibers with Ultra High Molecular Weight polyethylene (UHMW-PE) ones and massively replacing clinker with limestone fillers. In a first step, the background literature is synthesized. Secondly, the mix-design approach is presented, with the development of a new implementation of a packing model. Thirdly, the experimental methods are described, highlighting the challenges of tensile tests and the solutions proposed. The results obtained with different mixes are then compared and analyzed in detail in terms of influence factors such as size effect of the specimen and put into perspective with literature. Finally, the properties, advantages, and potentials of the optimal mix are brought forward.

2. Background

2.1 Matrix optimization

At the beginning of the 20th century, Abrams [7] related the strength of cementitious materials to the water-cement ratio and the grain size. Later, in 1960 Powers [8] introduced the porosity dependence of strength and explained the relationship between water-cement ratio and porosity. In 1970 Gitzen [9] derived empirical relations to describe the effect of grain size and the limitations imposed by porosity on the material strength. Considering both the water-binder ratio and the porosity, Bentz and Aitcin [10,11] introduced the distance between binder particles as the fundamental influencing factor on strength, the smaller the spacing, the higher the density of the microstructure.

UHPFRC were originally conceptualized by Bache in 1981 [12] and have been in development for the last five decades. Bache introduced ultrafine particles as a specific component of UHPC matrixes and DSP (Densified Systems containing homogeneously arranged, ultra-fine Particles) was the result of his work in which fine cement, low w/b ratio (0.18 – 0.25) and high silica fume and superplasticizer content were used that resulted in a compressive strength of 120-250 MPa. Six years later, Compact Reinforced Composite (CRC) was developed by adding rebars and fine fibers to DSP [13] to achieve high deformability. The influential researches of Bache lead to the development of Reactive Powder Concrete (RPC) and Ultra-High Performance Concrete (UHPC) during the 1990's [14,15] with elimination of coarse aggregates to enhance the homogeneity. Continuing this trend, maximizing the packing density of the dry mix and minimizing the water-binder ratio are the keys to further improve the matrix of UHPFRC.

Reducing the w/b ratio results in a smaller spacing between the grains. Thus, in a mix design, reducing the water amount for a given amount of binder while maintaining proper workability, enhances the mechanical and durability properties of the material. The total batching water can be divided into (I) void filling water that should fill the voids between the granular skeleton and fibers, and (II) lubricating water that lubricates the grains and fibers and improves workability. Considering the concrete mixture as a solid granular skeleton and voids [16], increasing the packing density reduces the voids in the solid grains skeleton and accordingly reduces the amount of void filling water. Hence, increasing the packing improves the overall workability-strength performance of cementitious materials. Furthermore, maximizing the packing density reduces the size of the interfacial transition

zone (ITZ) and increases its density [17] which enhances the bond between matrix and fibers.

Beginning as 1907, Fuller and Thompson [18] suggested a curve to optimize the particle packing which was later modified by Andreasen and Andersen [19] and Funk and Dinger [20]. However, the geometric effect of the grains on each other and the energy of mixing were not considered in any of these methods still frequently used for the formulation of UHPC mixes [21–23]. In 1994, inspired from Mooney's model [24], de Larrard introduced the Solid Suspension Model (SSM) [15] to optimize the matrix of UHPC. Later, in 1999, the Compressible Packing Model (CPM) was developed [25] to model the packing density of cementitious materials. CPM considered the energy required to compact a mix of several monosized particle classes as well as the loosening effect on large particles by interstitial small ones, and the wall effect within assemblies of small particles near a large one or a fiber or a container wall. Sedran [26] generalized the CPM to consider the interaction of multiple grain classes with arbitrary Particle Size Distributions (PSD). Focusing on the interaction equations for particles smaller than 125 μm, Fennis et al. [27] developed the Compaction-Interaction Packing Model (CIPM) which was an extension of the CPM, taking into account surface forces like van der Waals forces, electrical double layer forces and steric forces acting among particles with a diameter below 0.125 mm. This model was successfully applied to reduce the cement content in concrete mixtures by a factor of 3 while maintaining the mechanical properties [28].

Using a low w/b ratio and a high packing density in UHPFRC mixes made the implementation of highly effective chemical admixtures essential to ensure adequate workability. Among different types of superplasticizers (SP), the polycarboxylate-based SP are the most widely used in UHPFRC mixes, because of their excellent water reduction ability of up to 40% [29,30]. The interaction between superplasticizer, cement and grains with a diameter lower than 0.125 mm that they deflocculate with mainly a steric effect, has complex influential parameters such as chemistry and length of the backbone, number and length of the side chains, amount of anionic and ionic groups, bond type between backbone and side chain, and overall charge density of those polymers [31–34]. It affects both fresh and hardened properties of UHPFRC [35]. Thus, the compatibility of SP and powders used in UHPC formulation is of great importance.

Hence, towards further improvement of UHPFRC mixes, the use of suitable packing models and superplasticizers is required to reduce the w/b ratio to the minimum practically feasible and enhance the microstructure of the mix with minimum voids.

2.2 Synthetic fiber reinforced cementitious materials

Beginning as early as the 1990's, interest in developing a synthetic fiber reinforced cementitious material with a high tensile deformation capacity has been gaining ground. Attempts to employ synthetic fibers to achieve strain hardening can be traced back to works of Li et al. in 1992 [36] who used micromechanics theory with the aim of obtaining evenly distributed multiple microcracks under tension with openings smaller than durability related limits of 0.1 mm [37]. ECC (Engineered Cementitious Composite) was the result of this research [38], materials with discontinuous Polyethylene fibers, a tensile strength around 4.5 MPa, and 5% strain hardening capacity. It was shown that the same mechanical properties could be achieved using PolyVinyl Alcohol fibers (PVA) [39]. Kunieda et al. [40] and Kamal [41] tried to develop a material with the advantages of both UHPFRC and Strain Hardening Cementitious Composites (SHCC) with high strength and high modulus PE fibers. Although they achieved UHP-SHCC materials with a dense matrix, significant strain hardening capacity (close to 1%) and relatively high average compressive strength (83 MPa) compared to normal SHCC (20.2 MPa), the tensile strength of the UHPC matrix was significantly decreased (from 12 with steel fibers to 4.5 MPa) by the dense network of synthetic fibers that hindered efficient de-airing at fresh state. Curosu et al. [42] developed high-strength strain-hardening cement-based composites (HS-SHCC) with PE, aramid and PBO fibers. The compressive strength of the HS-SHCC reached 140 MPa on average, however, the tensile elastic limit of the mixes remained below 6 MPa and PE reinforced mixes had a tensile elastic limit of 3.8 MPa. Rigaud et al. [43,44] developed an ultra high performance reinforced concrete containing glass fibers (GF-UHPFRC) for thin-plate applications. They used 450x145x20 mm 4-point bending specimens and achieved a deflection hardening material with 17 MPa flexural strength using 2% fibers which corresponds to 8 MPa tensile strength based on their inverse analysis method. This trend was further continued by Ranade et al. [45] using UHMW-PE fibers with an elastic modulus of 100 GPa, which led to High-Strength, High-Ductility Concrete (HSHDC) with an increase in the tensile strength up to 14 MPa. The tensile elastic limit remained however low (in the range of 5 MPa) and the specimens were cured at 90°C for 7 days at an early age, which is impossible to use for cast-on-site applications. Moreover, the tensile hardening domain of these materials had a stress fluctuation range of 10 MPa.

Insufficient mechanical properties, lack of robust hardening and long-term durability concerns are the main reasons for not employing synthetic fiber reinforced cementitious materials in structural applications. Thus, a practical structural UHPFRC mix with synthetic

fibers should have the required mechanical properties as well as robust hardening behavior without special treatment and curing procedures.

2.3 Clinker replacement with SCM

Nehdi et al. [46], studied combinations of limestone filler, cement and silica fume in high-performance mortars with cement replacement by filler up to 25% mass. They concluded that cement with limestone filler contents up to about 10 to 15% by volume did not significantly affect the strength of mortars at early ages. This was confirmed by Bonavetti et al. [47], who experimentally investigated the effect of cement replacement by limestone filler up to 20% mass on the hydration process (gel-space ratio and degree of hydration) in pastes with w/c=0.25 to 0.50 and low slump concretes with w/c=0.30 and 0.34. Denarié et al. [48], proposed a general methodology for the formulation of UHPFRC from local components, based on the massive use of limestone filler to replace clinker that was successfully applied on sites in Slovenia and Switzerland [49]. Huang et al. [50] investigated the effect of replacing clinker with limestone in UHPC mixes and reported better workability and higher compressive strength for up to 54% replacement. Limestone powder is currently the most promising SCM for UHPFRC, due to its very small production energy. Along with developing studies on limestone filler, quartz and glass powder have been taken into consideration as SCM. Bornemann et al. [51] showed that it is possible to replace significant amounts of the cement in UHPC mixes by quartz powders of closely controlled size and distribution, keeping the absolute water added constant, without significantly decreasing the compressive strength up to a replacement ratio of 40%. On the other hand, Du et al. [52] and Soutsos et al. [53] reported successful replacement of more than 30% of cement with waste glass materials in conventional concrete and UHPC which enhance the mechanical properties due to their pozzolanic reactions. Sharifi et al. [54] showed that replacing up to 20% of cement with ground waste glass could improve the fresh properties of self-compacting concrete. These trends were confirmed by Soliman et al. [55] for UHPC containing glass sand and glass powder. Yu et al. [22] showed that replacement of 30% clinker with granulated blast-furnace slag (GGBS) does not affect the compressive strength of UHPFRC. Moreover, MCS/EPFL developed jointly with HOLCIM [56] High-performance Impermeable Fiber reinforced COMposite (HIFCOM) a type of UHPFRC using CEM III/B, in which 66-80% of clinker is replaced with granulated blast furnace slag. Therefore, considering the high amount of clinker in first generation UHPFRC mixes and their very low degree of hydration, it is possible to replace a massive part of it with SCM without reducing the mechanical properties, which is the trend of mix design of UHPFRC for over 10 years [57].

3. Mix design approach

3.1 Methodology

In this study, coarse aggregates were not employed and d_{max} was limited to 0.6 mm. Two types of limestone filler with different gradings were chosen as SCM to partially replace the cement. Furthermore, the effect of different proportions of fine sand and quartz powder on the mechanical properties of the mixes was investigated. In order to estimate and optimize the packing density of the dry mix and accordingly minimize the water-binder ratio, porosity and the distance between binder particles, the generalized CIPM model was developed and used, based on the works of Fennis [58]. The model considers the interaction of grain classes with arbitrary PSD as well as the interaction equations for the particles smaller than 125 μm that are necessary for UHPFRC. Among different types of synthetic fibers, considering mechanical and durability properties, UHMW-PE fibers were selected because of their high elastic modulus and tensile strength. Moreover, UHMW-PE fibers are not sensitive to an alkaline environment or UV rays, which are concerns in case of glass and PBO fibers, respectively [59,60]. The fiber length and diameter were selected so as to make sure that the fibers are pulled out rather than having fiber failure. After preliminary investigation on the effect of fiber dosage on workability of the fresh mix, 2% vol. dosage was selected in this study, due to the adverse effect of fibers on workability above that value.

3.2 Generalized CIPM Model development

The CPM model [25], predicts the packing density of a mix containing n monosized classes by considering the geometrical parameters (loosening and wall effects) and energy of mixing. In order to implement more realistically the variance in compaction energy of the different granular fractions in the CIPM, Fennis et al. [27] used Eq. 1, which was, originally proposed by de Larrard [25]. The actual packing density (Φ) is obtaining by solving Eq. 1 for Φ used in Eq. 2.

$$K = \sum_{i=1}^{n} \frac{\varphi_i / \varphi_i^*}{1 - \varphi_i / \varphi_i^*}$$

Eq. 1

Where φ_i/φ_i^* is written as Eq. 2.

$$\frac{\varphi_i}{\varphi_i^*} = \frac{r_i\Phi}{\beta_i\left(1 - \sum_{j=1}^{i-1}[1 - b_{ij}(1 - 1/\beta_j)]r_j\Phi - \sum_{j=i+1}^{n}[a_{ij}\beta_i/\beta_j]r_j\Phi\right)}$$
<div align="right">Eq. 2</div>

Where,

K = Compaction index depending on the compaction energy applied to the mixture

r_i = Volume fraction of size class i

β_i = virtual packing density of size class i (Eq. 3)

$$\beta_i = \alpha_i(1 + \frac{1}{K})$$
<div align="right">Eq. 3</div>

Where,

α_i = Experimentally determined packing density of class i for a prescribed packing process and K value (Table 1)

Table 1_ K values for various packing processes [25]

Packing process		K value
Dry	Pouring	4.1
	Sticking with a rod	4.5
	Vibration	4.75
	Vibration + compression 10 kPa	9
Wet	Smooth thick paste	6.7
	Normal paste - Vicat needle [26,61]	4.8
	Proctor test [62]	12
	Mixing power peak [58]	12.2
Concrete	Concrete mixers – workability EN [58]	9
Virtual	-	∞

The geometrical interaction between size classes is represented by a_{ij} for the loosening effect and b_{ij} for the wall effect as is shown in Eq. 4 and Eq. 5 respectively. In order to consider the interaction of the particles smaller than 125 μm, Fennis et al. [27] modified the de Larrard's [25] interaction functions on the basis of the works of Schwanda [63].

$$a_{ij} = \begin{cases} 1 - \dfrac{\log_{10}(d_i/d_j)}{w_{0,a}} & \log_{10}(d_i/d_j) < w_{0,a}, \\ 0 & \log_{10}(d_i/d_j) \geq w_{0,a} \end{cases} \qquad w_{0,a} = \begin{cases} w_a \times C_a & d_j < d_c \\ w_a & d_j \geq d_c \end{cases}$$ Eq. 4

$$b_{ij} = \begin{cases} 1 - \dfrac{\log_{10}(d_j/d_i)}{w_{0,b}} & \log_{10}(d_j/d_i) < w_{0,b}, \\ 0 & \log_{10}(d_j/d_i) \geq w_{0,b} \end{cases} \qquad w_{0,b} = \begin{cases} w_b \times C_b & d_i < d_c \\ w_b & d_i \geq d_c \end{cases}$$ Eq. 5

In which,

d_i and d_j are the diameter of size class i and class j, respectively.

d_c is the transition diameter in the CIPM below which compaction-interaction is taken into account.

$w_{0,a}$ and $w_{0,b}$ are the functions for maximum range of loosening effect and wall effect respectively.

w_a and w_b are the constants denoting the maximum range of loosening effect and wall effect respectively.

C_a and C_b are the compaction-interaction constant within the loosening effect and wall effect respectively.

However, in reality, the multiple components which are used in UHPFRC are not monosized. In order to consider this, Sedran [26] derived Eq. 6 for CPM considering M different material and n different size classes.

$$K = \sum_{i=1}^{n} \frac{\sum_{k=1}^{M} \dfrac{p_k \cdot r_{k,i}}{\beta_{k,i}}}{1/\Phi - 1/\gamma_{k,i}}$$ Eq. 6

In which,

p_k = Volume fraction of material k

$r_{k,i}$ = Volume fraction of material k in class i

$\beta_{k,i}$ = virtual packing density of material k in class i

$$\gamma_{k,i} = 1/p_k \left[\left[\sum_{j=1}^{i-1} [1 - b_{ij}(1 - 1/\beta_{k,j})] r_{k,j} + \sum_{j=i+1}^{n} a_{ij} r_{k,j}/\beta_{k,j} \right] \right]$$

In order to generalize the CIPM model for M different material and n different size classes, Eq. 1 was generalized as Eq. 7, starting from Eq. 6 [64].

$$K = \sum_{i=1}^{n} \frac{\displaystyle\sum_{k=1}^{M} \frac{\varphi_{k,i}}{\beta_{k,i}}}{\displaystyle\sum_{k=1}^{M} \varphi_{k,i}^{*}/\beta_{k,i} - \sum_{k=1}^{M} \varphi_{k,i}/\beta_{k,i}}$$

Eq. 7

Where,

$$\varphi_{k,i} = p_k \cdot r_{k,i} \cdot \Phi$$

Eq. 8

$$\varphi_{k,i}^{*} = \beta_{k,i}\, p_k \left[1 - \left[\sum_{j=1}^{i-1}[1 - b_{ij}(1 - 1/\beta_{k,j})]r_{k,j}\Phi + \sum_{j=i+1}^{n} a_{ij} r_{k,j}\Phi/\beta_{k,j} \right] \right]$$

Eq. 9

3.3 Materials and mixture design

Combinations of three types of matrixes, two types of HRWRA and three types of fibers were investigated in this study. The matrixes were classified as (I) without sand, *PE07*, (II) with sand, *PE10* and (III) with quartz powder, *PE21*. Six different powders including cement CEM I 52.5 HTS (Lafarge), two types of limestone filler of different gradings: Betoflow D® and Betocarb SL® (OMYA), white silica fume from SEPR (BET = 14 m²/g), quartz powder and quartz sand were used in the mixes. Fig. 2 shows the SEM images of the powder components. Each matrix was optimized by means of the aforementioned generalized CIPM using the measured packing density of the components. After Fennis [27], cementitious material with superplasticizer can be modeled with $w_a = w_b = 1$, $C_a = 1.5$, $C_b = 0.2$ and $d_c = 25$ μm and a value of 9 was considered for the compaction index (K) for the wet mix of all components. Furthermore, the packing density of the fine powders was measured using the water demand method based on mixing energy [65]. The mixture proportions of the three mixes and the corresponding packing density values are given in Table 2. Moreover, Fig. 3 shows the particle size distribution (PSD) of the solid materials used in the formulation of the matrixes.
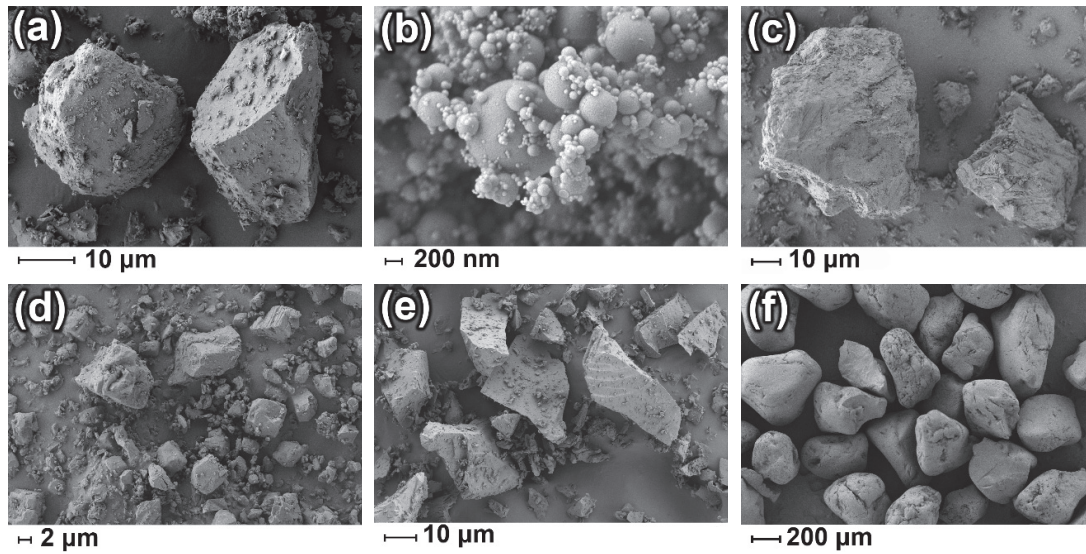
Fig. 2_ SEM images of the powder components: (a) Cement, (b) Silica fume, (c) Betocarb®- HP SL, (d) Betoflow®-D, (e) Quartz powder, and (f) Fine sand

Table 2_ Mix proportions of the UHPFRC with synthetic fibers

Components (kg/m³)	PE07	PE10	PE21
Cement	724	544	508
Silica fume	253	190	178
Betocarb®- HP SL	242	182	170
Betoflow®-D	554	416	389
Quartz Powder	0	0	223
Fine Sand	0	616	525
Water	226	170	165
Water/fines	0.146	0.146	0.124
Water/cement	0.357	0.357	0.357
HRWRA	53	40	27
Ca(NO$_3$)$_2$	18	14	11
Defoaming agent	0.1	0.1	0.1
UHMW PE fiber (Dyneema® SK99)	19.6	19.6	19.6
Packing density (K=9)	0.76	0.82	0.81

Ca(NO$_3$)$_2$ was employed in the form of water-soluble powder in order to optimize the performance of the superplasticizer and reduce the air content [66].

Two types of HRWRA, a modified Polycarboxylates-based, SIKA Viscocrete P5 (SP1) and a Polycarboxylates-based, GLENIUM SKY 561 (SP2) were used to maintain flowability and rheology of the mixture at the very low w/fines ratio.
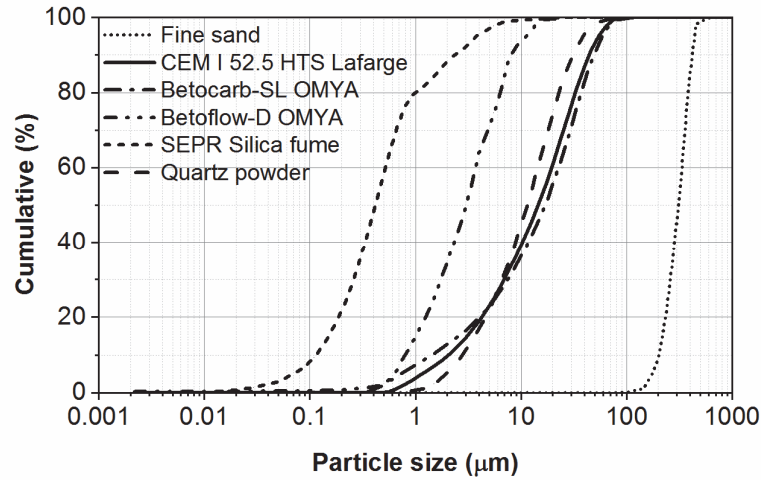
Fig. 3_ PSD of the components

Three types of fiber, including SK62, SK78, and SK99 from DSM Dyneema® were investigated. The mechanical and physical properties of these PE fibers are given in Table 3. The fibrous mix consisted of 2% vol. 6 mm long chopped UHMW-PE fibers with a diameter of 12 μm. Fig. 4 shows the SEM images of SK99 at different scales.

Table 3_ Geometry and mechanical properties of PE Fiber

Fiber properties	*SK62*	*SK78*	*SK99*
Nominal strength (MPa)	2800	3400	4100
Nominal Young's modulus (GPa)	86	113	155
Elongation at break (%)	3.5	3.5	3.5
Specific weight (kg/m^3)	975	975	975
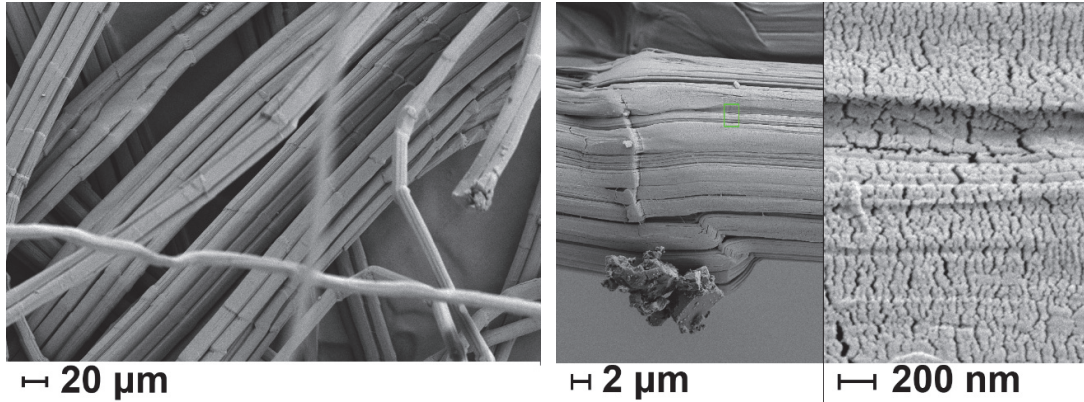
Fig. 4_ SEM images of PE fibers (SK99) at different scales

4. Experimental methods

4.1 Packing density of the components

Although a number of theoretical packing models have been developed, accurate measurement of the packing density of very fine materials, such as the cementitious materials used in concrete, remains a difficult task. In order to measure the packing density of the fine powders more accurately, the water demand method based on mixing energy [65] has been used. A mass of 2000 g of powder was mixed in a mortar mixer, with a constant water (water + superplasticizer) supply during the entire mixing time. During mixing, the voltage, power consumption and the phase shift between the voltage and the power consumption of the mixer were registered to determine the power consumption. The water demand of the mix was determined as the water (water + superplasticizer) addition at which maximum power use was measured. The packing density of the component α can be calculated after [58] by using Eq. 10 according to the water (water + superplasticizer) demand.

$$\alpha = \frac{1000}{1000 + \rho \frac{M_w}{M_p}}$$

Eq. 10

Where,

M_w = mass of the water or water + superplasticizer

M_p = mass of the powder

ρ = density of the powder mix in kg/m^3

The packing densities of the components were measured with and without superplasticizer. The packing density with superplasticizer was measured at the saturation point that is the dosage beyond which the superplasticizer no longer has any effect on the rheological properties of the mix. This point was determined by the lowest flow time in the Marsh cone test. As the presence of cement is necessary for the superplasticizer to play its role, the packing densities of SCM in presence of superplasticizer were determined by a linear extrapolation based on the packing densities of 80%/20% and 90%/10% mixes of SCM/Cement.

4.2 Fresh Properties

ASTM C1437 [67] and mini cone slump test (Fig. 5) were used to investigate the rheological behavior of the mixes. The selected geometry for the mini cone was inspired by the one used by Roussel et al. [68]. The final flow diameter d_{final} that is representative of the flowing ability, and the time to flow at 250 mm diameter t_{250} that is linked to the dynamic viscosity of the mix were measured.
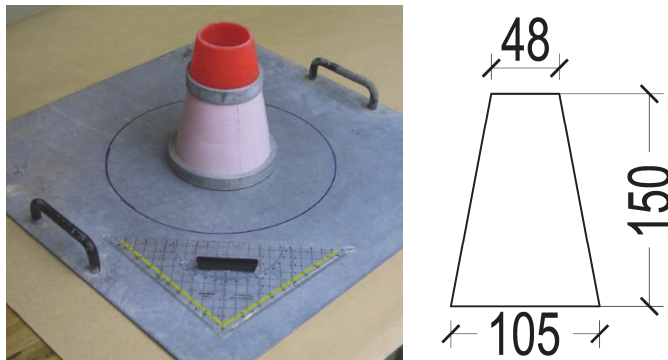
Fig. 5_ Mini cone test set-up and geometry (dimensions in mm)

4.3 Mechanical Properties

4.3.1 Tensile test

The tensile test set-up was designed in a way to avoid eccentricities and bending effects with geometry and size representative of practical applications. Two types of specimen, SType1 and SType2, were used to investigate the tensile behavior of the mixes. The specimens were cast horizontally in the molds from one end to the other, in a systematically repetitive procedure to obtain reproducible fiber orientation and distribution. The top surface of the specimen was covered immediately after pouring with a Controlled Permeability Formliner (CPF) - Zemdrain® sheet attached to a wood panel to guarantee a flat and uniform upper

surface and avoid surfacing after setting. The specimens were kept sealed after casting for 2 days at room temperature of 20 ± 5°C. Thereupon demolding, the specimens were stored at room temperature of 20 ± 5°C under 95 % RH at 28 days.

The geometry of SType1 was based on JSCE recommendations [69], Fig. 6. The specimens were gripped on their end faces in a fixed-fixed type of end constraints using a wedge-clamping system. The tests were performed using a 50 kN W+B universal testing machine under quasi-static uniaxial loading, under displacement control with a stroke rate of 0.003 mm/sec. Two pairs of LVDT, set in two perpendicular planes, were used to determine the elongation of the specimen and check eccentricities under loading. The gauge lengths of the LVDT were 150 mm and 175 mm in XY and YZ planes, respectively. The specimen thickness was 13 mm.
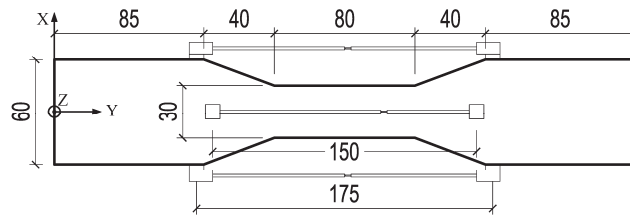
Fig. 6_ Stype1 specimen geometry (dimensions in mm)

SType 2 was an original dumbbell specimen that was designed with a thickness of 30 mm representative of that found in numerous applications of UHPFRC, either cast-on-site for rehabilitation or in structural uses with thin precast ribbed members. As it is shown in Fig. 7, the specimen had a total length of 750 mm from which 290 mm was a constant cross-section with a width of 80 mm. In order to limit as far as possible the stress concentrations in the transition zone, Neuber's model [70] was applied to determine the geometry of the 100 mm long transition zone between the specimen's ends and its central part. Moreover, the lateral internal faces of the molds along the shoulders were covered with 1 mm thick, deformable tape, to prevent eigenstresses and restrained shrinkage cracks at an early age.
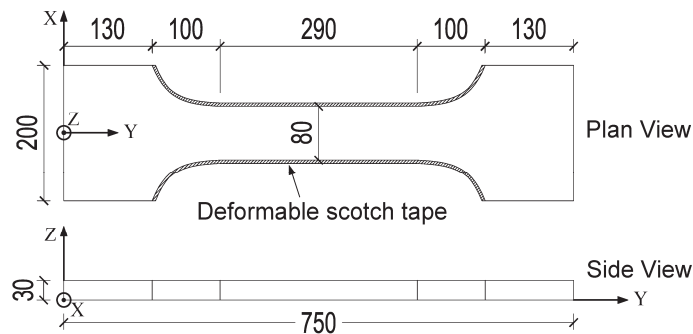
Fig. 7_ SType2 specimen geometry (dimensions in mm)

In order to avoid as far as possible bending effects during the test, an optimized set-up was used with: (1) a stiff (4 columns) testing machine, (2) fixed/fixed support conditions for the specimen, and (3) a highly accurate alignment of the specimen thanks to a special procedure to link it directly to the machine without clamping. The specimens were attached to the testing set-up by means of the "gluing without bonding" approach proposed by [71], and applied to dumbbell specimen by [72], Fig. 8. A steel shoe formed of plates with indented internal faces (c) on Fig. 8, was used as a form to cast resin indentations glued to the specimen, that help transmit loads from the machine to the specimen by interlocking. In order to avoid adherence between the specimen and the indented metallic shoe, a demolding spray was applied on the internal indented faces of the later, before inserting the specimen coated with resin on its ends in the shoe. This system guaranteed a uniform stress transfer without lateral restraint of the specimen. The top and bottom indented steel shoes were tightly bolted to stiff steel plates, (d) on Fig. 8, bolted directly on the machine's heads without any hinge.
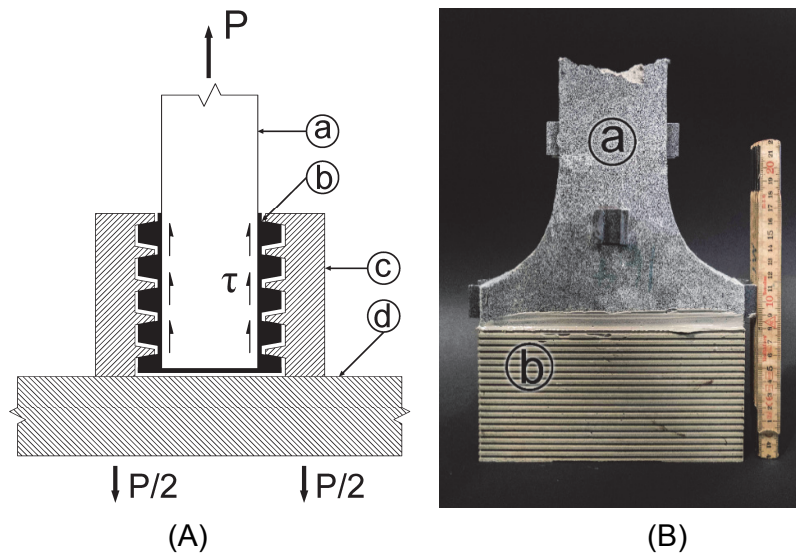
Fig. 8_ (A) Schematic sketch of the fixture set-up of the uniaxial tensile test (adapted after [71]) and (B) Tensile specimen after testing, with (a) specimen, (b) hardened resin indentations glued to the specimen surface, (c) indented steel plate, and (d) base plate

The uniaxial tensile tests were conducted on SType2 specimens with a universal AMSLER testing machine (capacity: 1000 kN). The test was controlled by the mean value of two LVDT fixed on the specimen with a gauge length of 515 mm, as shown in Fig. 9, with a closed-loop deformation rate of 0.003 mm/sec. Two additional pairs of LVDT, set in two perpendicular planes, were used to determine the elongation of the specimen and check eccentricities under loading. The gauge lengths of the LVDT were 400 mm and 275 mm in XY and YZ planes, respectively.
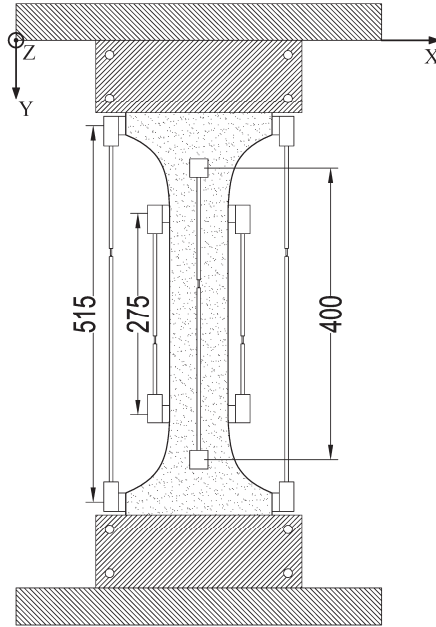
Fig. 9_ Test setup and instrumentation of the SType2 specimen (dimensions in mm)

4.3.2   Three-point bending test

The measurements were performed on $40 \times 40 \times 160$ mm prismatic specimens. The fresh mix was placed into the molds and compacted using a vibrating table for 10 seconds. After demolding at an age of 2 days, the specimens were cured at 20 ± 5 °C under 95 % RH until testing at 28 days.

Compressive and flexural strength tests were carried out according to EN 196-1 standard. The three-point flexural strength was determined using 200 kN W+B servo-hydraulic testing machine. Compressive strength tests were done on the two fragments of each mortar from above flexural tests, using the same machine. The flexural strengths were determined by taking the average of three test results whereas the compressive strengths were determined by taking the average of six test results. The test was displacement controlled at a constant rate of 0.1 mm/s. The span between supports was equal to 100 mm, and the specimens were loaded in the midspan. The supports allowed rotations because of a cylindrical bearing.

4.3.3 Compressive test

The compressive strength of the mixes was also investigated by using 70 x 140 mm cylinders according to SIA 2052:2017 [5].

4.4 Protective Properties

Capillary absorption tests were conducted based on EN13057:2002 standard [73]. Six cylinders with a 100 mm diameter and 30 mm depth were cut from a plate that was cured under standard laboratory conditions at the temperature of 20 ± 5 °C under 95 % RH. Before testing at 28 days, the cylinders were oven dried until constant weight, at 50°C. In order to ensure one-dimensional liquid transport, the side faces of the cylinders were sealed with paraffin and thereafter, the specimens were kept in the laboratory ambient conditions (20 ± 5°C) for at least 12 hours before being placed in the standard capillary absorption setup. Throughout the absorption tests, the immersion depth was kept constant at 2 mm. The standard capillary absorption setup is schematically shown in Fig. 10. The sorption coefficient was obtained from the slope of the cumulative mass of water absorbed per unit of area of inflow surface versus square root of time, calculated for 24 h.
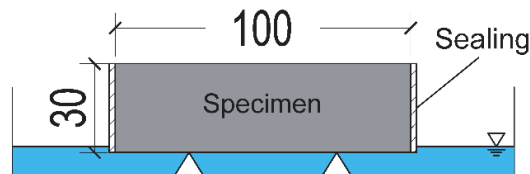
Fig. 10_ Schematic diagram of capillary absorption setup, (dimensions in mm)

4.5 Porosity measurements

An image analysis-based method was used in order to quantify the porosity and size distribution of the voids on cuts, after [74]. Approximately 40 x 40 x 10 mm samples were cut from the three-point bending specimens with a diamond saw. To achieve a flat surface, each sample was carefully polished using DIFLEX diamond grinding discs (220 grit, then 400 grit, 600 grit, 1500 grit, and finally 3000). To reinforce the perimeter of air voids and avoid eroding them while polishing, a 3:1 mixture of acetone and nail polish was applied to the surface of the sample prior to grinding. To improve the contrast between matrix and air voids, which was needed for image processing, the polished surfaces were blackened and then a fine limestone powder was pressed into the air voids, resulting in a black background with white air void profiles. Afterward, the samples were scanned at 3200 dpi resolution

with an Epson Perfection V370 flatbed scanner using 8-bit grayscale digital imaging. The grayscale images were converted to binary format and the porosity properties were investigated using a MATLAB script.

5. Results and Discussion

5.1 Packing density of the components

Fig. 11 shows the steps of measuring the water demand of the cement. The corresponding images of the steps, which are shown in Fig. 11, are presented in Fig. 12. The packing densities of the components are presented in Table 4.
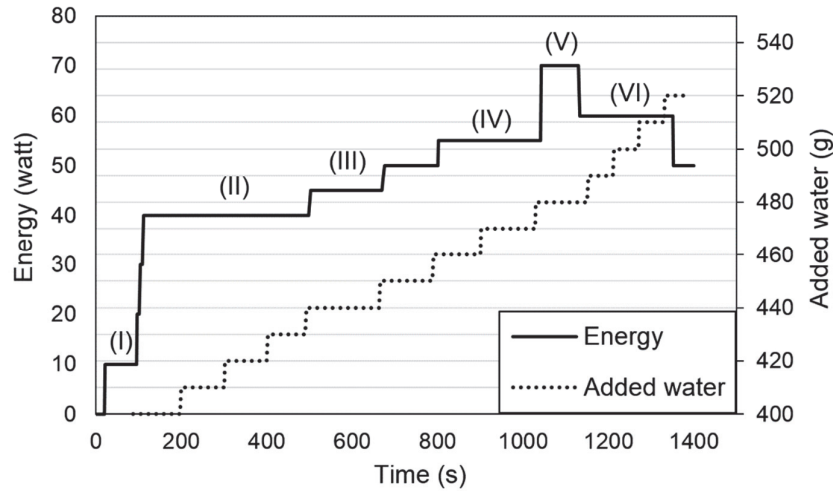
Fig. 11_ Energy of the mixer and added water versus time for 2000 g of cement
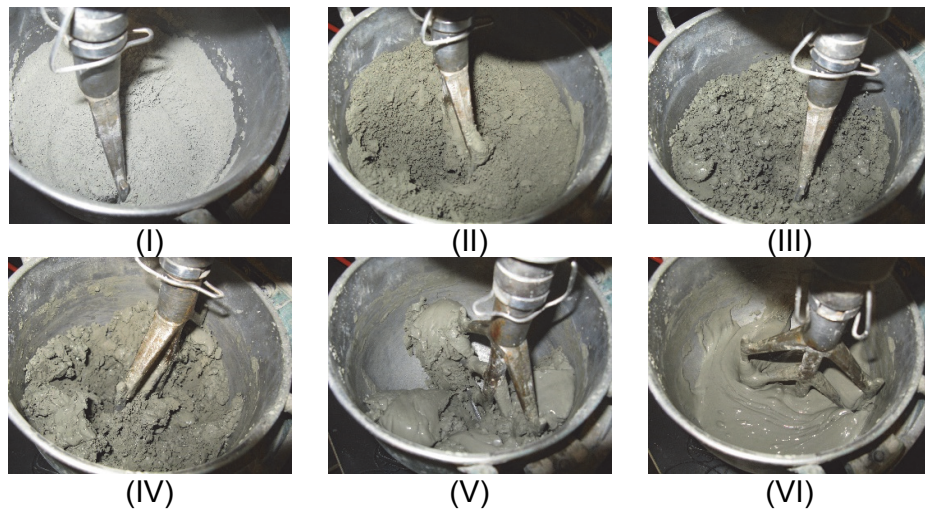
Fig. 12_ Steps of measuring the water demand

Table 4_ Packing density of the components with and without superplasticizer

Component	α	
	Without SP	With SP
Cement	0.56	0.66
Betoflow®-D	0.67	0.67
Betocarb®-HP SL	0.63	0.67
Silica fume	0.62	0.63 [15]
Quartz powder	0.54 [58]	0.56
Sand*	0.56	-

*Dry packing

5.2 Matrix optimization

5.2.1 Powder mix

The effect of different powder mixes on the tensile behavior was investigated by comparing the tensile response of mixes PE07, PE10 and PE21. Six JSCE tensile specimens (SType1) were prepared for each mix, using HRWRA type SP1 and SK99 fibers.
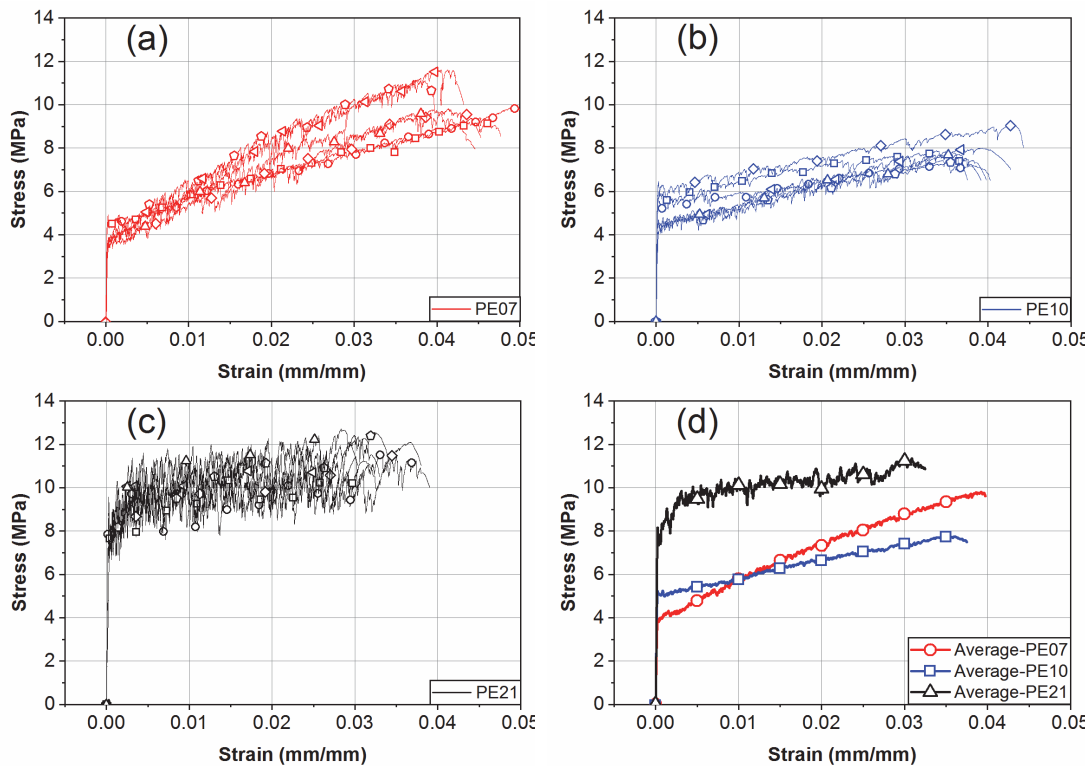
Fig. 13_ Tensile response of mix (a) PE07, (b) PE10 (c) PE21 and (d) Averages

Comparing mix PE07 and PE10, Fig. 13 (a) and (b), both the elastic limit and ultimate strength were affected by the amount of fine sand. The elastic limit increased by more than 1 MPa in the mixes with the higher sand amount. However, the strength showed an opposite trend and it was higher in the case of mixes without sand. Both, the properties of the matrix and the fibrous mix influence the elastic limit of the composite. Considering the same fibrous mix for mixes PE07 and PE10, increasing the sand amount increased the elastic limit of the matrix, which is in accordance with packing density values of the mixes. On the other hand, increasing the sand amount decreased the slope of hardening and accordingly the tensile strength. Table 5 shows a comparison between the sizes of different particles using d_{50} as reference. Considering the fiber diameter of 12 μm, quartz sand has a negligible role in the bond between matrix and fibers. Therefore, reducing the slope of hardening zone in the mixes with sand can be explained considering that adding sand decreased 25% volume of the other powders that can contribute to the bond.

Table 5_ Geometrical parameters of components' particles

Powders	d_{50} (μm)	specific surface[*] (m^2/g)	BET (m^2/g)	Form factor
Silica fume	0.4	14	14	1
Betoflow®-D	3	1.5	2	1.3
Quartz powder	11.4	0.29	1.85	6.4
Cement	14.5	0.37	0.64	1.7
Betocarb®-HP SL	17	0.54	0.65	1.2
Quartz sand	250	0.008	0.011	1.4

[*] Calculated from PSD, based on Fig. 3, with an assumption of spherical particles

The comparison between the tensile behavior of the mixes with quartz powder (PE21) and without quartz powder (PE07 and PE10), Fig. 13 (c) and (a,b), shows that using the quartz powder in the mixture considerably enhanced the mechanical properties and the bond between matrix and fibers. The elastic limit of the mix with quartz powder increased by more than 3 MPa and the tensile strength reached 11.7 MPa. Table 6 presents the average of the tensile elastic limit (6x SType1), tensile strength (6x SType1), compressive strength (3x cylinder) and capillary absorption coefficient of the three mixes (6x specimen).

Table 6_ Mechanical and protective properties of Mixes PE07, PE10 and PE21, average (standard deviation)

Properties		PE07	PE10	PE21
Tensile Elastic limit, f_{Ute}	(MPa)	3.7 (0.5)	4.6 (0.8)	7.7 (0.7)
Tensile strength, f_{Utu}	(MPa)	10 (0.9)	7.9 (0.6)	11.7 (0.6)
Compressive strength, f_{Uc}	(MPa)	81[*] (7)	115.5 (14)	119 (2.6)
Sorptivity	(g/m^2√h)	132 (41)	60 (12)	24 (3)

[*] converted from 40x40x160 specimens using the coefficient of 1.4

The effect of quartz powder on improving the mechanical properties of cementitious materials has been reported by other researchers [75–78] and can be explained by two mechanisms. First, by looking at the roughness of the quartz powder particles. The specific surface calculated from PSD, based on Fig. 3, with an assumption of spherical particles was 0.29 m^2/g for quartz powder while the measured BET was 1.85 m^2/g. This means a form factor (BET over specific surface based on PSD with an assumption of spherical particles) of 6.4 for quartz powder compared to a form factor of 1.7 for cement and 1.2-1.3 for limestone fillers within a similar particle size range. The extra roughness of quartz powder particles improved the interlocking of the grains and enhanced the bond between matrix and fibers. The second mechanism is the pozzolanic effect of quartz powder that can interact with the free lime liberated during the hydration. Although a temperature higher than 80 °C is recommended [77,78] to trigger the pozzolanic effect of quartz powder, Mosaberpanah et al. [75] reported the positive effect of this powder on mechanical properties even for the specimens without thermal curing. Benezet et al. [79,80] found that below a critical diameter of 5 μm associated with a critical surface area of 1 m^2/g, quartz powder particles possess strong pozzolanic reactivity arising from their high surface to volume ratio. Furthermore, the w/f ratio of mix PE21 is significantly lower than that for PE07 or PE10 which can lead to higher elastic limit and better bond.

5.2.2 Admixture effect

Furthermore, in order to investigate the effect of the superplasticizer on the mechanical properties, the pore size distribution of mix PE07 without fibers with HRWRA types SP1 and SP2 was measured based on the aforementioned image analysis method and is shown in Fig. 14 for the range of 10 to 1000 μm. Moreover, the mechanical properties from the 3-point bending test, the fresh density, rheological properties from the mini cone, and total air content of the two mixes are presented in Table 7.
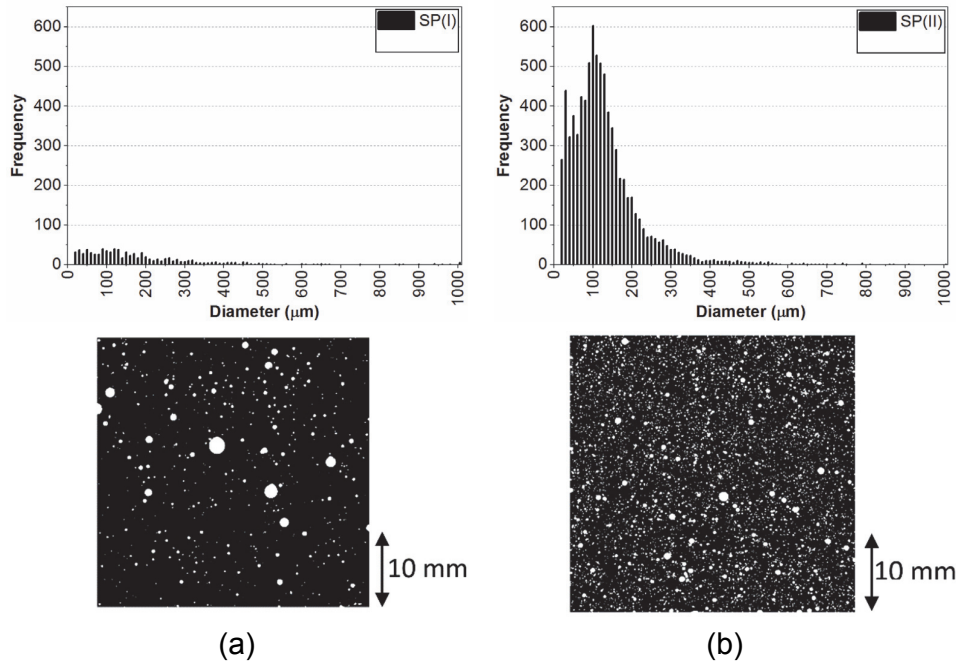
Fig. 14_ Effect of HRWRA on the porosity of mix (a) SP1 and (b) SP2

The properties of the two mixes are presented in table 6. The two mixes had similar workability at the fresh state; however, the chemical compatibility of the admixture and powders played an important role on the air content and accordingly on mechanical properties of the hardened specimens. The modulus of rupture and the compressive strength of the mix with SP1 was respectively 90% and 30% more than that for the mix with SP2.

Table 7_ Hardened and fresh properties of the matrix of mix PE07 with two different types of HRWRA

Properties	SP1	SP2
MOR (MPa)	19	10
Compressive (MPa)	120.5	93
Density (kg/m^3)	2247	2035
d_{final} (mm)	270	270
t_{250} (s)	7	12
Air content (%)	3.4	12.6

5.3 Fibrous mix optimization

Fig. 15 shows the tensile behavior of mixes PE10 and PE21 reinforced with different fibers. In both cases, the elastic modulus of the fibers has an influence on the elastic limit of the

composite. In case of the mixes PE10, increasing the elastic modulus of the fibers from 86 to 155 GPa, increased the elastic limit of the composite by more than 2 MPa. Accordingly, for the PE21 mix (with quartz powder), the average elastic limit of the composite increased from 6 to 8 MPa by 37% increase in the elastic modulus of the fibers.

(a)   (b)
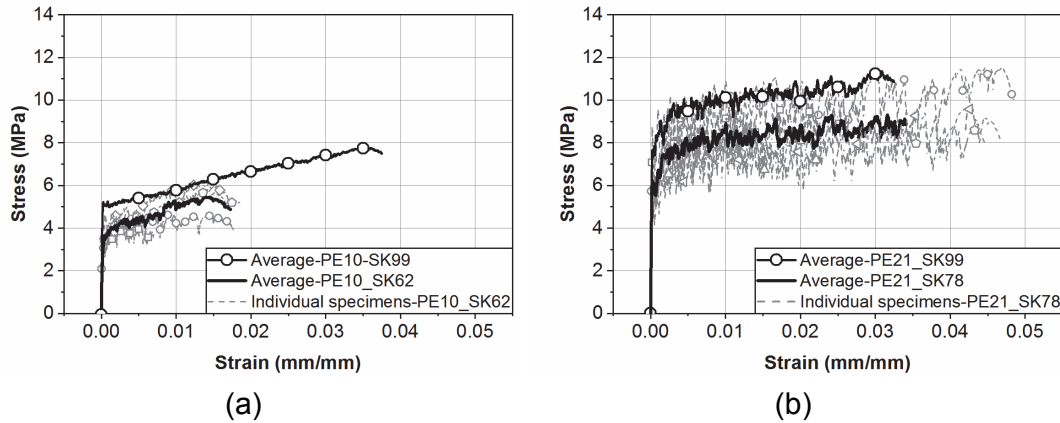
Fig. 15_ Tensile response of (a) mix PE10 with SK99 and SK62 and (b) mix PE21 with SK99 and SK78 fibers

5.4 Inverse analysis of matrix-fiber bond

A meso-mechanical model from Wuest-Oesterlee [56,81] for predicting the UHPFRC tensile hardening response was used to model the tensile behavior of mix PE21 with SK99 and SK78 fibers and perform an inverse analysis of the matrix-fiber bond strength. The properties of the fibers from Table 3, 50 J/m^2 and 39 GPa for the matrix fracture energy and elastic modulus, and 0.5 and 0.75 for the fiber orientation factor and efficiency factor were selected as the inputs of the model. The bond between matrix and fibers (τ) was varied to fit the predictions of the model to the experimental results, Fig. 16. The bond values of 3 MPa and 2.4 MPa for SK99 and SK78 fibers, respectively, gave the closest correlation with the experimental results. These values correspond well with the range that is given in the literature. Curosu et al. [42] reported 2.2 MPa for the bond of 20 µm diameter PE fiber in HS-SHCC matrix with w/b ratio of 0.18. Additionally, Kozawa et al. [82] investigated 12 µm diameter PE fiber in UHP-SHCC mix with 0.18 w/b and found 3.3 MPa for the bond between matrix and fiber.

43
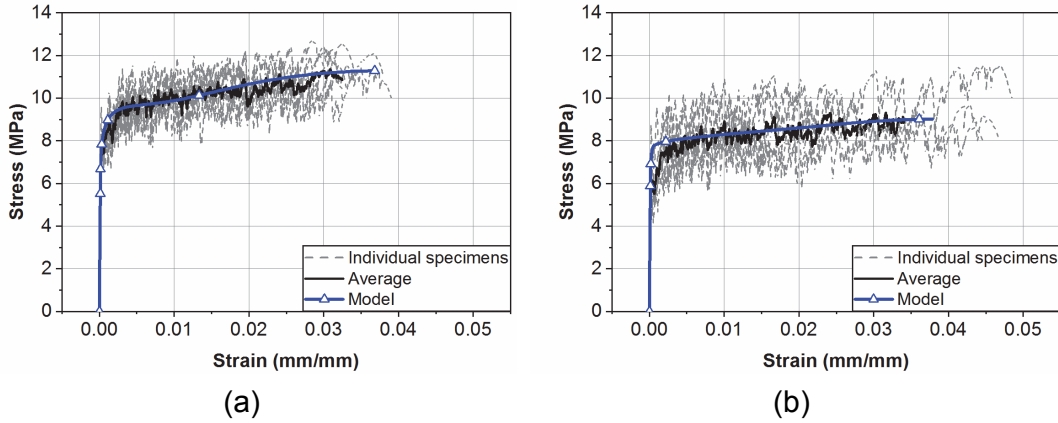
Fig. 16_ Modelling the tensile behavior of mix PE21 with (a) SK99 and (b) SK78 fibers

5.5 Specimen size effect

The average tensile response and its scatter band for mix PE21 + SK99 fibers with two different specimen types is shown in Fig. 17. The results are an average of those obtained with six 10 mm thick SType1 specimens with 300 mm² cross-section, and three 30 mm thick SType2 specimens with 2400 mm² cross section. The average stress-strain curves of both types of samples were almost superimposed, however, SType1 had a larger scatter band compared to SType2. This indicates less sensitivity of these mixes to the fiber orientation that can be explained by looking at the number of fibers per unit area of the samples. Considering the diameter, length and percentage of the PE and steel fibers in a mixture with similar mechanical properties, there are almost 30 times more PE fibers than steel ones in the mix. Thus, the fibers are oriented more uniformly, and the tensile properties are less sensitive to the specimen's thickness and cross section.
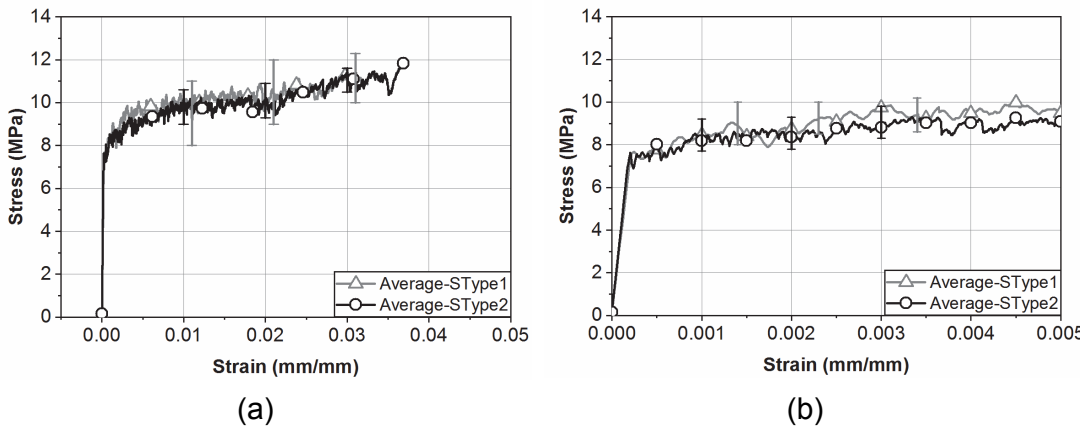
Fig. 17_ Tensile response of mix PE21 with SK99 fibers, average and scatter band (a), and close up until 0.005 mm/mm average responses (b)

Moreover, it should be noted that an extensive effort was made to avoid eccentricity and bending effects while testing in both types of specimens, like preparing specimens with flat surfaces, measuring deformation in all sides of specimens, etc. Neglecting or underestimating these procedures, especially in case of SType1, may result in overestimating the strength and deformability of the material due to the bending effects.

5.6 Environmental impact

Table 8 presents the EE of the mixes with synthetic fibers (SK99) and Ductal® NaG3 TX UHPFRC mix with steel fibers, which was used in rehabilitation of Chillon viaducts [83] and is frequently used on the Swiss market. The total EE of the synthetic fiber mixes is reduced by 60-70% compared to that of a typical UHPFRC mix with steel fibers, from which 80% is the effect of replacing steel fibers with UHMW-PE ones, and 20% is the effect of replacing 50% clinker with limestone filler. The EE data for the individual components was taken from [3,84].

Table 8_ Comparison of EE between the mixes

Mixes	PE07	PE10	PE21	NaG3 TX UHPFRC
Total EE (MJ/m^3)	8,150	7,200	6,790	20,360

5.7 PE-UHPFRC

After optimizing the mix design and investigating the influence factors on the tensile behavior, Mix PE21 with SK99 fibers, henceforth referred to as *PE-UHPFRC,* was the most promising. Fig. 18 shows the tensile behavior of this mix including the softening part.
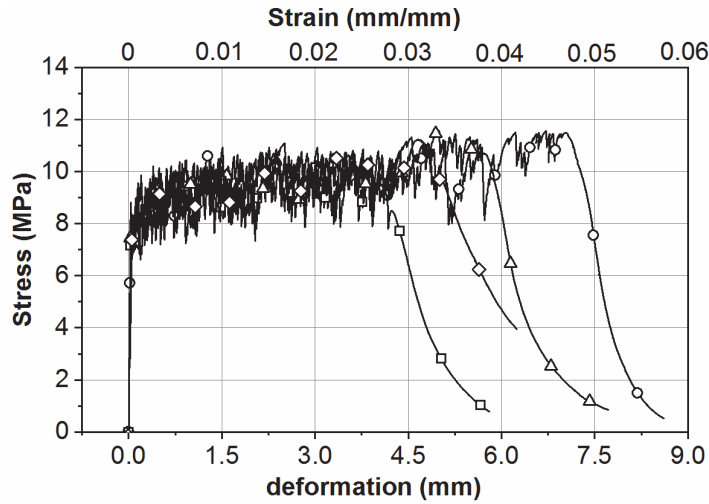
Fig. 18_ Tensile behavior of PE-UHPFRC including the softening (SType1 specimens, YZ plane)

As previously mentioned, the testing methods and boundary conditions are highly important in uniaxial tensile test [6] and the bending effects due to eccentricities can severely bias the results. Fig. 19 and Fig. 20 show the stress versus strain from both LVDT in a plane and the bending effect due to eccentricity for SType1 and SType2 specimens, respectively. The bending effect due to eccentricity was calculated based on the difference between the LVDT measurements in each plane and it was below 0.5 MPa in both tensile test setups. Care was taken to make sure that the measurements from the LVDT were corrected to account for their distances from the surface of the specimen while calculating the bending effect due to eccentricity.

(a)

(b)
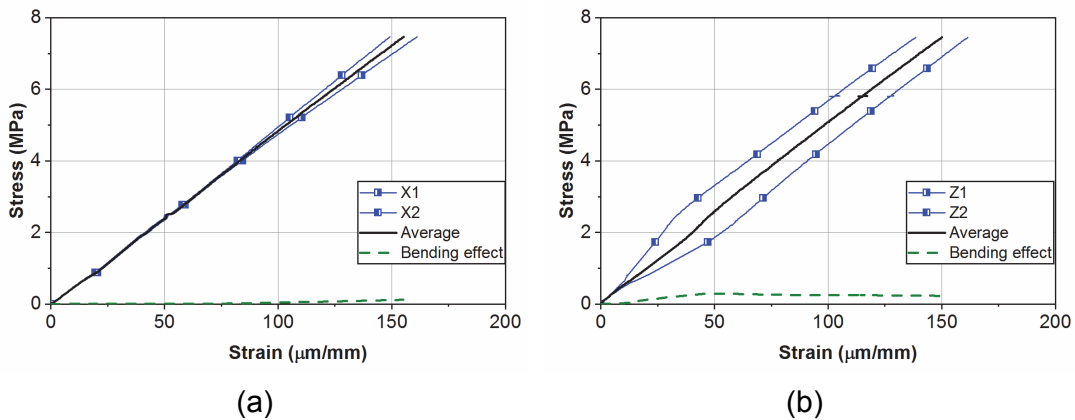
Fig. 19_ Stress versus strain from both LVDT in a plane and the bending effect due to eccentricity in (a) XY plane and (b) ZY plane for SType1

(a)   (b)
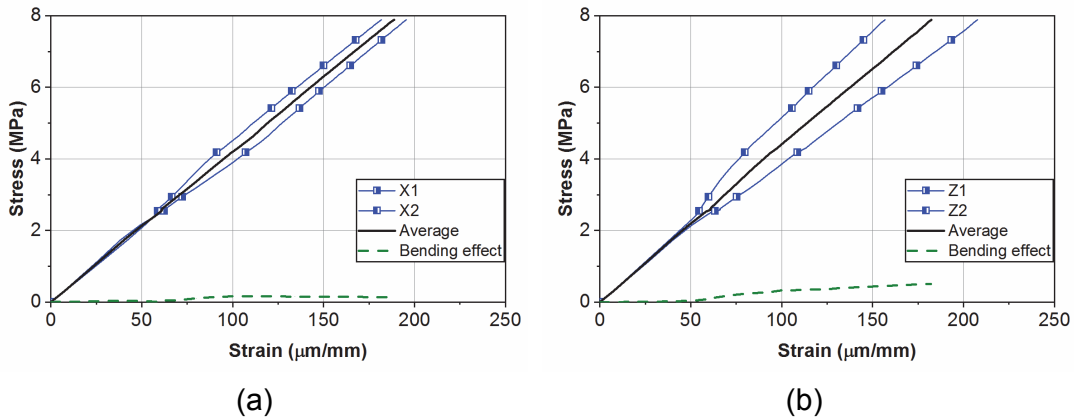
Fig. 20_ Stress versus strain from both LVDT in a plane and the bending effect due to eccentricity in (a) XY plane and (b) ZY plane for SType2

Fig. 21 shows the fracture surface of a PE-UHPFRC tensile specimen. This figure highlights the fundamental difference between the fibrous mix of the PE-UHPFRC and that of conventional UHPFRC.
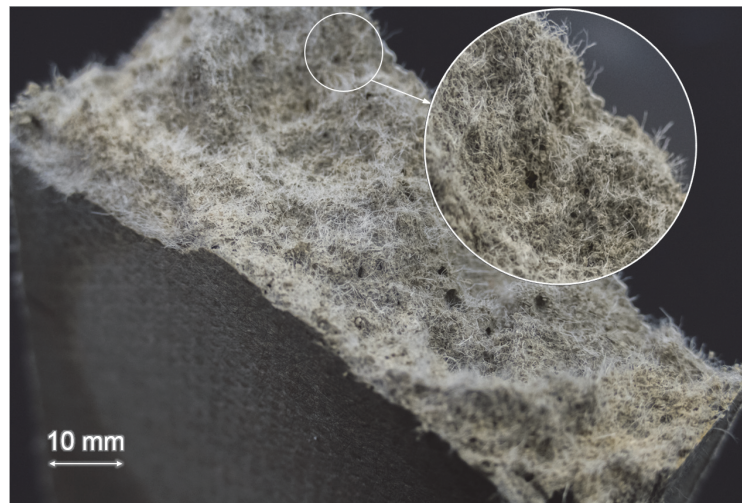
Fig. 21_ Fracture surface of a PE-UHPFRC tensile specimen (total fiber length = 6 mm)

The mechanical properties of PE-UHPFRC and the requirements for UHPFRC based on SIA 2052 [5] are presented in Table 9. The newly developed PE-UHPFRC fulfills the tensile, deformability and capillary absorption requirements for UHPFRC type UA and it is very close to type UB. Fig. 22 compares the tensile elastic limit and compressive strength of PE-UHPFRC with different types of strain hardening synthetic fiber cementitious materials together with the UHPFRC definition limits based on French standard [4] and Swiss recommendations [5] on UHPFRC.

47

Table 9_ Mechanical properties of PE- UHPFRC and SIA 2052 [5] requirements for UHPFRC

Properties	PE-UHPFRC	SIA 2052		
		U0	UA	UB
f_{Utuk} (MPa)	11.7	≥ 4.9	≥ 7.7	≥ 12.0
f_{Utek} (MPa)	7.7	≥ 7.0	≥ 7.0	≥ 10.0
f_{Utuk}/f_{Utek}	1.46	> 0.7	> 1.1	> 1.2
ε_{Utuk} (‰)	35	-	> 1.5	> 2.0
f_{Uck} (MPa)	120	≥ 120	≥ 120	≥ 120
Sorptivity (g/m²√h)	24	≤ 100	≤ 100	≤ 100
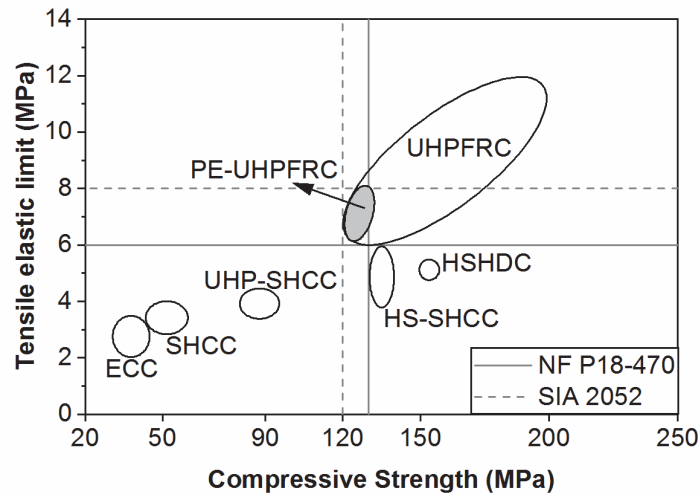
Fig. 22_ Tensile elastic limit and compressive strength of different classes of synthetic fiber cementitious materials. NB: elastic limit after SIA 2052 based on average values, and after NF P18-470 on fractile 5%

At the fresh state, the flow of the PE-UHPFRC after ASTM C1437 [59], was 48% with a final diameter after 25 blows of 150 mm. Moreover, the density and the air content at the fresh state were 2222 kg/m³ and 4.3%, respectively. The capillary absorption coefficient of the PE-UHPFRC was 24 g/m²√h, which is in the expected range for UHPFRC materials. For comparison, a concrete often used to build bridge curbs (exposure classes XD3, XF4 after EN 206-1 [85]) has a sorptivity around 300 g/m²√h when it is properly placed and cured [86].

5.8 Potential synergies with rebar

Adding a thin overlay of UHPFRC on reinforced concrete (RC) slabs and bridge decks is a common technique for design or strengthening of concrete structures [72,86,87]. Fig. 23 shows a typical cross-section of an RC slab strengthened with UHPFRC. Considering the extremely high deformation capacity of PE-UHPFRC, this material is optimal from a structural level viewpoint for use with rebar.
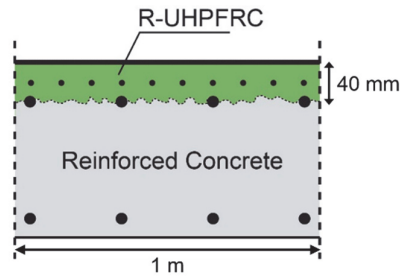
Fig. 23_ A typical cross-section of an RC slab strengthened with UHPFRC

Fig. 24 depicts the force-strain curve of an R-UHPFRC section with depth of 40 mm reinforced with Ø12@125 mm B500B steel rebars, under tension, using two types of UHPFRC material, PE-UHPFRC (Fig. 24 a) and steel fiber UHPFRC (Fig. 24 b), assuming that the tensile responses of the two materials can be added for similar deformations. The tensile elastic limit and ultimate tensile strength were assumed 8 MPa and 12 MPa, respectively for both UHPFRC materials. Moreover, the ultimate tensile strain was considered to be 30‰ and 4‰ for PE-UHPFRC and S-UHPFRC, respectively and the softening response was neglected in both cases. As it is shown in Fig. 24, using PE-UHPFRC opens up an extremely high deformation capacity and therefore structures with PE-UHPFRC could be designed with full structural ductility, however, structures with steel fibers UHPFRC should be designed considering limited structural ductility.

(a)   (b)
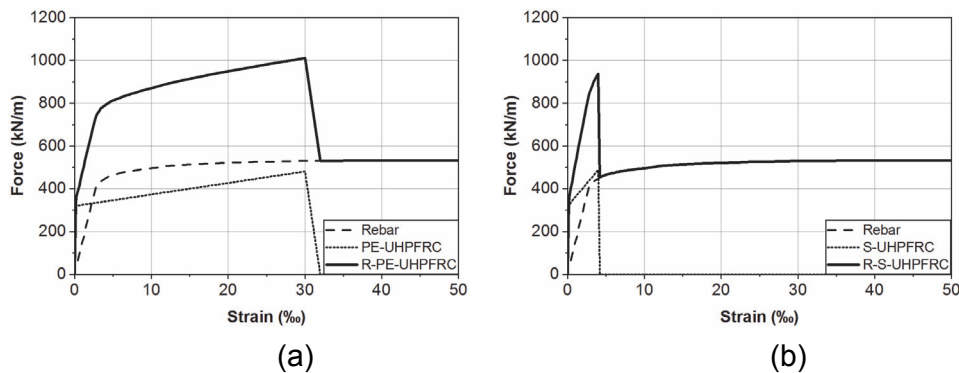
Fig. 24_ Force-strain curve of the R-UHPFRC section under tension using (a) PE-UHPFRC and (b) steel fiber UHPFRC

6. Conclusions

- A structural UHPFRC with synthetic fibers was developed with 120 MPa compressive strength, 43 GPa elastic modulus, 7.7 MPa tensile elastic limit, 11.7 MPa tensile strength, and more than 3% tensile deformation capacity. The mix showed a robust strain hardening and the amplitude of the stress fluctuations in the hardening zone were much lower compared with that in other results from the literature [45].

- The environmental impact in terms of embodied energy of the new PE-UHPFRC mix is reduced by 70% compared to that of a typical UHPFRC mix with steel fibers with similar properties, by replacing steel fibers with UHMW-PE fibers and replacing 50% vol. of clinker with limestone fillers.

- The capillary absorption coefficient of the PE-UHPFRC was 24 $g/m^2\sqrt{h}$ which is in the range of very low and it is comparable with that of classical UHPFRC mixes with steel fibers.

- The newly developed mix is optimal from a structural level viewpoint for use with rebar considering its extremely high deformation capacity. Reinforced PE-UHPFRC structures can be designed with full structural ductility.

- The generalized Compaction-Interaction Packing Model (CIPM), which considers multiple grain classes with arbitrary PSD as well as interaction functions for the particles smaller than 125 μm, was developed as a tool to optimize the matrix.

- Use of quartz sand in the mixture improved the tensile elastic limit of the mix. However, the tensile strength of the mix with sand was lower than that of the mix without sand.

- Using quartz powder in the mix design considerably improved both the tensile elastic limit and tensile strength of the mixes.

- The elastic modulus of the fibers affected both the tensile elastic limit and tensile strength of the mixes. The average elastic limit of the composite increased from 6 to 7.5 MPa by a 37% increase in the elastic modulus of the fibers from SK78 to SK99.

Acknowledgments

References

1. Habert, G., Denarié, E., Šajna, A. & Rossi, P. *Lowering the global warming impact of bridge rehabilitations by using Ultra High Performance Fibre Reinforced Concretes*. Cement and Concrete Composites 38, 1–11 (2013).

2. Stengel, T. & Schießl, P. *Life cycle assessment (LCA) of ultra high performance concrete (UHPC) structures*. in *Eco-efficient construction and building materials* (eds. Pacheco-Torgal, F., Cabeza, L. F., Labrincha, J. & de Magalhães, A. B. T.-E. C. and B. M.) 528–564 (Woodhead Publishing, 2014). doi:https://doi.org/10.1533/9780857097729.3.528

3. Stengel, T. & Schießl, P. *Sustainable construction with UHPC–from life cycle inventory data collection to environmental impact assessment*. in *Proceedings of the 2nd international symposium on ultra high performance concrete. Kassel University Press, Kassel* 461–468 (2008).

4. *NF P18-470: Bétons fibrés à ultra-hautes performances – Spécification, performance, production et conformité*. AFNOR (2016).

5. *SIA 2052, "Béton fibré ultra-performant (BFUP): Matériaux, dimensionnement et exécution"*. (Cahier Technique, 2017).

6. Kanakubo, T. *Tensile Characteristics Evaluation Method for Ductile Fiber-Reinforced Cementitious Composites*. Journal of Advanced Concrete Technology 4, 3–17 (2006).

7. Abrams, D. A. *Design of concrete mixtures*. bulletin 1, Structural materials research laboratory. Chicago: Lewis Institute (1919).

8. Powers, T. C. *Physical Properties of Cement Paste*. in *Proceeding of 4th International Symposium chemistry of cement* 2, 577–613 (1960).

9. Gitzen, W. H. *Alumina as a ceramic material*. (American Ceramic Society, 1970).

10. Bentz, D. P. & Aitcin, P.-C. *The hidden meaning of water-cement ratio*. Concrete international 30, 51–54 (2008).

11. Aïtcin, P.-C. *The importance of the water–cement and water–binder ratios*. in *Science and Technology of Concrete Admixtures* 3–13 (Elsevier, 2016).

12.   Bache, H. H. *Densified cement/ultra-fine particle-based materials*. in *CBL Report No 40* (Aalborg Portland, 1981).

13.   Bache, H. H. *Compact Reinforced Composite Basic Principles*. in *CBL Report No 41* (Aalborg Portland, 1987).

14.   Richard, P. & Cheyrezy, M. *Composition of reactive powder concretes*. Cement and Concrete Research 25, 1501–1511 (1995).

15.   de Larrard, F. & Sedran, T. *Optimization of ultra-high-performance concrete by the use of a packing model*. Cement and Concrete Research 24, 997–1009 (1994).

16.   Powers, T. C. *The properties of fresh concrete*. (Wiley, 1968).

17.   Vogt, C. *Ultrafine particles in concrete: Influence of ultrafine particles on concrete properties and application to concrete mix design*. in *Doctoral dissertation* (KTH, 2010).

18.   Fuller, W. B. & Thompson, S. E. *The laws of proportioning concrete*. ASCE J. Transport 59, 67–143 (1907).

19.   Andreasen, A. H. M. & Andersen, J. *Über die Beziehung zwischen Kornabstufung und Zwischenraum in Produkten aus losen Körnern (mit einigen Experimenten)*. Colloid & Polymer Science 50, 217–228 (1930).

20.   Funk, J. E., Dinger, D. R. & Funk Jr, J. E. *Coal Grinding and Particle Size Distribution Studies for Coal Water Slurries at High Solids Loading*. Alfred University Research Foundation, Alfred, New York (1980).

21.   Yang, R. *et al. The physical and chemical impact of manufactured sand as a partial replacement material in Ultra-High Performance Concrete (UHPC)*. Cement and Concrete Composites 99, 203–213 (2019).

22.   Yu, R., Spiesz, P. & Brouwers, H. J. H. *Development of an eco-friendly Ultra-High Performance Concrete (UHPC) with efficient cement and mineral admixtures uses*. Cement and Concrete Composites 55, 383–394 (2015).

23.   Alkaysi, M., El-Tawil, S., Liu, Z. & Hansen, W. *Effects of silica powder and cement type on durability of ultra high performance concrete (UHPC)*. Cement and Concrete Composites 66, 47–56 (2016).

24.   Mooney, M. *The viscosity of a concentrated suspension of spherical particles*. Journal of colloid science 6, 162–170 (1951).

25.   De Larrard, F. *Concrete mixture proportioning: a scientific approach*. (CRC Press, 1999).

26.   Sedran, T. *Rhéologie et rhéométrie des bétons. Application aux bétons autonivelants*. Doctoral thesis (1999).

27. Fennis, S., Walraven, J. C. & Den Uijl, J. A. *Compaction-interaction packing model: regarding the effect of fillers in concrete mixture design*. Materials and structures 46, 463–478 (2013).

28. Haist, M., Moffatt, J. S., Breiner, R. & Müller, H. S. *Entwicklungsprinzipien und technische Grenzen der Herstellung zementarmer Betone*. Beton□und Stahlbetonbau 109, 202–215 (2014).

29. Zhang, Y. & Kong, X. *Correlations of the dispersing capability of NSF and PCE types of superplasticizer and their impacts on cement hydration with the adsorption in fresh cement pastes*. Cement and Concrete Research 69, 1–9 (2015).

30. Schröfl, C., Gruber, M. & Plank, J. *Preferential adsorption of polycarboxylate superplasticizers on cement and silica fume in ultra-high performance concrete (UHPC)*. Cement and Concrete Research 42, 1401–1408 (2012).

31. Yamada, K., Takahashi, T., Hanehara, S. & Matsuhisa, M. *Effects of the chemical structure on the properties of polycarboxylate-type superplasticizer*. Cement and concrete research 30, 197–207 (2000).

32. Winnefeld, F., Becker, S., Pakusch, J. & Götz, T. *Effects of the molecular architecture of comb-shaped superplasticizers on their performance in cementitious systems*. Cement and Concrete Composites 29, 251–262 (2007).

33. Flatt, R. & Schober, I. *Superplasticizers and the rheology of concrete*. in *Understanding the rheology of concrete* 144–208 (Elsevier, 2012).

34. Schmidt, W., Brouwers, H. J. H., Kuehne, H.-C. & Meng, B. *Effects of the characteristics of high range water reducing agents and the water to powder ratio on rheological and setting behavior of self-consolidating concrete*. Advances in Civil Engineering Materials 3, 127–141 (2014).

35. Hirschi, T. & Wombacher, F. *Influence of different superplasticizers on UHPC*. in *Proceedings of the Second International Symposium on Ultra High Performance Concrete, Kassel University Press, Kassel* 77–84 (2008).

36. Li, V. C. & Wu, H.-C. *Conditions for pseudo strain-hardening in fiber reinforced brittle matrix composites*. Applied Mechanics Reviews 45, 390–398 (1992).

37. Maalej, M. & Li, V. C. *Introduction of strain-hardening engineered cementitious composites in design of reinforced concrete flexural members for improved durability*. Structural Journal 92, 167–176 (1995).

38. Li, V. C. *From micromechanics to structural engineering-the design of cementitous composites for civil engineering applications*. Structural Eng./Earthquake Eng. 10, 37–48 (1993).

39. Li, V. C., Wang, S. & Wu, C. *Tensile strain-hardening behavior of polyvinyl alcohol engineered cementitious composite (PVA-ECC)*. ACI Materials Journal-American Concrete Institute 98, 483–492 (2001).

40. Kunieda, M., Denarié, E., Brühwiler, E. & Nakamura, H. *Challenges for strain hardening cementitious composites–deformability versus matrix density*. in *HPFRCC5* (2007).

41. Kamal, A. *Material development of UHP-SHCC for repair applications and its evaluation*. Doctoral thesis (2008).

42. Curosu, I., Liebscher, M., Mechtcherine, V., Bellmann, C. & Michel, S. *Tensile behavior of high-strength strain-hardening cement-based composites (HS-SHCC) made with high-performance polyethylene, aramid and PBO fibers*. Cement and Concrete Research 98, 71–81 (2017).

43. Rigaud, S., Chanvillard, G. & Chen, J. *Characterization of bending and tensile behavior of Ultra-High Performance Concrete containing glass fibers*. in *High Performance Fiber Reinforced Cement Composites 6* 373–380 (Springer, 2012).

44. Chen, J. & Chanvillard, G. *UHPC composites based on glass fibers with high fluidity, ductility, and durability*. Ultra-High Performance Concrete and Nanotechnology in Construction. Proceedings of Hipermat, Kassel 265–272 (2012).

45. Ranade, R., Li, V. C., Stults, M. D., Heard, W. F. & Rushing, T. S. *Composite Properties of High-Strength, High-Ductility Concrete*. ACI Materials Journal 110, (2013).

46. Nehdi, M., Mindess, S. & Aïtcin, P.-C. *Optimization of high strength limestone filler cement mortars*. Cement and Concrete Research 26, 883–893 (1996).

47. Bonavetti, V., Donza, H., Menendez, G., Cabrera, O. & Irassar, E. F. *Limestone filler cement in low w/c concrete: A rational use of energy*. Cement and Concrete Research 33, 865–871 (2003).

48. Denarié, E. & Houst, Y. *Cement matrices for high performance fibre reinforced cementitious composites (HPFRCCs), in particular ultra high performance fibre reinforced concretes (UHPFRCs)*. *European patent* (2009).

49. Denarié, E., Kazemi Kamyab, M., Brühwiler, E., Haddad, B. G. & Nendaz, S. *Béton fibré ultra performant pour la maintenance, un nouvel élan. tracés n°12* 20–23 (2011).

50. Huang, W., Kazemi-Kamyab, H., Sun, W. & Scrivener, K. *Effect of cement substitution by limestone on the hydration and microstructural development of ultra-high performance concrete (UHPC)*. Cement and Concrete Composites 77, 86–101 (2017).

51. Bornemann, R. & Schmidt, M. *The Role of Powders in Concrete*. in *6th International Symposium on High Strength / High Perfomrance Concrete* 863–872 (2002).

52. Du, H. & Tan, K. H. *Waste glass powder as cement replacement in concrete*. Journal of Advanced Concrete Technology 12, 468–477 (2014).

53. Soutsos, M. N., Le, T. T. & Millard, S. G. *Reactive glass powder concrete (RGPC)-" green" flags for" green" pavements*. in *2nd RILEM International Workshop on Concrete Durability and Service Life Planning - ConcreteLife'09* (ed. Kovler, K.) 327–335 (2009).

54. Sharifi, Y., Afshoon, I. & Firoozjaie, Z. *Fresh properties of self-compacting concrete containing ground waste glass microparticles as cementing material*. Journal of Advanced Concrete Technology 13, 50–66 (2015).

55. Soliman, N. A., Omran, A. F. & Tagnit-Hamou, A. *Laboratory Characterization and Field Application of Novel Ultra-High-Performance Glass Concrete*. ACI Materials Journal 113, (2016).

56. Oesterlee, C. *Structural Response of Reinforced UHPFRC and RC Composite Members*. Doctoral thesis (2010).

57. Denarié, E. *ARCHES D06: Recommendations for the tailoring of UHPFRC recipes for rehabilitation*. in *European project 6th FWP / ARCHES Assessment and Rehabilitation of Central European Highway Structures, WP 5 – 'Harden Structures to last with UHPFRC'* (2009).

58. Fennis, S. *Design of ecological concrete by particle packing optimization*. Doctoral thesis (2011).

59. S. P. Shah J. I. Daniel, and B. Mobasher, D. L. *Toughness-Durability of Glass Fiber Reinforced Concrete Systems*. Materials Journal 85, (1988).

60. Said, M. A. *et al. Investigation of ultra violet (UV) resistance for high strength fibers*. Advances in Space Research 37, 2052–2058 (2006).

61. Lecomte, A., Mechling, J. M. & DILIBERTO-JEANNOT, C. *Indice de serrage des pâtes cimentaires de consistance normale*. des journées scientifiques du RF2B (2006).

62. Pouliot, N., Sedran, T., de LARRARD, F. & Marchand, J. *Prediction of the compactness of roller-compacted concrete using a granular stacking model*. Bulletin des Laboratoires des Ponts et Chaussées (2001).

63. Schwanda, F. *Das rechnerische Verfahren zur Bestimmung des Hohlraumes und Zementleimanspruches von Zuschlägen und seine Bedeutung für Spannbetonbau*. Zement und Beton 37, 13 (1966).

64. Denarié, E. *The generalized CIPM derivation*. (Internal communication: MCS-EPFL, 2016).

65. Marquardt, I. *Ein Mischungskonzept für selbstverdichtenden Beton auf der Basis der Volumenkenngrößen und Wasseransprüche der Ausgangsstoffe*. Doctoral thesis (2001).

66.   Flatt, R. J. & Palacios, M. *Using calcium nitrate in order to reduce alkali sulfate concentration and improve the performance of superplasticizer*. in (Internal communication: MCS-IfB, 2015).

67.   *ASTM C1437-15, Standard Test Method for Flow of Hydraulic Cement Mortar*. (ASTM International, 2015).

68.   Roussel, N., Stéfani, C. & Leroy, R. *From mini-cone test to Abrams cone test: measurement of cement-based materials yield stress using slump tests*. Cement and Concrete Research 35, 817–822 (2005).

69.   *Recommendations for Design and Construction of High Performance Fiber Reinforced Cement Composites with Multiple Fine Cracks (HPFRCC)*. (Japan Society of Civil Engineers, 2008).

70.   Neuber, H. *Der zugbeanspruchte Flachstab mit optimalem Querschnittsübergang*. Forschung im Ingenieurwesen A 35, 29–30 (1969).

71.   Helbling, A. & Brühwiler, E. *Eine neue Halterung für Zugversuche mit Beton-Probekörper*. Material und Technik 15, 103–107 (1987).

72.   Denarie, E. & Brühwiler, E. *Structural Rehabilitations with Ultra-High Performance Fibre Reinforced Concretes (UHPFRC)/Strukturelle Instandsetzung von Betonbrücken mit Ultra-hochleistungsfähigem Faserfeinkornbeton (UHFB)*. Restoration of Buildings and Monuments 12, 93–108 (2006).

73.   *BS EN 13057:2002, Determination of resistance of capillary absorption*. (British Standards Institution, 2002).

74.   Fonseca, P. C. & Scherer, G. W. *An image analysis procedure to quantify the air void system of mortar and concrete*. Materials and Structures 48, 3087–3098 (2015).

75.   Mosaberpanah, M. A. & Eren, O. *Effect of quartz powder, quartz sand and water curing regimes on mechanical properties of UHPC using response surface modelling*. ADVANCES IN CONCRETE CONSTRUCTION 5, 481–492 (2017).

76.   Nikdel, A. *Mechanical Properties of Concrete Containing Quartz Powder as a Filler Instead of Using Silica Fume*. (2014).

77.   Yang, Q., Zhang, S., Huang, S. & He, Y. *Effect of ground quartz sand on properties of high-strength concrete in the steam-autoclaved curing*. Cement and Concrete Research 30, 1993–1998 (2000).

78.   Rashad, A. M. & Zeedan, S. R. *A preliminary study of blended pastes of cement and quartz powder under the effect of elevated temperature*. Construction and Building Materials 29, 672–681 (2012).

79.   Benezet, J. C. & Benhassaine, A. *Grinding and pozzolanic reactivity of quartz powders*. Powder technology 105, 167–171 (1999).

80. Benezet, J. C. & Benhassaine, A. *The influence of particle size on the pozzolanic reactivity of quartz powder*. Powder Technology 103, 26–29 (1999).

81. Wuest, J., Denarié, E. & Brühwiler, E. *Model for predicting the UHPFRC tensile hardening*. in *Ultra High Performance Concrete (UHPC): Proceedings of the Second International Symposium on Ultra High Performance Concrete, Kassel, Germany* 153 (2008).

82. Kozawa, K., Kunieda, M. & T Kanda. *Bond properties of synthetic fiber embedded in ultra high strength matrix [in Japanese]*. Japan Concrete Institute 30, 231–236 (2008).

83. Denarié, E., Sofia, L. & Brühwiler, E. *Characterization of the tensile response of strain hardening UHPFRC-Chillon viaducts*. in *AFGC-ACI-fib-RILEM Int. Symposium on Ultra-High Performance Fibre-Reinforced Concrete, UHPFRC 2017* 242–250 (2017).

84. Hammond, G., Jones, C., Lowrie, F. & Tse, P. *Inventory of carbon & energy: ICE*. 5, (Sustainable Energy Research Team, Department of Mechanical Engineering …, 2008).

85. *EN206-1. Concrete-Part 1: Specification, performance, production and conformity*. CEN 69, 23 (2000).

86. Denarié, E. & Brühwiler, E. *Cast-on site UHPFRC for improvement of existing structures–achievements over the last 10 years in practice and research*. 7th workshop on High Performance Fiber Reinforced Cement Composites, 1-3, June 2015, Stuttgart, Germany (2015).

87. Brühwiler, E. & Denarié, E. *Rehabilitation and strengthening of concrete structures using ultra-high performance fibre reinforced concrete*. Structural Engineering International: Journal of the International Association for Bridge and Structural Engineering (IABSE) 23, 450–457 (2013).

Appendix A

Evolution of damage in PE-UHPFRC under tension

The evolution of damage in PE-UHPFRC under tension is an important property, which can be characterized by determining the apparent E modulus at different tensile strains by performing unloading-loading cycles. Fig. 1 shows the tensile response of a SType2 PE-UHPFRC specimen and unloading-loading cycles at strain levels of 0.15, 0.4, 1, 2 and 3 %.
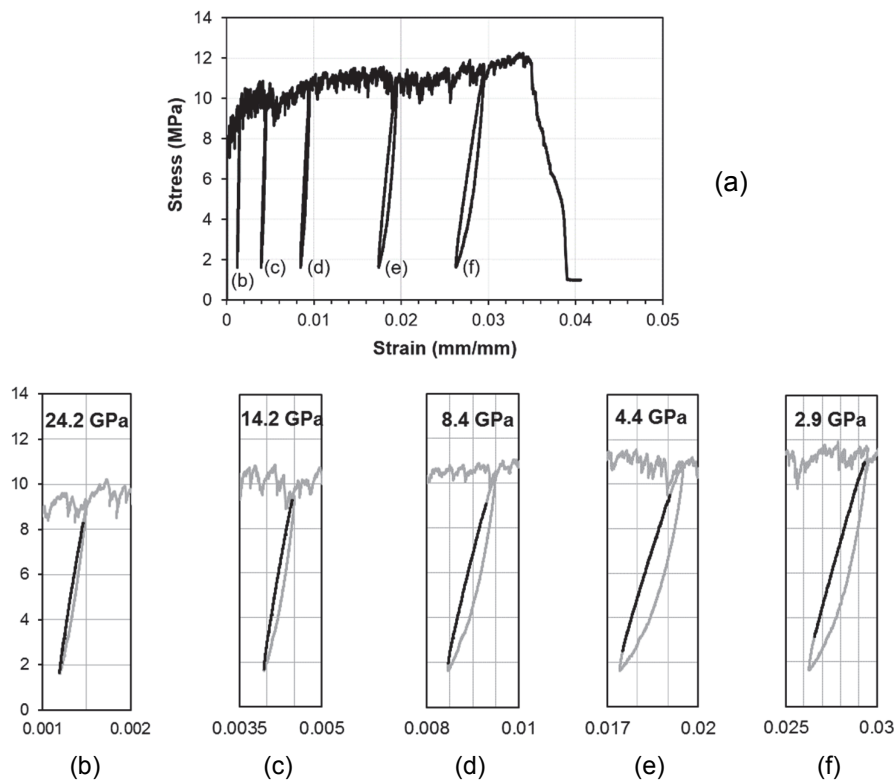
Fig. 1_ Tensile response of PE-UHPFRC and unloading-loading cycles at different strain levels

Fig. 2 shows the apparent E modulus of PE-UHPFRC compared with that of conventional UHPFRC with steel fibers from [1] as a function of tensile strain before unloading. The evolution of damage was considerably slower in PE-UHPFRC compared with that in conventional UHPFRC with steel fibers.
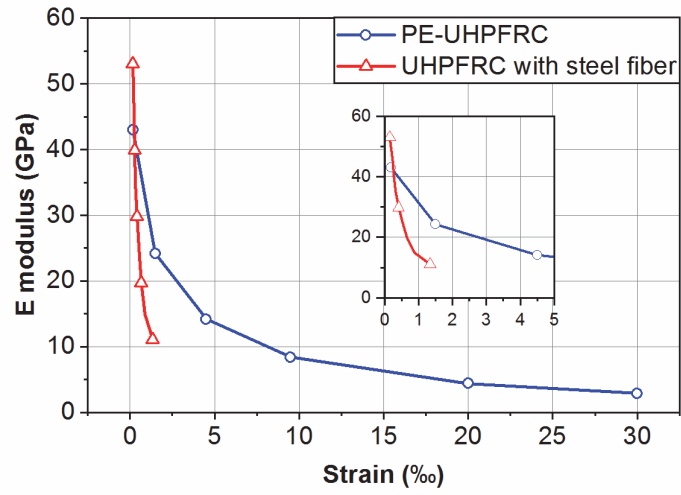
Fig. 2_ Apparent E modulus of PE-UHPFRC at various tensile strains compared with that of a conventional UHPFRC with steel fiber from [1]

References

1.   T. Makita, *Fatigue behaviour of UHPFRC and R-UHPFRC - RC composite members*, Dr. Thesis. (2014).

Appendix B

Validation of tensile setup on SType1 with aluminum specimen

In order to validate the tensile tests on SType1 specimens, an aluminum specimen with the same dimensions and thickness of 10 mm was tested. Four LVDTs was used in order to measure the strain and eccentricity in two perpendicular directions X and Z shown in Fig. 1.
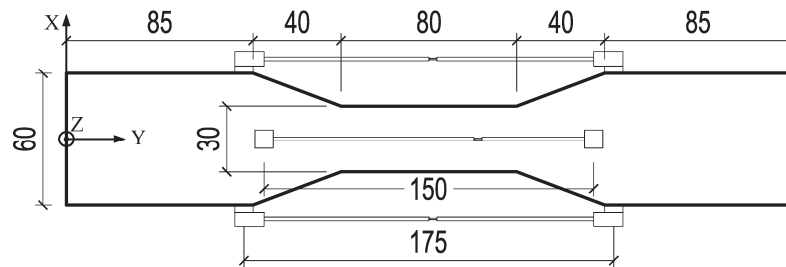
Fig. 1_ Position of LVDTs in SType1 aluminum specimen (dimensions in mm)

- Validation of Elastic modulus

Elastic modulus of the aluminum specimen was calculated in order to validate the testing setup. As the LVDT were not positioned only within the constant cross-section of the specimen, a correction factor was needed to consider the effect of a variable cross-section. The correction factor for the LVDT in XY plane was calculated by transforming the variable width of the specimen within the LVDT's length into three parts with constant width as it is shown in Fig. 2 and rewriting Hooke's Law.
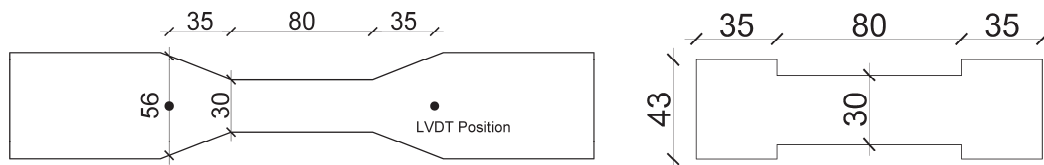
Fig. 2_ Transformation the variable width for calculating the correction factor in XY plane

$$L_1 = 35 + 35 = 70, L_2 = 80$$

$$(\sigma = E\varepsilon, \varepsilon = \Delta L \big/ L \rightarrow \Delta L = L \sigma \big/ E)$$

$$\Delta L = \Delta L_1 + \Delta L_2 = L_1 \frac{\sigma_1}{E} + L_2 \frac{\sigma_2}{E} = P \big/ E (\frac{L_1}{A_1} + \frac{L_2}{A_2})$$

$$\rightarrow E = P \big/ \Delta L \frac{A_2 L_1 + A_1 L_2}{A_1 A_2}$$

The expected elastic modulus of the aluminum alloy used is between 71 and 72 GPa and the measured value from the tensile test should be in this range. Fig. 3 shows the E modulus versus deformation considering the correction factor, which confirms the validity of the tensile tests on SType1 specimens.
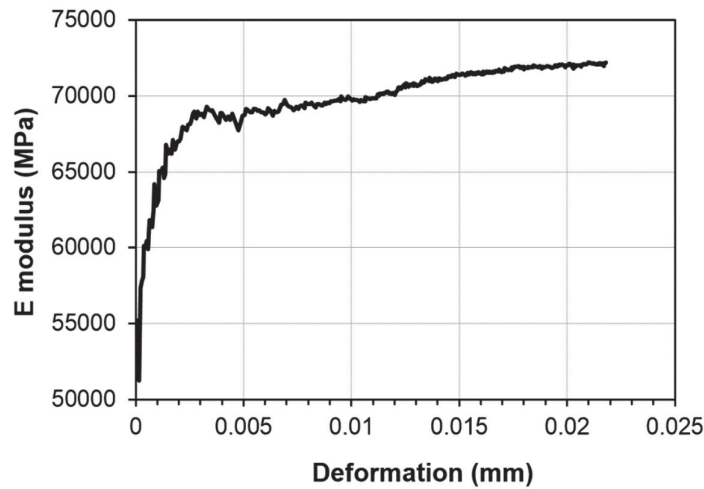
Fig. 3_ Corrected E modulus versus deformation for the aluminum specimen

- *Validation of Elastic modulus*

Fig. 4 shows the stress versus strain from both LVDT in a plane and the bending effect due to eccentricity for aluminum specimen. The bending effect due to eccentricity was calculated based on the difference between the LVDT measurements in each plane and it was below 0.2 MPa in both planes. Care was taken to make sure that the measurements from the LVDTs were corrected to account for their distances from the surface of the specimen while calculating the bending effect due to eccentricity.
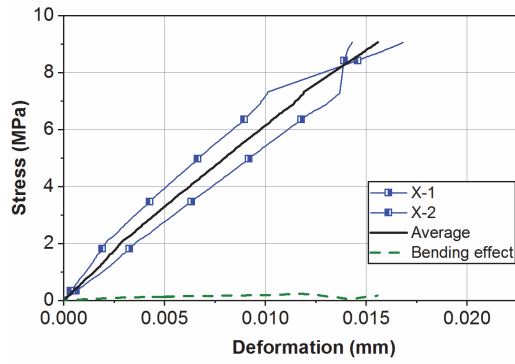
(a)
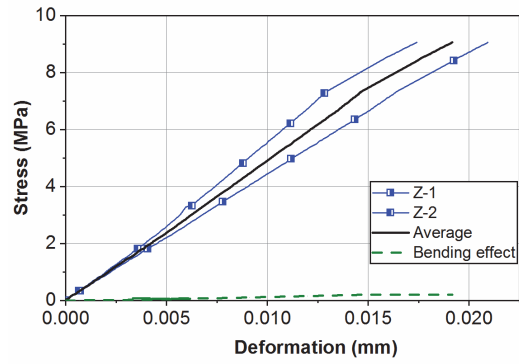
(b)

Fig. 4_ Stress versus strain from both LVDTs in a plane and the bending effect due to
eccentricity in (a) XY plane and (b) ZY plane for SType1

Chapter 3

Paper 2

Tensile response of PE-UHPFRC under imposed shrinkage deformations

Reference: A. Hajiesmaeili[1], M. A. Hafiz[2], E. Denarié[3], Tensile response of PE-UHPFRC under imposed shrinkage deformations, *to be submitted to Materials and Structures, June 2019.*

1 – corresponding author - conducted the experiments on UHPFRC with PE fibers along with the writing of the full article
2 – providing data for UHPRC mixes with steel fibers
3 – thesis supervisor

Abstract

PE-UHPFRC is a new Ultra High-Performance Fiber Reinforced Concrete (UHPFRC), which is developed to reduce the environmental impact of conventional UHPFRC by replacing the steel fibers with synthetic ones and reducing the clinker content in the mix. The development of the dynamic elastic modulus, the evolution of free autogenous deformations and the eigenstresses development with age, under full and partial restraint conditions, were investigated for PE-UHPFRC and the results were put into perspective with that for conventional UHPFRC with steel fibers. Furthermore, the tensile responses of different mixes under imposed shrinkage were compared and discussed. The results showed a shorter setting time and consequently an earlier initiation of elastic modulus development for PE-UHPFRC compared with that of conventional UHPFRC. Furthermore, the developed eigenstresses under full restraint conditions in a PE-UHPFRC layer compared with that for conventional UHPFRC were reduced by more than 70%, which is highly beneficial especially for cast-in place rehabilitation applications.

Keywords: UHPFRC; UHMW-PE; PE-UHPFRC; Autogenous shrinkage; Eigenstresses; TSTM; Tensile response

1. Introduction

The aging of transportation infrastructures together with the increasing demand of the society have intensified the need for effective and sustainable structural rehabilitation and strengthening techniques. In this regard, the concept of rehabilitation and strengthening of existing bridges with UHPFRC, using a thin UHPFRC overlay in zones of severe mechanical and environmental exposure, has gained the ground over the past decades [1].

Composite UHPFRC-Concrete members are subjected to internal deformations and to external actions. The internal autogenous deformations are mainly due to chemical shrinkage, self-desiccation after setting, drying shrinkage (more or less pronounced depending on UHPFRC recipes) and thermal effects caused by the heat of hydration in the new layer. These deformations starting at early age are restrained by the existing structure as well as the reinforcement bars, if any, in the UHPFRC layer [2]. The very high degree of restraint (load level of the overlay with respect to that for full restraint) of cast-in-place applications with thin overlays (often close to 90%) [3] leads to the development of pronounced tensile eigenstresses in the UHPFRC layer [4–7] which constitute a net loss of the performance in terms of potential tensile capacity.

Several authors reported results on the effect of restrained shrinkage for UHPFRC mixes with steel fibers. Schachinger et al. [8,9] investigated the cracking risk of two types of UHPC with CEM I 42.5 R/HS and CEM III B 42.5 NW/HS, due to restrained autogenous deformation until 28 days, and reported that a cracking risk exists within the first 15 h for the mixes with CEM I 42.5 R/HS. Habel et al. [6] studied the evolution of autogenous deformations and their associated eigenstresses in UHPFRC under incremental restraint, at 20°C. The comparison of the developed eigenstresses and tensile properties of UHPFRC until 7 days showed that the cracking risk is higher during the first two days. The study of Kamen et al. [4] on the thermo-mechanical response of UHPFRC at early age showed that even though increasing the curing temperature from 20 to 30°C prepones the initiation of eigenstresses development, it has a negligible effect on the eigenstresses at 7 days and no evidence of damage was observed. Yoo et al. [10] studied the effect of the restraint ratio on the cracking behavior of UHPFRC until 7 days by conducting restrained ring-tests with different ring thicknesses, in which the specimen with thicker steel rings (corresponding to a higher degree of restraint) demonstrated a faster cracking time than the ones with thinner steel rings. The influence of the degree of restraint on the cracking risk was confirmed by [11] who investigated the effect of specimen thickness on restrained shrinkage and cracking behaviors of thin UHPFRC slabs until 9 days. The authors studied two different thicknesses

of 35 and 45 mm for the UHPFRC layer and showed that the degree of restraint and the cracking risk were reduced as the thickness of the specimen increased. Furthermore, Weimann et al. [12] reported multiple cracks with crack widths smaller than 50 µm in Engineered Cementitious Composites (ECC), in a ring test subjected to approximately 90% restrained shrinkage, due to the relatively low tensile elastic limit of this material.

Even though it was shown that the cracking risk is higher at an early age for UHPFRC mixes, it should also be considered that eigenstresses continue to increase with age as a consequence of the autogenous shrinkage, and they may reach the Strain hardening domain at a later age. However, only a few notable studies investigated the eigenstresses development in UHPFRC beyond 28 days. Hafiz et al. [13] studied the development of eigenstresses in UHPFRC under full restraint conditions and showed that these stresses could reach values higher than the elastic limit and even reach the tensile strain hardening domain of the material after one month at 20°C curing.

PE-UHPFRC is a UHPFRC mix in which 50% vol. of the clinker is replaced with limestone fillers [14] and the steel fibers are replaced with Ultra High Molecular Weight Polyethylene (UHMW-PE) ones. This newly developed mix has the potential to reduce the eigenstresses in UHPFRC by reducing the autogenous shrinkage and increasing the viscoelastic response of the material. Kang et al. [15] showed that autogenous shrinkage decreases proportionally with the increase in limestone filler content. The autogenous shrinkage decreased by more than 30% by replacing 50% mass of cement with limestone filler. Furthermore, Hafiz et al. [13] reported a higher viscoelastic response for a mix with 50% mass replacement of clinker with limestone filler. Additionally, Bissonnette et al. [16] found higher tensile creep for a concrete mix with smaller diameter steel fibers. Therefore, the much smaller diameter of the PE fibers (0.012 mm) compared with that of steel fibers (0.16 to 0.2 mm) can have a potential to increase the tensile creep of PE-UHPFRC, and consequently reduce the eigenstresses by providing greater stress relaxation compared to the mixes with steel fibers.

The present study reports on the delayed response under imposed shrinkage deformations of PE-UHPFRC compared with that of conventional UHPFRC. In a first step, the investigated materials and their properties are presented. Secondly, the methods are described, highlighting the use of a Temperature Stress Testing Machine (TSTM) to investigate the eigenstresses development under full restraint conditions, and the Vibration Resonance Frequency test (VRF) to study the development of the dynamic elastic modulus with age. The development of the elastic modulus, the evolution of autogenous deformations, and the development of eigenstresses are investigated for three types of UHPFRC mixes including

(1) PE-UHPFRC with PE fiber and 50% vol. replacement of clinker with limestone filler, (2) S-UHPFRC with steel fibers, and (3) S-LF-UHPFRC with steel fibers and 50% mass replacement of clinker with limestone filler. Finally, the tensile responses of different UHPFRC mixes under imposed shrinkage deformations are put into perspective and the effect of the viscoelastic response on reducing the apparent elastic modulus of different mixes at very low loading rates is discussed.

2. Materials

Four mixes were used: (1) a newly developed UHPFRC mix, named PE-UHPFRC, in which the steel fibers were fully replaced by UHMW-PE ones and 50% volume of the clinker was replaced by limestone fillers [17], (2) a conventional UHPFRC mix with steel fibers from the CEMTEC$_{multiscale}$© family [18], optimized and modified at MCS/EPFL[19,20], designated as S-UHPFRC, (3) a UHPFRC mix based on S-UHPFRC in which 50% of the cement was replaced with inert limestone filler henceforth referred to as S-LF-UHPFRC [13], and (4) a mix similar to that of PE-UHPFRC with less sand and without quartz powder, named PE09. Six different powders including cement CEM I 52.5 HTS Lafarge, two types of limestone fillers of different gradings: Betoflow D® and Betocarb SL® (OMYA), white silica fume from SEPR (BET = 14 m^2/g), quartz powder (d_{50}=11.4 μm) and fine quartz sand (d_{50}=250 μm) were used in the mixes. The detailed compositions of the mixes are given in Table 1.

Table 1_ Mix proportions of the PE-UHPFRC, PE09, S-UHPFRC and S-LF-UHPFRC

Components (kg/m³)	(1) PE-UHPFRC	(2) S-UHPFRC	(3) S-LF-UHPFRC	(4) PE09
Cement	508	1467	733.7	627.8
Silica fume	178	381.4	293.5	220
Betocarb®- HP SL	170	-	223	210
Betoflow®-D	389	-	501.6	480.6
Fine Sand	525	-	-	348.4
Quartz Powder	223	-	-	-
Water	165	225.8	217.9	224
Water/fines	0.124	0.129	0.129	0.146
Water/cement	0.357	0.163	0.310	0.357
UHMW-PE fiber	19.6	-	-	19.6
Steel fibers	-	706.5	706.5	-
HRWRA	27	20.5	14.7	26.4
Ca(NO$_3$)$_2$	11	-	-	13.2
Defoaming agent	0.1	-	-	0.1

The PE-UHPFRC and PE09 have a fibrous mix containing 2% UHMW-PE fiber (6/0.012 mm) type SK99 (E modulus = 155 GPa) and SK 62 (E modulus = 86 GPa), respectively. The fibrous mix of both S-UHPFRC and S-LF-UHPFRC consisted of two types of micro (with a semi-circular section with variable dimensions) and macro (with l_f = 10 mm, d_f =0.2 mm) fibers. The mechanical properties of the mixes 1, 2, and 3 in the hardened state are shown in Table 2. The tensile properties are the average of 15 and 8 uniaxial tensile tests on dumbbell specimens with a thickness of 30 mm, for PE and steel fiber UHPFRC mixes, respectively. The compressive strength is the average of results on three cylinders after [21]. The average compressive strength of mix PE09 on three cylinders 7/14 cm after [21] was 119.7 at 28 days.

Table 2_ Mechanical properties of the PE-UHPFRC, S-UHPFRC, and S-LF-UHPFRC, average (standard deviation)

Properties	PE-UHPFRC	S-UHPFRC	S-LF-UHPFRC
Tensile strength (MPa)	11.7 (0.6)	18 (3.1)	15.1 (2.7)
Tensile elastic limit (MPa)	7.7 (0.5)	12.3 (1.7)	11.1 (1.9)
Tensile strain at peak stress (‰)	35 (10)	1.64 (0.44)	1.27 (0.51)
Compressive strength (MPa)	120 (2.6)	230.5 (0.85)	169.7 (0.5)
Young's modulus (GPa)	42.6 (2.2)	51 (2.3)	46.3 (1.3)

3. Experimental procedure

3.1 Delayed response

The free autogenous deformations and eigenstresses development of the UHPFRC mixes under full and partial restraint conditions were investigated using a Temperature Stress Testing Machine [22–24] at MCS/EPFL [25] from a very early age, directly after casting. Quasi–isotherm temperature conditions of 20 °C were ensured in the specimen with the help of a cooling circuit surrounding the molds. The TSTM setup is shown in Fig. 1.
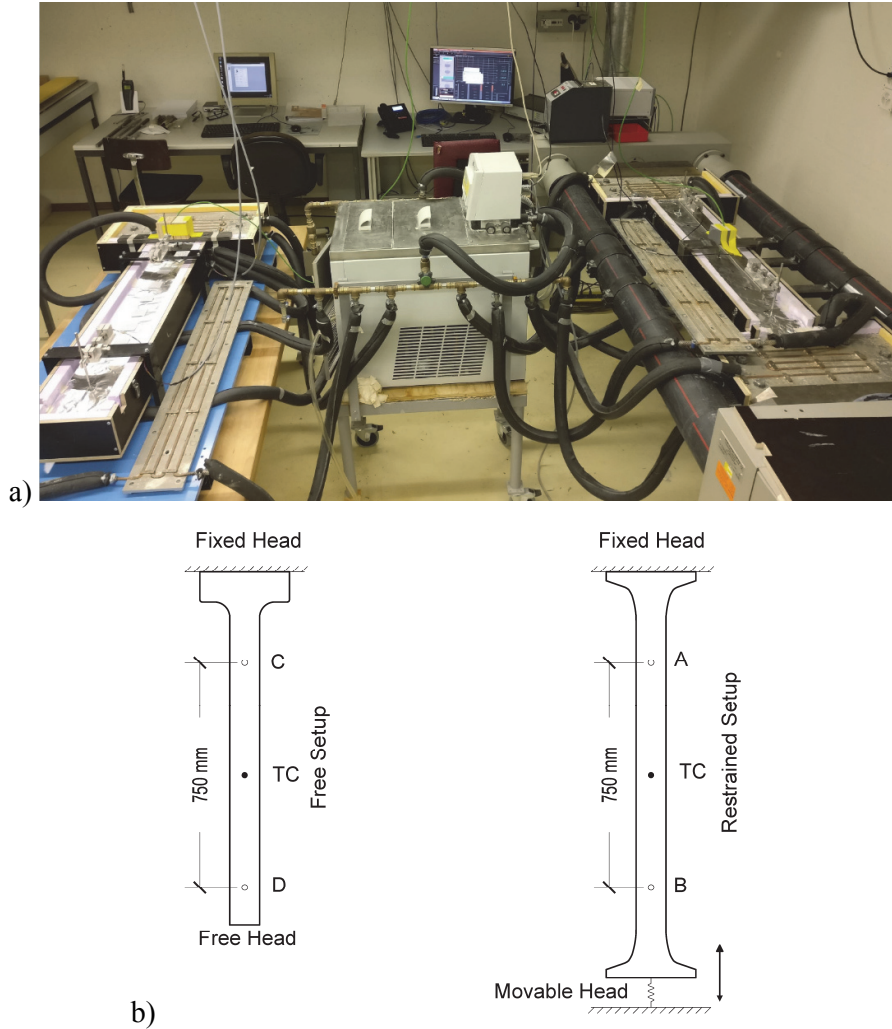
Fig. 1_TSTM setup: (a) overview with cooling system, (b) schematic representation of the specimen's geometry and location of measurement points of transducers (A, B, C, D) and thermocouples (TC)

The setup consisted of two parts. The free autogenous deformations were measured with the Free Setup and the eigenstresses development under full and partial restraint conditions were investigated using the Restrained Setup with the help of a load cell and an electromechanical actuator linked to a closed loop control system. The associated free deformations in the restrained specimen, as well as the free deformations in the free system, were determined by means of the measurements of two LVDT in each specimen, attached to a rod inserted in the material immediately after casting, through openings in the molds. In the Restrained Setup, two LVDT (A and B) with a range of ± 0.5 mm were placed 750 mm apart, whereas in the Free Setup, two LVDT (C and D) with a range of ± 2.5 mm were installed 750 mm apart

from each other, as shown in Fig. 1. The eigenstresses were calculated by dividing the force measured by the load cell with the cross-sectional area of the specimen. In both devices, fully sealed specimens of cross-sectional dimensions 50 mm x 100 mm were used. Further details regarding the TSTM setup can be found in [25–28].

The autogenous shrinkage was calculated by dividing the difference of displacements shown by LVDT C and D by the distance between them, assuming a linear variation of the autogenous deformation from one end to the other in the Free Setup. The partial restraint test was conducted using stroke control, in which the stroke was kept in the same relative position without any movement, throughout the test. The partial restraint imposed by the finite stiffness of the machine in this test was determined by comparing the free deformations in the restrained system and the free deformations in the free system. For the full restraint tests, in order to ensure fully restrained condition in the Restrained Setup, the deformations were controlled actively after setting to keep the relative displacement between the two points A and B at zero. However, at the fresh state and in the very early age close to setting time, the material stiffness was too low to impose a closed loop force or deformation control. As such, the tests were started under stroke control (passive control) with the stroke remaining in the same position as that at the start of the test. The monitored development of eigenstresses under passive stroke control was used to determine the stress to activate the deformation control leading to full restraint condition. A value of 0.2 MPa in tension (equivalent to 100 kg acting on the specimen cross section) was chosen as the trigger value, to be low enough to minimize the impacts on the viscous effects of the loading history induced by the passive stroke control timeframe after setting, while being high enough to reach a sufficient stiffness of the specimen to respond to a closed loop deformation control without yielding out of control.

Table 3 gives an overview of all the tests performed using the TSTM set-up. For mixes 1, 2, and 3, two full restraint tests were carried out. Additionally, one partial restraint test was carried out on PE09.

Table 3_ overview of the performed tests with TSTM

Material	Duration	Restraint condition
PE-UHPFRC	30 days & 65 days	Full
S-UHPFRC	31 days & 65 days	Full
S-LF-UHPFRC	32 days & 65 days	Full
PE09	28 days	Partial (0.65)

3.2 Development of elastic modulus

The vibration resonance frequency (VRF) test method [26,29] was used to determine the dynamic elastic modulus of the mixes from an early age and assess its development with age. The method is based on the measurement and analysis of natural vibration frequencies of the first two longitudinal modes of vibration of a cylindrical specimen using the Rayleigh-Ritz method, which relates the frequencies of vibration to the elastic modulus and the density of the material for a given geometry. Cylindrical specimens with a diameter of 70 mm and a length of 140 mm were used for the tests. The measurements of the frequencies started shortly after setting time of the material. A 10 mm diameter steel ball suspended with a steel thread was used to hit the center of one of the circular faces of the specimen. The hits were done automatically using an arm connected to a step motor with a magnetic head, once per minute. The propagated longitudinal waves were then captured by a miniature accelerometer at the opposite face of the specimen. The captured waves were digitized and analyzed using signal processing to obtain the 1st and 2nd resonance frequency of the specimen. The elastic modulus at different age was calculated using the resonance frequencies of the specimen and the density of the material. In order to estimate the setting time and start the measurement from the beginning of elastic modulus development, the temperature evolution was monitored in another specimen, using a thermocouple inserted right after casting.
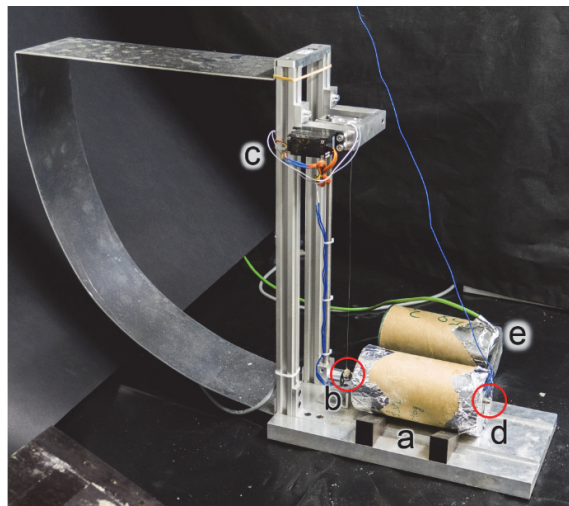
Fig. 2_ VRF setup: (a) cylindrical VRF specimen, (b) steel ball, (c) automatic hitting system, (d) accelerometer, (e) specimen for measuring temperature evolution

4. Results and Discussion

4.1 Development of elastic modulus

The development of the dynamic elastic modulus is shown in Fig. 3 on a semi-log scale for the mixes 1, 2 and 3. As expected, the final dynamic elastic modulus of the mix with steel fibers was higher than that for the PE-UHPFRC. The dynamic elastic modulus was slightly higher than the static ones (Table 2) and reached above 51 GPa in S-UHPFRC and S-LF-UHPFRC mixes, and 45 GPa in PE-UHPFRC mixes, after 14 days.
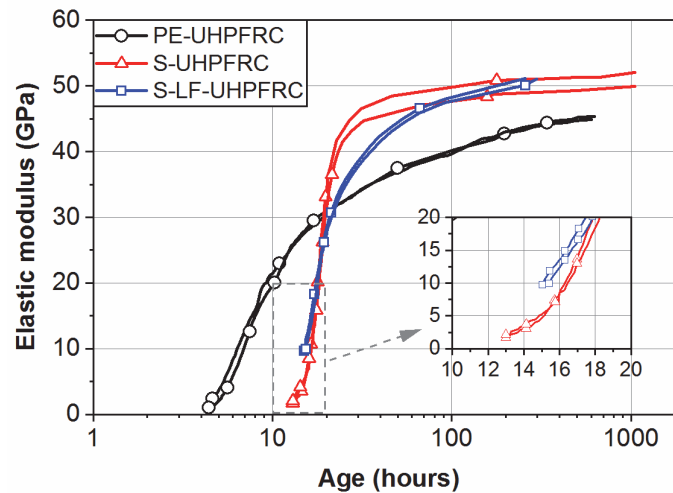
Fig. 3_ Development of dynamic elastic modulus for PE-UHPFRC, S-UHPFRC, and S-LF-UHPFRC

The development of the elastic modulus started in S-LF-UHPFRC slightly earlier than in S-UHPFRC, and it started in PE-UHPFRC approximately 10 hours earlier than the other two mixes. The difference between the results for the two steel fiber mixes can be explained considering the difference in their superplasticizer dosage. S-LF-UHPFRC had 14.7 kg/m^3 superplasticizer whereas S-UHPFRC had 20.5 kg/m^3. The retarding effect of the superplasticizer can delay the setting time and consequently the initiation of the elastic modulus development. The considerable difference between the PE-UHPFRC and the other two mixes can be attributed to the accelerating effect of $Ca(NO_3)_2$ used in the mix with PE fibers. Bost et al. [30] showed a significant accelerating effect of calcium nitrate on Portland cement even at a very low concentration. Thus, the $Ca(NO_3)_2$ in PE-UHPRC mixes reduced the setting time and accordingly preponed the initiation of elastic modulus development. Additionally, the effect of limestone filler in accelerating the hydration of cement grains by acting as crystallization nucleus [31], and in reducing the interparticle spacing product (at a constant liquid content and for limestone particles finer than cement) [32] played a role in

reducing the setting time and therefore bringing forward the initiation of the elastic modulus development in PE-UHPFRC and S-LF-UHPFRC. A similar trend was reported in [32–34].

Even though the development of the elastic modulus started earlier in the PE-UHPFRC mix compared with that for the other two mixes, at the age of 20 hours all the mixes reached an elastic modulus of 30 GPa as the result of different development rates. Fig. 4 shows the rate of elastic modulus development in UHPFRC mixes 1, 2, and 3. The rate of elastic modulus development had a higher peak in the S-UHPFRC mix compared with the other two mixes which had a similar trend. This can be attributed to the dilution effect of the limestone filler by increasing the water/cement (w/c) ratio in the mixes. The w/c ratio of the S-UHPFRC was 0.15 while the w/c ratio of PE-UHPFRC and S-LF-UHPFRC were 0.32 and 0.30, respectively. Considering the increase in the rate of drop of relative humidity with a decrease in the w/c ratio [35] and taking into account the similar kinetics of the rate of hydration and the changes in the relative humidity, the different rates of elastic modulus development of the mixes can be explained. The rate of elastic modulus development approached zero after 14 days.
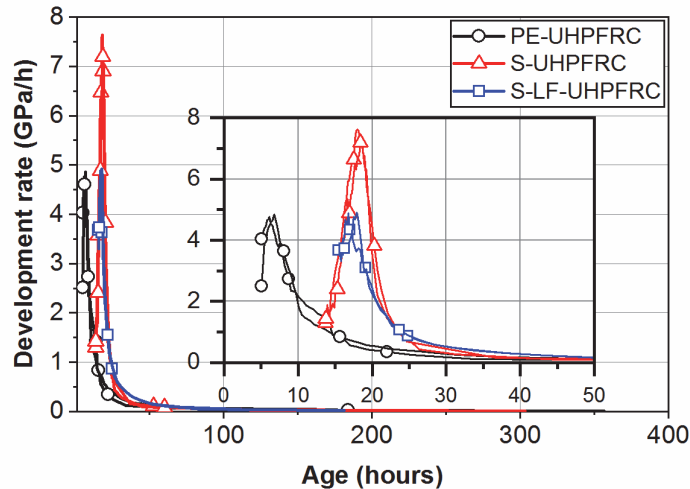
Fig. 4_ Rate of elastic modulus development in PE-UHPFRC, S-UHPFRC, and S-LF-UHPFRC

4.2 Free autogenous deformations

The evolution of the free autogenous deformations ($\varepsilon_{free}^{free}$) of the UHPFRC mixes are presented in Fig. 5. In this figure, the deformations are zeroed at the end of swelling and increasing strains indicate shrinkage. All the mixes showed a fast autogenous shrinkage in

the first few days. This trend can be explained by the progress of the hydration process and refinement of the pore structure with fast consumption of water [26].
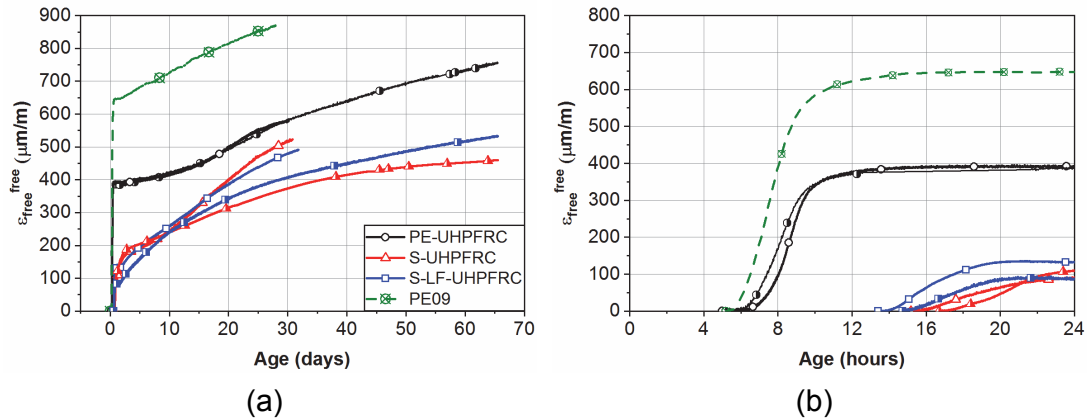
Fig. 5_ Evolution of free autogenous deformations of different UHPFRC mixes (a) zoom until 24h (b) (increasing strains indicate shrinkage)

The results of both full restraint test series on the PE-UHPFRC mix were almost superimposed which showed a very good reproducibility. The PE09 mix showed a higher shrinkage than that in PE-UHPFRC at an early age until 12 h. The higher autogenous shrinkage of PE09 can be explained by a lower sand content in this mix (348.5 kg/m^3 compared with 525 kg/m^3 in PE-UHPFRC) and also its higher water/fines ratio. Cheyrezy and Behloul [36] found that below w/b of 0.17, the autogenous shrinkage decreases with the w/b ratio. The autogenous deformations were higher in PE-UHPFRC compared to that in UHPFRC mixes with steel fibers. The stiff and very dense steel fibers skeleton in S-UHPFRC and S-LF-UHPFRC resists against the autogenous deformations and reduces the autogenous shrinkage at early ages [37–39] while the flexible PE fibers cannot hinder those autogenous deformations. This difference was reduced as the stiffness of the matrix increased with age and the role of the fibers' stiffness in controlling the deformations was lessened. A trend similar to that of PE-UHPFRC mixes was reported for the autogenous deformations of a PVA fiber reinforced Engineered Cementitious Composites (ECC) in [40].

Contrary to the finding of [15] regarding the effect of limestone filler in reducing the autogenous shrinkage in UHPFRC mixes, no considerable difference was observed between the autogenous shrinkage of S-UHPFRC and S-LF-UHPFRC in which 50% of cement was replaced with limestone filler. This discrepancy can be explained by considering a similar effect as that of the relative volume fraction of the fibrous mix and sand on the yield stress of the fresh mix, which indicates the resistance of a material against deformation, for

autogenous shrinkage. Martinie et al [41] showed that the yield stress of fresh cementitious composites is strongly correlated to the sum of the relative volume fraction of the fibers and the relative volume fraction of the granular skeleton: $\Phi_f/(r/4)+\Phi_s/\Phi_m$, where Φ_f is the volume fraction of fibers, r is the aspect ratio of the fiber (length/diameter), and Φ_s and Φ_m are the volume fraction and the dense packing fraction of the sand respectively. The investigated mix in [15] had 162 kg/m^3 steel fibers (13/0.2 mm) and 873 kg/m^3 of fine sand while the S-UHPFRC and S-LF-UHPFRC mixes had 471 kg/m^3 steel fibers (10/0.2 mm) and 235.5 kg/m^3 of steel wool that has a similar effect as sand. Considering 0.6 and 0.13 (experimental values) for dense packing fractions of the sand and the steel wool, respectively, the total relative volume fraction of the rigid inclusions is 0.87 and 0.98 for the mix studied in [15] and the UHPFRC mixes with steel fiber in this study, respectively. Thus, similar to the effect of increasing the total relative volume fraction of the rigid inclusions on increasing the yield stress of the fresh mix, it can be assumed that increasing the total relative volume fraction of the rigid inclusions in S-UHPFRC and S-LF-UHPFRC led to increasing the resistance to deformation and reduced the effect of limestone filler on the autogenous shrinkage.

4.3 Eigenstresses under full/partial restraint

Fig. 6 shows the eigenstresses development of PE-UHPFRC, S-UHPFRC, and S-LF-UHPFRC under full restraint and PE09 under partial restraint condition. The degree of restraint was 0.65 for the partial restraint test (estimated from the ratio of the free deformations in the restrained set-up to the free deformations in the free set-up). Even though the autogenous shrinkage of PE09 was approximately 1.5 times higher than that for the PE-UHPFRC mix, the eigenstresses development of these two mixes followed a very similar trend and were almost superimposed, despite the very different degrees of restraint. This can be explained by the opposing effects of a higher shrinkage (almost 1.5 times more for mix 4) but of a lower restraint (0.65) also for mix 4($1.5 \times 0.65 \approx 1$).
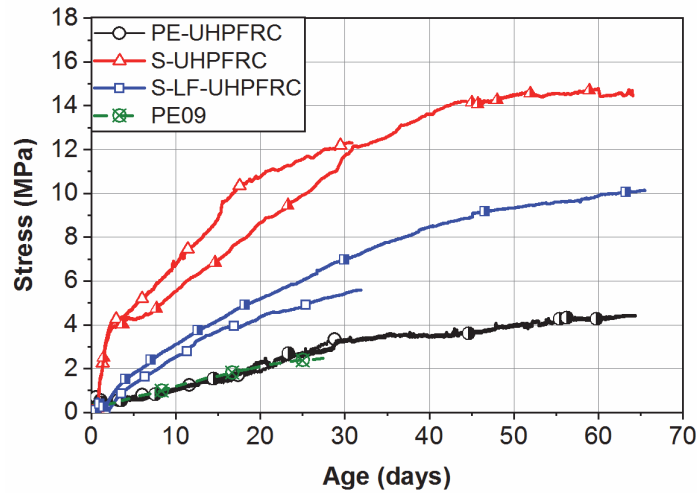
Fig. 6_ Eigenstresses development of different UHPFRC mixes, quasi isotherm curing conditions at 20°C

The value of eigenstresses in a 50 mm thick layer of PE-UHPFRC at 28 days decreased by a factor of 2 and 4 compared with that for S-LF-UHPFRC and S-UHPFRC, respectively. The lower value of eigenstresses in PE-UHPFRC might be explained in two levels; from a matrix and from a fibrous mix point of view. Regarding the matrix, Hafiz et al. [13] showed a higher viscoelastic response for the mixes with a higher dosage of limestone filler in creep tests starting at 14 days age, which consequently results in a higher relaxation potential and help to mitigate the developed eigenstresses. Concerning the fibrous mix, it was shown that using fibers in a cementitious matrix increases creep in tension [16,42,43] especially in the case of fibers with a smaller diameter [16]. Thus, the smaller diameter of the PE fibers compared to the steel fibers can lead to higher tensile creep in PE-UHPFRC mixes. Furthermore, Garas et al. [44] found a higher tensile creep for the UHPFRC specimens cured at room temperature compared with that for the thermally treated specimens due to the relatively lower stiffness of fiber/matrix interfaces in the former specimens. Accordingly, a higher volume of relatively low-stiffness fiber/matrix interface in PE-UHPFRC mixes due to the higher number of PE fibers compared with steel fibers may lead to a higher tensile creep in these mixes. Consequently, the higher tensile creep capacity of PE-UHPFRC mixes can provide greater stress relaxation compared to the mixes with steel fibers and reduce the developed eigenstresses.

4.4 Tensile response under imposed shrinkage deformations

Fig. 7 shows the tensile response of the UHPFRC mixes under imposed shrinkage deformations with very low loading rates. For the full restraint specimens, the free

autogenous shrinkage deformation from the Free Setup was considered as the deformation acting on the specimen in Restraint Setup and causing the eigenstresses development. In case of the partial restraint specimen (PE09), 65% of the free autogenous shrinkage deformation from Free Setup, which was the real deformation acting on the specimen according to the degree of restraint, was used for the strain calculations.
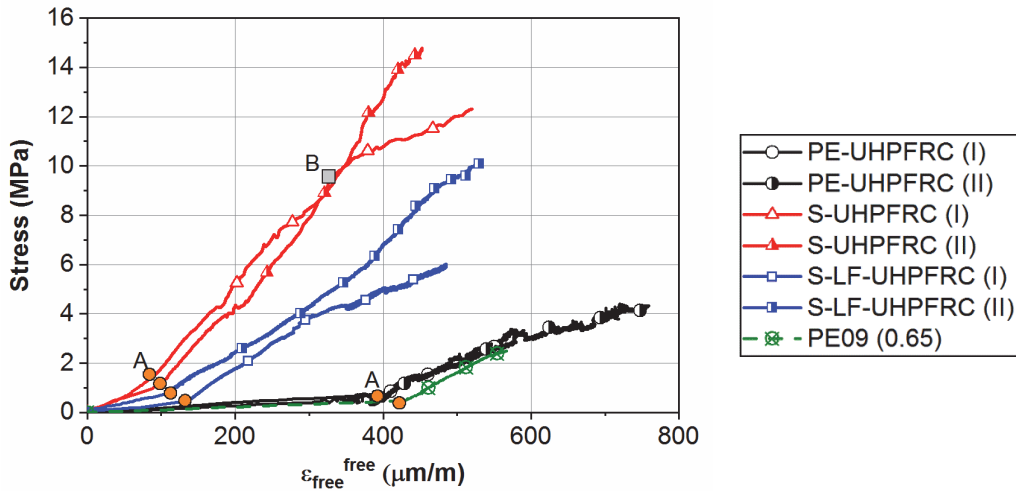
Fig. 7_ Tensile response of UHPFRC mixes under imposed shrinkage deformations

All the mixes showed a bilinear tensile response (until the elastic limit) starting with smaller slope and continuing with a higher slope. The first linear part with a lower slope finished at approximately 25 h, 45 h and 150 h for S-UHPFRC, S-LF-UHPFRC, and PE-UHPFRC, respectively (point A, orange circles in Fig. 7). Considering the development of elastic modulus in Fig. 3, the first linear part of the tensile response finished when the dynamic elastic modulus reached 43 GPa in all the mixes. The second slope of the tensile response corresponded to the elastic modulus of the materials at a very low loading rate (that of the shrinkage deformations), which intrinsically includes the effect of relaxation due to the viscoelastic response. The average slopes of the second linear part were 37 GPa, 22 GPa, and 14 GPa for S-UHPFRC, S-LF-UHPFRC, and PE-UHPFRC, respectively. The tensile response of PE09 under partial restraint condition was almost superimposed on that for the PE-UHPFRC specimens under full restraint condition. This indicates that the tensile behavior of the material under shrinkage deformation is independent of the degree of restraint; however, it takes longer for a partial restraint specimen to reach a given stress level than for a full restraint specimen. Furthermore, assuming that the deviation from linearity in the second slope indicates the beginning of the tensile hardening domain, it can be noticed that the eigenstresses in S-UHPFRC (I) reached the elastic limit at 10 MPa (point B in Fig.

7) and the specimen entered the hardening domain. This highlights the importance of considering eigenstresses in designing UHPFRC layers for rehabilitation.

5. Conclusions

- The development of the elastic modulus started earlier in PE-UHPFRC compared with the other two mixes; however, the rate of development was higher for S-UHPFRC. The dynamic elastic modulus reached 45 GPa and 50 GPa for PE-UHPFRC and steel fiber mixes, respectively.
- The autogenous shrinkage was 2-3 times more in PE-UHPFRC compared to that in conventional UHPFRC with steel fibers, in the first days; however, this difference was reduced to 25% at 28 days. The sand amount and steel fibers had a considerable effect on reducing the autogenous shrinkage.
- Replacing cement with limestone filler had a considerable effect on reducing the eigenstresses. Furthermore, using PE fibers instead of steel ones helped in reducing the eigenstresses. PE-UHPFRC showed 70% and 50% lower eigenstresses in the two tests under full restraint conditions compared with that in S-UHPFRC and S-LF-UHPFRC, respectively.
- The tensile response of UHPFRC mixes under imposed shrinkage deformations can be considered as bilinear, until the elastic limit. The first part with the smaller slope finished when the dynamic elastic modulus of the material reached 43 GPa. The tensile response of the material under shrinkage deformation was independent of the degree of restraint. The eigenstresses in one of the S-UHPFRC specimens passed the elastic limit and entered the hardening domain, which highlights the importance of considering eigenstresses in designing UHPFRC layers for rehabilitation.

Acknowledgments

References

1. Denarié, E. & Brühwiler, E. *Cast-on site UHPFRC for improvement of existing structures–achievements over the last 10 years in practice and research*. 7th workshop on High Performance Fiber Reinforced Cement Composites, 1-3, June 2015, Stuttgart, Germany (2015).

2. Denarié, E., Silfwerbrand, J. & Beushausen, H. *Structural Behaviour*. in *Bonded Cement-based Material Overlays for the Repair, the Lining or the Strengthening of Slabs or Pavements: State-of-the-art Report of the RILEM Technical Committee 193-RLS* 81–106 (Springer Science & Business Media, 2011).

3. Denarié, E. *SAMARIS D25b-Guidance for the use of UHPFRC for rehabilitation of concrete highway structures*. (2006).

4. Kamen, A., Denarié, E., Sadouki, H. & Brühwiler, E. *Thermo-mechanical response of UHPFRC at early age—Experimental study and numerical simulation*. Cement and Concrete Research 38, 822–831 (2008).

5. Habel, K. *Structural behaviour of elements combining ultra-high performance fibre reinforced concretes (UHPFRC) and reinforced concrete*. Doctoral thesis (2004).

6. Habel, K., Charron, J.-P., Denarié, E. & Brühwiler, E. *Autogenous deformations and viscoelasticity of UHPFRC in structures. Part I: experimental results*. Magazine of Concrete Research 58, 135–145 (2006).

7. Bernard, O. *Comportement à long terme des éléments de structure formés de bétons d'âges différents*. Doctoral thesis (2000).

8. Schachinger, I., Schmidt, K., Heinz, D. & Schießl, P. *Early-age cracking risk and relaxation by restrained autogenous deformation of ultra high performance concrete*. in *Proc. of the 6 International Symposium on Utilization of High Strength/High Performance Concrete, Leipzig* 16–20 (2002).

9. Schiessl, P., Beckhaus, K., Schachinger, I. & Rucker, P. *New results on early-age cracking risk of special concrete*. Cement, concrete and aggregates 26, 1–9 (2004).

10. Yoo, D.-Y., Park, J.-J., Kim, S.-W. & Yoon, Y.-S. *Influence of ring size on the restrained shrinkage behavior of ultra high performance fiber reinforced concrete*. Materials and structures 47, 1161–1174 (2014).

11. Yoo, D.-Y., Banthia, N. & Yoon, Y.-S. *Geometrical and boundary condition effects on restrained shrinkage behavior of UHPFRC slabs*. KSCE Journal of Civil Engineering 22, 185–195 (2018).

12. Weimann, M. B. & Li, V. C. *Hygral behavior of engineered cementitious composites (ECC)*. International Journal for Restoration of Buildings and Monuments (2003).

13. Hafiz, M. A., Hajiesmaeili, A. & Denarié, E. *Tensile response of low clinker UHPFRC subjected to fully restrained shrinkage*. Cement and Concrete Research (2019).

14. Hajiesmaeili, A. & Denarie, E. *Next Generation UHPFRC for Sustainable Structural Applications*. ACI Special Publication 326, (2018).

15. Kang, S.-H., Jeong, Y., Tan, K. H. & Moon, J. *High-volume use of limestone in ultra-high performance fiber-reinforced concrete for reducing cement content and autogenous shrinkage*. Construction and Building Materials 213, 292–305 (2019).

16. Bissonnette, B. & Pigeon, M. *Tensile creep at early ages of ordinary, silica fume and fiber reinforced concretes*. Cement and Concrete Research 25, 1075–1085 (1995).

17. Hajiesmaeili, A. & Denarié, E. *Development of Next Generation UHPFRC with synthetic fibers, for structural applications*. Cement and Concrete Composites (2019).

18. Rossi, P., Arca, A., Parant, E. & Fakhri, P. *Bending and compressive behaviours of a new cement composite*. Cement and Concrete Research 35, 27–33 (2005).

19. Denarié, E. *ARCHES D06: Recommendations for the tailoring of UHPFRC recipes for rehabilitation*. in *European project 6th FWP / ARCHES Assessment and Rehabilitation of Central European Highway Structures, WP 5 – 'Harden Structures to last with UHPFRC'* (2009).

20. Denarié, E. & Katrin, H. *SAMARIS D13: Report on preliminary studies for the use of HPFRCC for the rehabilitation of road infrastructure components*. (MCS/SAMARIS, 2004).

21. *SIA 2052, "Béton fibré ultra-performant (BFUP): Matériaux, dimensionnement et exécution"*. (Cahier Technique, 2017).

22. Bjøntegaard, Ø. *Thermal dilation and autogenous deformation as driving forces to self-induced stresses in high performance concrete*. Doctoral thesis (1999).

23. Kovler, K. *Testing system for determining the mechanical behaviour of early age concrete under restrained and free uniaxial shrinkage*. Materials and structures 27, 324 (1994).

24. Charron, J.-P. *Contribution à l'étude du comportement au jeune âge des matériaux cimentaires en conditions de déformations libre et restreinte*. Doctoral thesis (2003).

25. Kamen, A. *Comportement au jeune âge et différé d'un BFUP écrouissant sous les effets thermomécaniques*. Doctoral thesis (2007).

26. Kazemi Kamyab, M. *Autogenous Shrinkage and Hydration Kinetics of SH-UHPFRC under Moderate to Low Temperature Curing Conditions*. Doctoral thesis (2013).

27.   Switek, A. E. *Time-Dependent Response of Ultra High Performance Fibre Reinforced Concrete (UHPFRC) under Low to High Tensile Stresses*. Doctoral thesis (2011). doi:10.5075/epfl-thesis-4899

28.   Hafiz, M. A. & Denarié, E. *Experimental study of tensile response of Strain Hardening UHPFRC at early age*. in *International Conference on Strain-Hardening Cement-Based Composites* 308–315 (Springer, 2017).

29.   Kolluru, S. V, Popovics, J. S. & Shah, S. P. *Determining elastic properties of concrete using vibrational resonance frequencies of standard test cylinders*. Cement, concrete and aggregates 22, 81–89 (2000).

30.   Bost, P., Regnier, M. & Horgnies, M. *Comparison of the accelerating effect of various additions on the early hydration of Portland cement*. Construction and Building Materials 113, 290–296 (2016).

31.   Soroka, I. & Setter, N. *The effect of fillers on strength of cement mortars*. Cement and Concrete Research 7, 449–456 (1977).

32.   Kumar, A. *et al. Simple methods to estimate the influence of limestone fillers on reaction and property evolution in cementitious materials*. Cement and Concrete Composites 42, 20–29 (2013).

33.   Bentz, D. P., Sato, T., De la Varga, I. & Weiss, W. J. *Fine limestone additions to regulate setting in high volume fly ash mixtures*. Cement and Concrete Composites 34, 11–17 (2012).

34.   Vance, K., Aguayo, M., Oey, T., Sant, G. & Neithalath, N. *Hydration and strength development in ternary portland cement blends containing limestone and fly ash or metakaolin*. Cement and Concrete Composites 39, 93–103 (2013).

35.   Jensen, O. M. *Autogenous phenomena in cement-based materials*. in *Doctoral dissertation* (Department of Civil Engineering, Aalborg University, 2005).

36.   Cheyrezy, M. & Behloul, M. *Creep and shrinkage of ultra-high performance concrete*. Creep, Shrinkage and Durability Mechanics of concrete and other Quasi-Brittle Materials", édité par F.-J. Ulm, ZP Ba. ant and FH Witmann, Elsevier, Cambridge 527–538 (2001).

37.   Kanellopoulos, A., Nicolaides, D. & Karihaloo, B. L. *Autogenous shrinkage of CARDIFRC®*. in *CONCREEP7* (eds. G. Pijaudier-Cabot, Bruno, G. & Acker, P.) 7, 615–620 (2005).

38.   Meng, W. & Khayat, K. H. *Effect of hybrid fibers on fresh properties, mechanical properties, and autogenous shrinkage of cost-effective UHPC*. Journal of Materials in Civil Engineering 30, 4018030 (2018).

39. Garas, V. Y., Kahn, L. F. & Kurtis, K. E. *Preliminary investigation of the effect of steel fibers on the tensile creep and shrinkage of ultra-high performance concrete*. in *Proceedings of the 8th International Conference on Creep, Shrinkage and Durability Mechanics of Concrete and Concrete Structures* 1, 741–744 (2008).

40. Wang, S. & Li, V. C. *Polyvinyl alcohol fiber reinforced engineered cementitious composites: material design and performances*. in *Proc., Int'l Workshop on HPFRCC Structural Applications, Hawaii* (Citeseer, 2005).

41. Martinie, L., Rossi, P. & Roussel, N. *Rheology of fiber reinforced cementitious materials: classification and prediction*. Cement and Concrete Research 40, 226–234 (2010).

42. Bissonnette, B., Pigeon, M. & Vaysburd, A. M. *Tensile creep of concrete: study of its sensitivity to basic parameters*. ACI Materials journal 104, 360 (2007).

43. Altoubat, S. A. & Lange, D. A. *A new look at tensile creep of fiber reinforced concrete*. ACI Special Publication on Fiber Reinforced Concrete 143–160 (2003).

44. Garas, V. Y., Kurtis, K. E. & Kahn, L. F. *Creep of UHPC in tension and compression: effect of thermal treatment*. Cement and Concrete Composites 34, 493–502 (2012).

Chapter 4

Paper 3

Capillary flow in UHPFRC with synthetic fibers, under high tensile stresses

Reference: A. Hajiesmaeili[1], E. Denarié[2], Capillary flow in UHPFRC with synthetic fibers, under high tensile stresses, *to be submitted to Cement and Concrete Research, June 2019.*

1 – corresponding author - conducted all the experiments presented in the paper along with the writing of the full article

2 – thesis supervisor

Abstract

A novel Ultra High-Performance Fiber Reinforced Concrete (UHPFRC) mix with synthetic fibers and a low clinker matrix, henceforth referred to as *PE-UHPFRC*, has been developed for structural applications. It exhibits a high tensile elastic limit above 7 MPa, a tensile strength of more than 10 MPa, and a very high tensile hardening domain of above 3.5%. In order to effectively use this material, its protective properties have been investigated on the basis of the effect of tensile deformation and subsequent cracking on water transport properties, for a wide range of tensile strain. A special setup was developed to measure the capillary absorption of liquids while the specimen is under tension. The results show a considerable reduction in capillary absorption in case of PE-UHPFRC compared with Strain Hardening Cement-based Composites (SHCC). Moreover, the results highlight the considerable effect of the onset of cracking on capillary absorption.

Keywords: Capillary absorption; UHPFRC; PE-UHPFRC; UHMW-PE fibers; Tensile response; Crack characteristics

1. Introduction

The ever-increasing demand of society for the build environments on one hand and the limited material resources, on the other hand, have promoted the implementation of high and ultra-high-performance materials towards sustainability during the last few decades. Meanwhile, UHPFRC has successfully gained the ground and has proved its potential to be one of the solutions to contain the explosion of the costs (economy and environment) along with its numerous applications [1–3]. Continuing this trend, PE-UHPFRC is developed with 75% reduced environmental impact compared to conventional UHPFRC mixes by replacing the steel fibers with Ultra High Molecular Weight Polyethylene (UHMW-PE) ones and replacing 50% of the clinker with limestone fillers [4]. The high tensile elastic limit above 7 MPa, tensile strength of more than 10 MPa, and tensile deformation capacity of more than 3.5% make the newly developed UHPFRC well adapted for structural applications. In order to effectively use this material, its protective properties need to be investigated on the basis of the effect of tensile deformation and subsequent cracking on water transport properties and accordingly on the durability of the material

Deterioration mechanisms in cementitious materials are principally caused by insufficient protection followed by ingress of catalysts like water and aggressive agents in the material. Sorptivity and permeability are used as a measure for liquid transport properties and thereupon for the durability of cementitious materials. Permeability relates the movement of moisture through a saturated porous medium under a pressure gradient. Consequently, it is not entirely representative as structures made from cementitious materials are rarely saturated and exposed to strong pressure gradients in the building environment (excluding underground and offshore structures). Hence, sorptivity is a more realistic property to describe the liquid transport and durability of cementitious materials in structural applications were capillary flow prevails. There are two general approaches to model and analysis the sorptivity of cementitious materials in literature, which both yield a linear relationship between capillary absorption and the square root of time. The first approach is based on an extension of Darcy's law to unsaturated porous media [5] and the second approach is based on the Lucas–Washburn equation [6,7], which describes the dynamic flow equation of liquids in a capillary tube. The latter approach is more employed to describe the capillary absorption of cracked cementitious materials [8–10] in which the sorptivity corresponds to the square root of crack width. Furthermore, Zaccardi et al. [11] reported a better correlation between the water capillary absorption, and the fourth root of time for normal concretes with ordinary Portland cement and pozzolanic Portland cement.

Different measurements for evaluating the transport properties, such as capillary absorption, gas penetration, and liquid penetration were carried out on undamaged UHPFRC specimens [12–18], which all show a considerable improvement compared to ordinary and high strength concretes. Roux et al. [18] showed that the capillary absorption of UHPFRC is over ten times less than that of conventional concretes. Furthermore, they reported that the air permeability and chloride diffusion coefficient of UHPFRC are at least two orders of magnitude less than that of C30 and C80 concretes. Tam et al. [16] found that the water permeability coefficient of UHPFRC is lower than that of normal concrete by one or two orders of magnitude. The resistance of UHPFRC to the penetration of chloride ions was investigated by many researchers [3,14,18] and it was shown that UHPFRC has a much higher resistance to penetration of chloride ions than ordinary concretes and that the depth affected from the surface of exposed areas is remarkably lower in UHPFRC. Furthermore, numerous studies have confirmed the durability of structures built with UHPFRC after several years of exposure to severe conditions [19–23]. These features are attributed to the homogenous and highly dense microstructure of UHPFRC.

At service state, structural elements experience different levels of mechanical loading under both autogenous (eigenstresses) and exogenous actions (climate conditions, live loads, deadweight, accidental actions, fire, etc.), well documented in the literature [24–26]. However, only a few notable studies were carried out on the effects of damage on the transport properties of UHPFRC [24–30]. Wang et al. [26] studied the influence of imposed compressive stresses on capillary absorption of UHPFRC and found that the absorbed water mass increased by a factor of two when the specimens were loaded up to 50% of their compressive strength. The effect of tensile stresses on capillary absorption was investigated by Wittmann et al. [24] and it was shown that the capillary absorption is significantly increased if the material is subjected to tensile stresses higher than 50 % of its tensile strength. Accordingly, Wang et al. [25] reported that the sorptivity of UHPFRC increases by 30%, 45%, 77% and 95% for load levels of 50%, 60%, 70% and 80% of its splitting tensile strength, respectively.

ECC (Engineered Cementitious Composite) [31], SHCC [32] and HSHDC (High Strength, High-Ductility Concrete) [33] are classes of synthetic fiber-reinforced cementitious composites with high tensile deformation capacity. Although from a mechanical properties point of view, HSHDC is the closest to PE-UHPFRC, to the best of authors' knowledge, no extensive research has been reported in the open literature on transport properties of this material. However, the durability of ECC and SHCC, which are designed to limit the ingress of potentially deleterious substances by controlling cracks width, were investigated in terms

of transport properties, as a function of different crack width and strain levels by several researchers [34–43]. The results show that the water permeability under pressure is very much linked to the crack features and cracking patterns. Regardless of the material type (SHCC, normal concrete and UHPFRC), the permeability to liquids under pressure starts increasing at a much faster rate with increasing crack width after 0.05 to 0.1 mm [30,40,41]. However, the capillary water absorption in SHCC specimens was found to increase drastically by increasing the strain in the specimens even before a crack opening of 0.1 mm [39]. Investigations by means of neutron radiography showed that pre-existing microcracks subjected to capillary absorption become water-filled only after a few minutes [44]. Furthermore, increasing strains from 0 to 0.5% results in almost a 72% higher water capillary absorption [42]. Although the crack width plays an important role on the capillary absorption of cementitious materials, its effects have been underestimated in the aforementioned studies as the capillary absorption was determined after unloading the specimens.

In this study, an original test setup was developed in order to measure the capillary absorption of materials under tensile loading. The water sorptivity of tensile specimens made from PE-UHPFRC was investigated over a wide range of tensile deformation with the help of the developed setup. Afterwards, the specimens were unloaded and the capillary absorption of the same specimens was determined in accordance with EN13057:2002 standard [45], in order to compare the sorptivity under load and after unloading. As the cracking behavior highly affects the capillary absorption, Digital Image Correlation (DIC) was used to analyze the crack characteristics including crack pattern and width and investigate their effect on sorptivity. Finally, the results were put into perspective with existing experimental data on related materials.

2. Material design

A newly developed UHPFRC mix, named "*PE-UHPFRC*" (ref. mix PE21), was used for the present study. The Embodied Energy (EE) of this mix is reduced by 75 % with respect to that of current UHPFRC mixes for structural applications, with steel fibers. In PE-UHPFRC mixes, the steel fibers are fully replaced by UHMW-PE ones and 50% volume of the clinker is replaced by limestone fillers. Considering that the optimization of packing density and low w/fines ratio are the keys for obtaining Ultra high-performance cementitious composites, a generalization of the Compaction-Interaction Packing Model (CIPM) model [46] was derived and applied to optimize the mixture design [4]. Six different powders including cement CEM I 52.5 HTS Lafarge, two types of limestone filler of different gradings: Betoflow D$^®$ and Betocarb SL$^®$ (OMYA), white silica fume from SEPR (BET =

14 m^2/g), quartz powder and fine quartz sand (d$_{50}$=0.250 mm) were used in the mixes. Moreover, a modified Polycarboxylates-based HRWRA was used to maintain flowability and rheology of the mixture at the very low w/fines ratio of 0.146. The composition of the PE-UHPFRC mix is given in Table 1. Moreover, Fig. 1 shows the particle size distribution (PSD) of the powders used and of the mix. The packing density of the final mix was 0.81 based on the generalized CIPM, by using a compaction index of 9 for the calculations.

Table 1_ Mix proportions of PE-UHPFRC (mix PE21)

Components	(kg/m^3)
Cement	508
Silica fume	118
Betocarb®- HP SL	170
Betoflow®-D	389
Quartz powder	223
Fine sand	525
Water	165
HRWRA	27
Ca(NO$_3$)$_2$	11
UHMW PE fibers (Dyneema® SK99)	19.6

Ca(NO$_3$)$_2$ was employed in the form of a water-soluble compound in order to optimize the performance of the superplasticizer and reduce its dosage and thus the air content. At fresh state, the air content and the specific weight of the material were 4.5 % and 2215 kg/m^3, respectively. Furthermore, the flow was 48% after ASTM C1437 [47], with a final diameter after 25 blows of 150 mm.
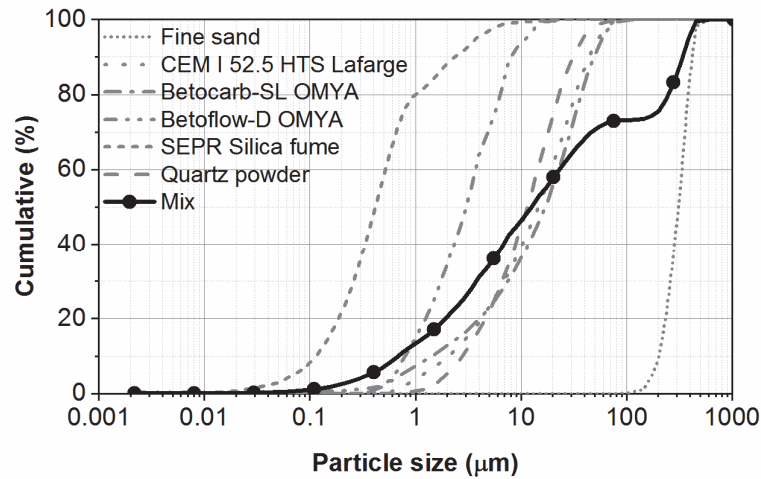
Fig. 1_ PSD of the components and final mix

The fibrous mix consisted of 2% vol. 6 mm long, chopped UHMW-PE fiber type SK 99 from DSM Dyneema®. The mechanical properties and the geometry of these PE fibers are given in Table 2.

Table 2_ Geometry and mechanical properties of PE Fiber

Fiber properties	Values
Diameter d_f (µm)	12
Length l_f (mm)	6
Nominal strength (MPa)	4100
Nominal Young's modulus (GPa)	155
Elongation at break (%)	3.5
Specific weight (kg/m^3)	980

3. Experimental procedure

3.1 Specimen design and preparation

An original dumbbell specimen was designed with a thickness of 30 mm representative of that found in numerous applications of UHPFRC, either cast-on-site for rehabilitation or in structural uses with thin precast ribbed members. The specimen had 290 mm length with a constant cross-section, with a width of 80 mm, on which three capillary chambers were installed (Fig. 2 and Fig. 5). The total length of the specimen was 750 mm. In order to limit as far as possible stress concentrations, Neuber's model [48] was applied to determine the geometry of the 100 mm long transition zone between the specimen's ends and its central part. Fig. 2 shows the corresponding specimen geometry.
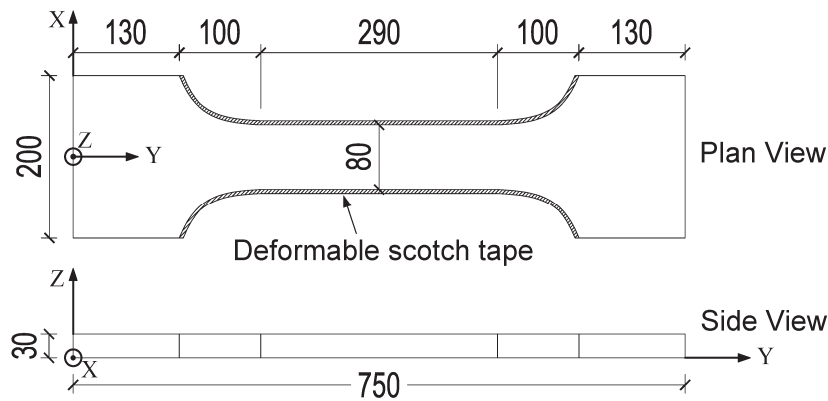
Fig. 2_ Dumbbell specimen geometry (dimensions in mm)

The specimens were cast horizontally in the molds from one end to the other, in a systematically repetitive procedure to obtain reproducible fiber orientation and distribution. The lower internal face of the molds was covered with a Controlled Permeability Formliner (CPF) - Zemdrain® sheet to avoid the water repellent effect of demolding oil. In order to avoid surfacing, the top surface of the specimen was covered immediately after pouring with a Zemdrain® sheet attached to a wood panel to guarantee a flat and uniform upper surface without air voids, after setting. Regarding the use of Zemdrain® sheets on the UHPFRC surfaces, it should be noted that according to [49], using these sheets had a negligible effect on the air permeability of concretes with a w/c ratio of 0.43. It can thus be assumed that their effect on the mechanical and transport properties of the UHPFRC skin are negligible. Moreover, the lateral internal faces of the molds along the shoulders were covered with 1 mm thick deformable tape to prevent eigenstresses and restrained shrinkage cracks at an early age. The specimens were kept sealed after casting for 2 days at room temperature of 20 ± 5°C. Thereupon demolding, the specimens were stored at room temperature of 20 ± 5°C under 95% RH. Before testing at 28 days, the specimens were washed with soap, to ensure removing of any fat with a water repellent effect. This was followed by a drying process at 50° C up to a constant weight. Eventually, the specimens were stored in the laboratory at ambient conditions (20 °C under 50% RH) for at least 12 hours.

3.2 Tensile test

In order to avoid as far as possible bending effects during the test, an optimized set-up was used with: (1) a stiff (4 columns) testing machine, (2) fixed/fixed support conditions for the specimen, and (3) a highly accurate alignment of the specimen thanks to a special procedure to link it directly to the machine without clamping. The dumbbell specimens were attached to the testing set-up by means of the "gluing without bonding" approach proposed by [50], and applied to dumbbell specimen by [51], Fig. 3. A steel shoe formed of plates with indented internal faces (c) on Fig. 3, was used as a form to cast resin indentations glued to the specimen, that helped transmit loads from the machine to the specimen by interlocking. In order to avoid adherence between the specimen and the indented metallic shoe, a demolding spray was applied on the internal indented faces of the later, before inserting the specimen coated with resin on its end in the shoe. This system guaranteed a uniform stress transfer without lateral restraint of the specimen. The top and bottom indented steel shoes were tightly bolted to stiff steel plates, (d) on Fig. 3, bolted directly on the machine's heads without any hinge.
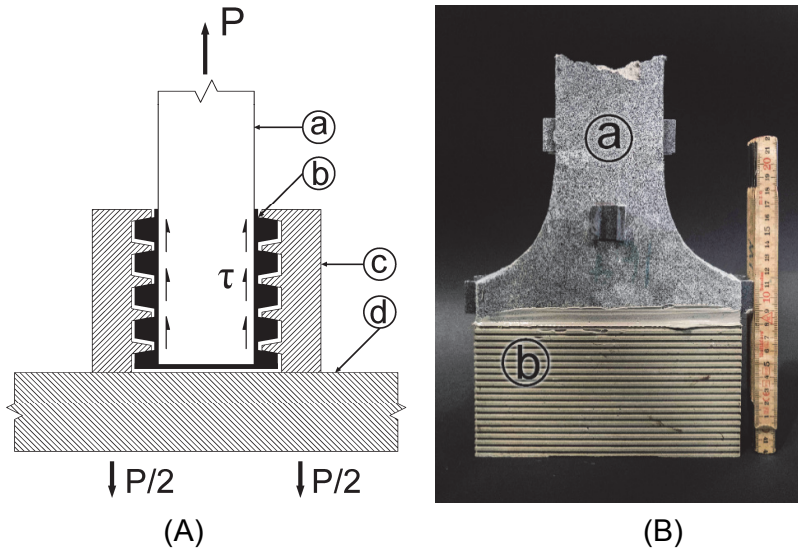
Fig. 3_ (A) Schematic sketch of the fixture set-up of the uniaxial tensile test (adapted after [50]) and (B) Tensile specimen after testing, with (a) specimen, (b) hardened resin indentations glued to the specimen surface, (c) indented steel plate, and (d) base plate

The uniaxial tensile tests were conducted with a universal AMSLER testing machine (capacity: 1000 kN). The test was controlled by the mean value of two LVDT fixed on the specimen with a gauge length of 515 mm, as shown in Fig. 4, with a closed-loop deformation rate of 0.003 mm/sec. Two additional pairs of LVDT, set in two perpendicular planes, were used to determine the elongation of the specimen and check eccentricities under loading. The gauge lengths of the LVDT were 400 mm and 275 mm in XY and YZ planes, respectively.
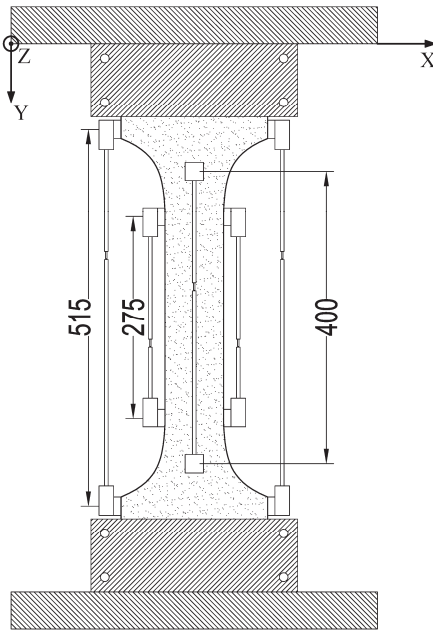
Fig. 4_ Test setup and instrumentation of the tensile specimen (dimensions in mm)

3.3 Crack measurement system

A 3D Digital Image Correlation (DIC) system, was used in order to measure the surface deformations. The system consisted of two 29 MP SVCam-hr29050 cameras with Zeiss *Distagon35* lenses, connected to a PC. The digital images were analyzed by the *Vic-3D 8* software in order to determine the surface deformation. In order to make an identifiable pattern, first the cast upper surface of the specimen was painted in white and then black aerosol paint spray was used to create the speckle pattern. The measurement area was 350 mm x 80 mm. The resolution of deformation measurement was 0.2 μm.

3.4 Capillary absorption test

An original setup was developed in order to measure capillary absorption while the specimen was loaded. The setup consisted of 3 cylindrical chambers with an internal diameter of 60 mm, which maintained the liquid in contact with the specimen surface. The chambers were made from Plexiglas that rested on an aluminum support. Two chambers (one for the specimen and the other one for the reference) were equipped with thermocouples in order to have a live measurement of the liquid temperature during the test.

For the capillary measurements, three chambers were clamped on the constant cross-section of the specimens with the help of 4 threaded rods. A rubber gasket was placed between the specimen surface and the chamber's support in order to ensure the water tightness. Each chamber was then connected to a graduated glass pipette with a flexible plastic tube. A drop of oil was put over the water in the pipette to avoid evaporation and the liquid level in the pipettes corresponded to the level of the chambers to avoid hydrostatic pressure at the beginning of the test. The subsequent changes of the liquid level were then recorded using a non-contact optical measurement system based on a digital camera and real-time image processing. As a reference, one chamber was clamped on an aluminum plate and was placed close to the specimen in order to record the variation of the water level due to the effect of ambient condition such as temperature variations and evaporation. This variation was then subtracted from the water level of the other three chambers in order to have only the effect of capillary absorption. The installation of the capillary absorption setup is presented in Fig. 5.
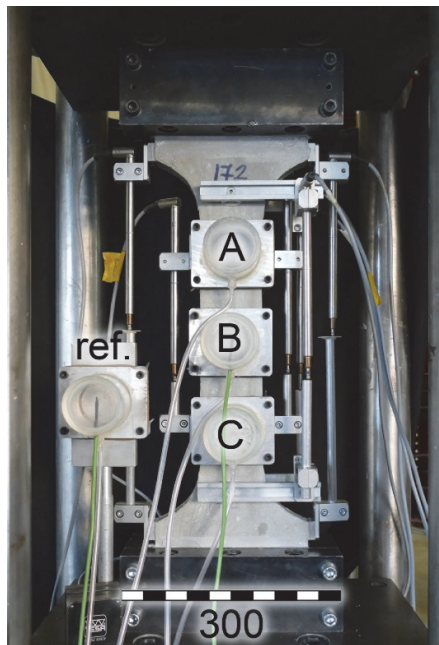
Fig. 5_ Capillary absorption measurement setup with chambers A, B and C installed on the tensile specimen, and additional reference chamber for compensation of effect of temperature variations

After the capillary absorption test under tension was completed, the damaged dumbbell specimens were unloaded, and cores were extracted for the capillary absorption tests based on EN13057:2002 standard [45]. Three cylinders were cut throughout the full depth (30 mm) of the tensile specimen with water jet, at the exact locations which were in contact with the

chambers during the capillary absorption measurement under tension, to be able to compare the results, Fig. 6 (a). Afterwards, the cylinders were oven dried until constant weight, at 50°C. In order to ensure one-dimensional liquid transport, the side faces of the cylinders were sealed with paraffin and thereafter, the specimen was kept in the laboratory ambient conditions (20°C) for at least 12 hours before being placed in the standard capillary absorption setup. Throughout the absorption tests, the immersion depth was kept constant at 2 mm. The standard capillary absorption setup is schematically shown in Fig. 6 (b).

<div align="center">(a)   (b)</div>
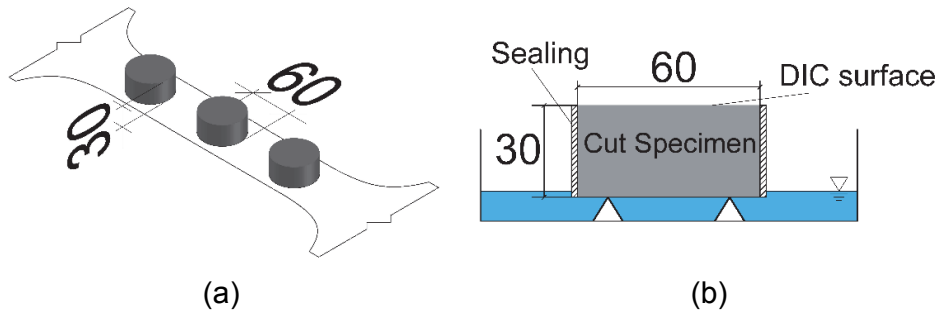
Fig. 6_ Dimensions and location of the cores extracted from the dumbbell specimen (a) and, a schematic sketch of standard capillary absorption setup (b) (dimensions in mm)

The capillary absorption coefficient was calculated based on Eq. 1, from the slope of the absorption versus square root of time in both cracked and uncracked states.

$$i = St^{0.5} \hspace{4cm} \text{Eq. 1}$$

Where i is the cumulative absorption, t is time, and S is a constant referred as the sorptivity (capillary absorption coefficient).

It should be born in mind that original UHPFRC made with a majority of reactive powders have a very low degree of hydration, due to their very low w/b ratio [52,53]. Thus, delayed hydration of the unhydrated binders when the material is in contact with water during permeability tests over several weeks may influence results, and require the use of different liquids not reacting with cement [27]. However, this effect was neglected in this study as the exposure time to water was short and also the amount of unhydrated binders was significantly lower for the investigated PE-UHPFRC compared with conventional mixes, because of the replacement of 50% of the clinker by limestone filler. The maximum degree of hydration for PE-UHPFRC was 52% and 60%, after Waller [54] and Jensen [55] models, respectively.

3.5 Overview of performed tests

Table 3 gives an overview of all the performed tests. Three uniaxial tensile tests until the end of hardening were performed in order to characterize the tensile behavior of the material. Capillary absorption tests were carried out on the specimens for a wide range of tensile strain levels. The investigated strain levels are 0.015%, 0.03%, 0.05%, 0.1%, 0.15%, 0.2%, 1% and 2%. First, the specimens were loaded to the defined strain levels, measuring the strain with the help of two LVDTs with the gauge length of 515 mm (Fig. 4). Meanwhile, the crack characteristics were recorded by means of DIC. Afterward, the chambers were installed on the surface of the specimens and the capillary absorption measurement started. Considering the effect of saturation conditions on the capillary absorption, a separate specimen was tested for each strain level. Repetition was done for the strain level of 0.05% to characterize the variability of the obtained results.

Table 3_ Overview of the performed tests

Specimen No.	Loaded until	Capillary absorption under tension	Capillary absorption after unloading	
1	ultimate strain	-	-	
2	ultimate strain	-	-	Tensile prop. & crack char.
3	ultimate strain	-	-	
4	0.015%	3x chambers	-	
5	0.03%	3x chambers	-	
6	0.05%	3x chambers	3x cylinders	
7	0.05%	3x chambers	-	Serviceability domain
8	0.1%	3x chambers	3x cylinders	
9	0.15%	3x chambers	3x cylinders	
10	0.2%	3x chambers	3x cylinders	
11	1%	3x chambers	3x cylinders	Large deformation
12	2%	3x chambers	3x cylinders	

4. Results and Discussion

4.1 Tensile response

The uniaxial tensile test results of all the tested specimens are shown in Fig. 7. The x-axis shows the average tensile strain computed from the extensions of two pilot LVDT that controlled the deformation with the gage length of 515 mm (setup shown in Fig. 4).

The specimens had a strain-hardening behavior and numerous multiple cracks developed gradually. As it is shown in Fig. 7, the elastic limit (first crack strength) was above 7 MPa. The average elastic modulus of the material in tension was 43 GPa, which was computed from the slope of the average straight line through the stress-strain data points of the specimen. Furthermore, it should be noted that compared to other results from the literature [33], the stress fluctuation in the hardening zone was much lower. Fig. 7 highlights highly reproducible tensile test results which confirm the robustness of the material and the effectiveness of the testing setup.

(a)   (b)
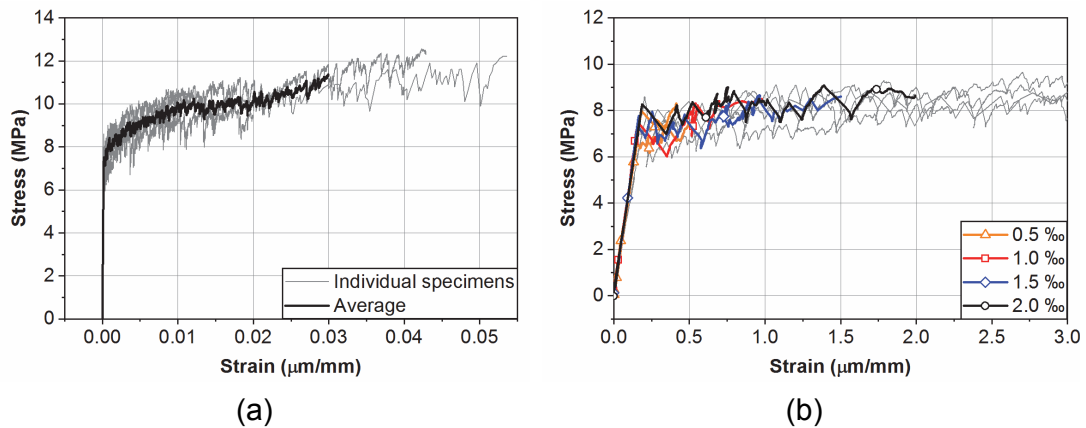
Fig. 7_Uniaxial tensile stress-strain responses of the tested PE-UHPFRC specimens (a) zoom until 0.3% strain level

4.2 Crack characteristics

The crack characteristics were analyzed up to the strain level of 4.5%. Considering the yield strain of approximately 0.2% for conventional steel reinforcement in structural members, 4.5% strain will never be reached under service loads in RC structures. However, investigating higher strains is still important to understand the full picture of the evolution of the cracks and of the associated capillary absorption. Fig. 8 shows the crack numbers, and average, maximum, minimum and standard deviation of the crack width (w_c) for a uniaxial tensile test. The specimen exhibited a multiple cracking behavior and the average crack widths did not exceed 0.1 mm even up to a very high strain level of 4.5%.
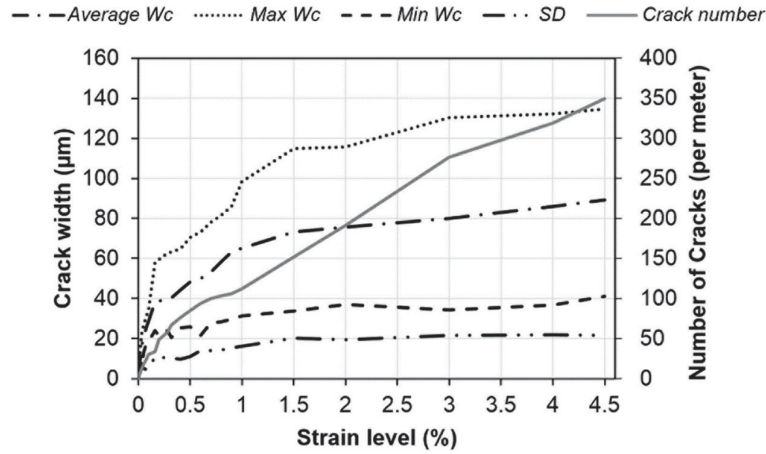
Fig. 8_ Crack number, and average, maximum, minimum and standard deviation of the crack width under tension of specimen No. 2

Fig. 9 shows the DIC images of the tensile specimen No. 2 at strain levels of 0.1, 0.2, 1, 2, 3 and 4% along with the crack analysis. The horizontal lines indicate the crack location and the dots show the corresponding crack width. The gauge length of the strain ε_{yy}, which is represented by the colored contour plot, was 20 pixels, which was 1.43 mm in this study.
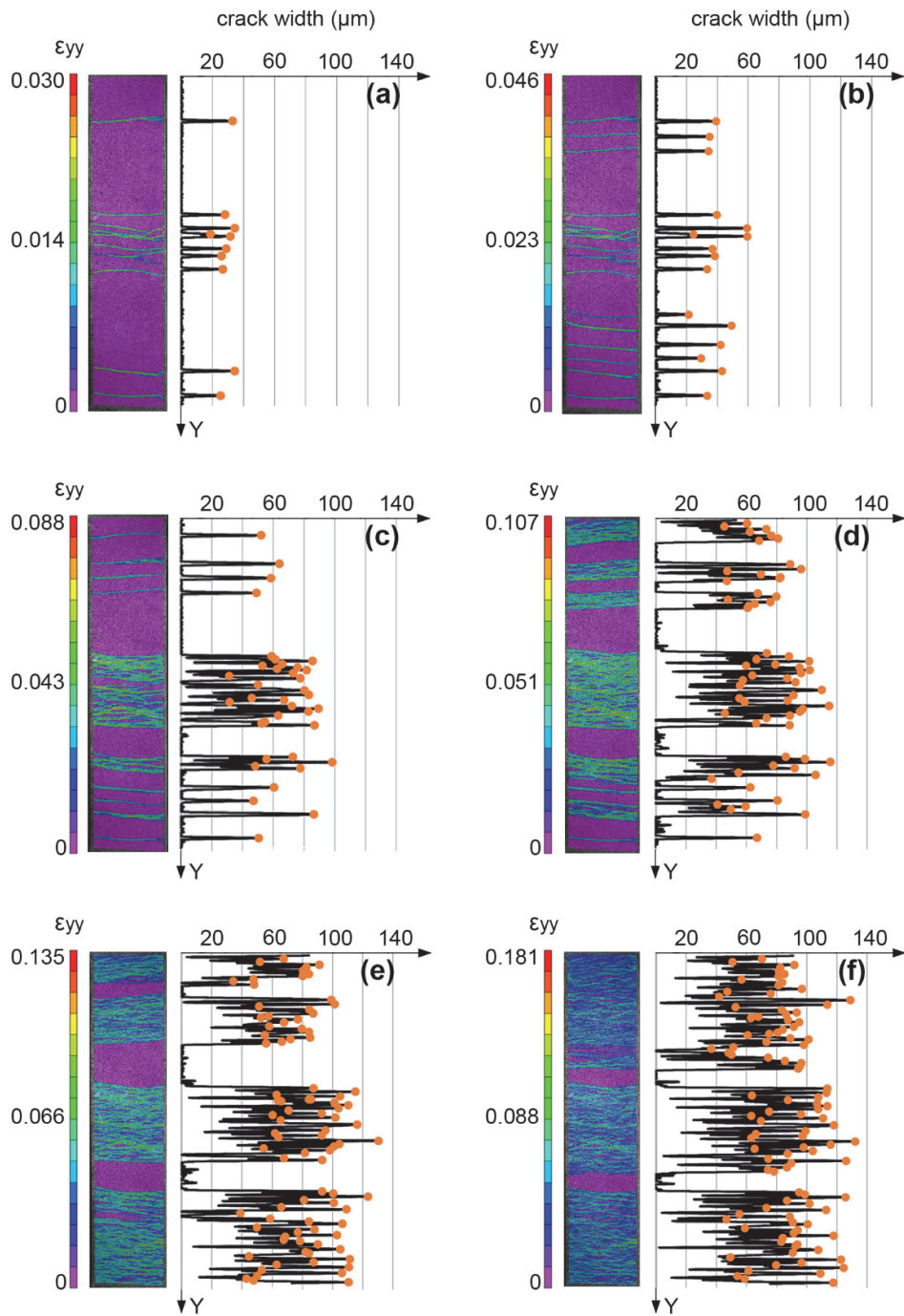
Fig. 9_ DIC images of the tensile specimen No.2 at different strain levels along with the crack analysis. (a) 0.1%, (b) 0.2%, (c) 1%, (d) 2%, (e) 3%, and (f) 4%

Fig. 10 represents the distribution of the crack width at the strain levels of 1, 2, 3 and 4%. For the strain levels of 1 and 2%, a lognormal distribution fits well on the results, as suggested in the literature for ECC and SHCC materials [37,38,56]. However, for the higher

strain levels of 3 and 4%, the distribution of the crack width was closer to a normal distribution, Fig. 10 (b).

(a)   (b)
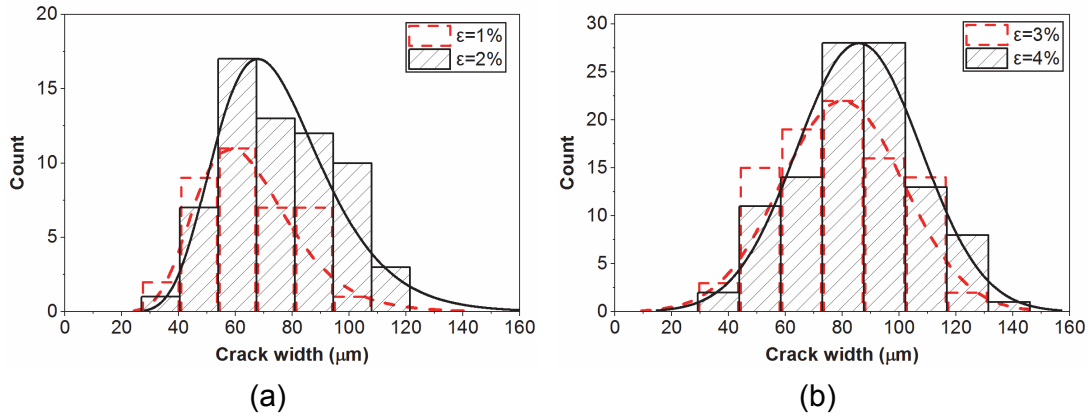
Fig. 10_ Crack width distribution: (a) for 1 and 2% strain levels - lognormal distribution, and (b) for 3 and 4% strain levels - normal distribution

4.3 Capillary absorption test under tension

Fig. 11 shows the average water capillary absorption under tension from the three chambers, for the strain level of 0.015 to 0.2%. Considering that the elastic limit of the material was around 0.02%, the strain level of 0.015% was in the elastic domain and the specimen was still uncracked. The capillary absorption coefficient for this strain level was in the extremely low range of 3 to 4 g/m²√h that confirms the very dense microstructure of the material. The strain level of 0.03% was just after the elastic limit at which there was only one crack on the specimen. Accordingly, only the chamber that was on the cracked area was showing higher values and the capillary absorption from the two other chambers remained close to 4 g/m²√h.
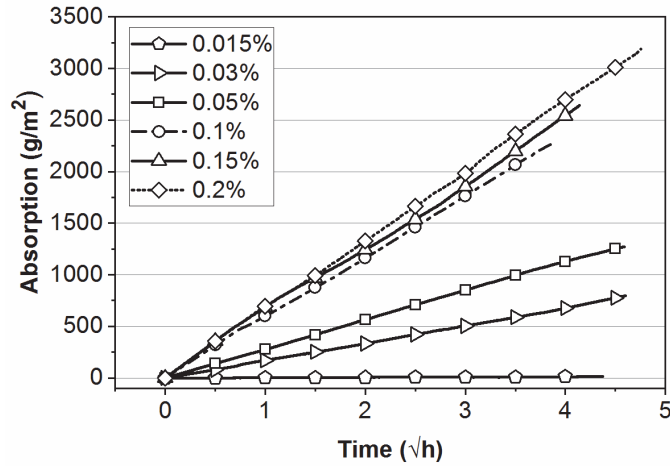
Fig. 11_ Average water capillary absorption under tension, from three chambers for the strain levels of 0.015 to 0.2%

Fig. 12 represents the crack patterns with respect to the location of the chambers as well as the crack widths for the strain levels of 0.05, 0.1, 0.15 and 0.2%. In this figure, the positions of the cracks are outlined by dashed lines and the circles show the position of the chambers on the specimens. At the strain level of 0.05%, two cracks with widths of 50.2 μm and 33.6 μm along a length of 29.7 mm and 38.1 mm, respectively, were present under the top chamber (A). One crack with a width of 38.8 μm along a length of 57.6 mm was present under the middle chamber (B). Finally, one crack with a width of 44 μm along a length of 58.7 mm was present under the bottom chamber (C). The average capillary absorption coefficient at this strain level was 293 and 313 $g/m^2\sqrt{h}$ for the first and the repeated specimen, respectively.

At the strain level of 0.1%, two cracks were present under chamber A, while there was one crack each within the area of both the other chambers. According to Table 4 and Fig. 12, the widest crack with a width of 70.7 μm highly influenced the capillary absorption in the top chamber while the other two chambers exhibited similar capillary absorption with a similar crack pattern.

For the strain level of 0.15%, nine cracks with an average width of 34 μm located under chamber A, and three cracks with an average width of 85 μm under chamber B, had a similar effect on capillary absorption. The capillary absorption of the bottom chamber (C), which did not experience any crack in its area, remained close to 4 $g/m^2\sqrt{h}$.

At the strain level of 0.2%, more cracks developed on the top and bottom part of the specimen compared to the center. Six cracks were found under chamber A. However, the cracks were situated close to the end of the chamber and therefore their lengths which were in direct contact with water, were shorter compared to that for the other two chambers. Two cracks with widths of 40.1 μm and 46.4 μm were present under chamber C. Four cracks with the width range of 50 to 100 μm were present in the middle of the bottom chamber and resulted in a higher capillary absorption for this chamber.
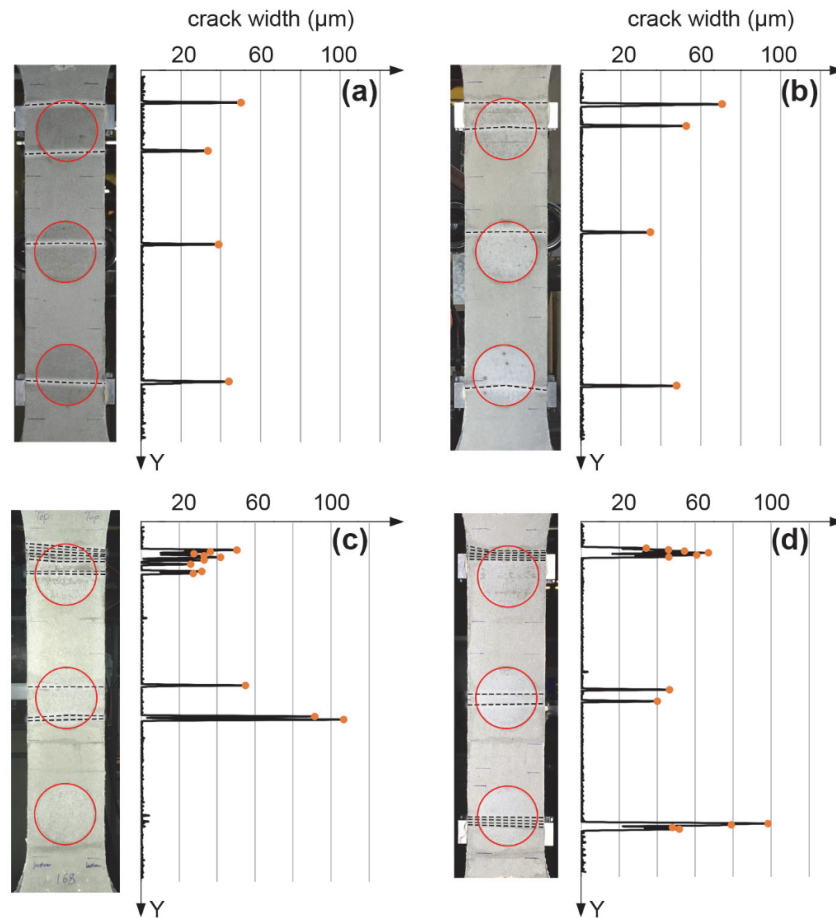
Fig. 12_ Crack positions and the corresponding crack width for the specimens loaded up to strain levels of (a) 0.05%, (b) 0.1%, (c) 0.15% and (d) 0.2%

Fig. 13 outlines the average water capillary absorption of the specimen from three chambers against the square root of hour, for the strain levels of 1 and 2%, under tensile loading. At 1% strain level, the specimen experienced 38 cracks along a length of 354.5 mm, which represents a crack density of 107 cracks per meter. The average of the crack width was 68.5 μm with a standard deviation of 17.4. The capillary absorption coefficient of the specimen varied from 1600 to 1900 g/m²√h for the three chambers.

The crack density at the 2% strain level was 236 cracks per meter with the average crack width of 68.2 μm and a standard deviation of 18.7. With respect to the crack characteristics at 1% strain level, the number of cracks increased by a factor of two, while the average crack width and standard deviation remained in a similar range. The average capillary absorption coefficient for the three chambers at a 2 % strain level was 3582 g/m²√h. This is a very high value comparable with the capillary absorption coefficient of red brick that is approximately 4000 g/m²√h.
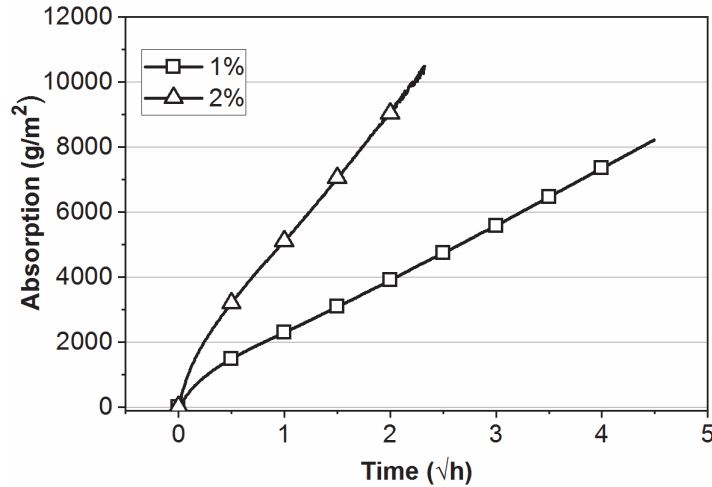
Fig. 13_ Average of water capillary absorption under tension, from three chambers for the strain levels of 1 and 2%

The capillary absorption coefficient was calculated for each individual chamber and is shown in Table 4 for the strain levels of 0.03 to 2%. The variation of the capillary absorption from different chambers at the strain levels below 0.2% is the result of a limited number of cracks and consequently non-uniform crack patterns at those strain levels. At the strain level of 0.03%, there was only one crack on the specimen under the chamber B. Similarly, as it is shown in Fig. 12, there was no crack under the chamber C at the strain level of 0.15%.

Table 4_ Capillary absorption coefficients (g/m²√h) under tension, from each chamber and the average values for strain levels of 0.03 to 2%

Strain level	0.03%	0.05%	0.05%	0.1%	0.15%	0.2%	1%	2%
Chamber A	4	315	348	976	935	651	1612	4341
Chamber B	502	314	300	390	932	689	1915	2682
Chamber C	4	250	291	397	4	717	1659	3724
Average	170	293	313	588	624	686	1729	3582

In order to highlight the effect of cracks on capillary absorption, Fig. 14 shows the capillary absorption as a function of crack area for the specimen tested at 0.05, 0.1, 0.15 and 0.2% strain level. In this figure, each point corresponds to one chamber and the crack area was calculated by the sum of the crack widths times crack lengths under the chamber. The results showed a linear relation relationship between the capillary absorption and the crack area.
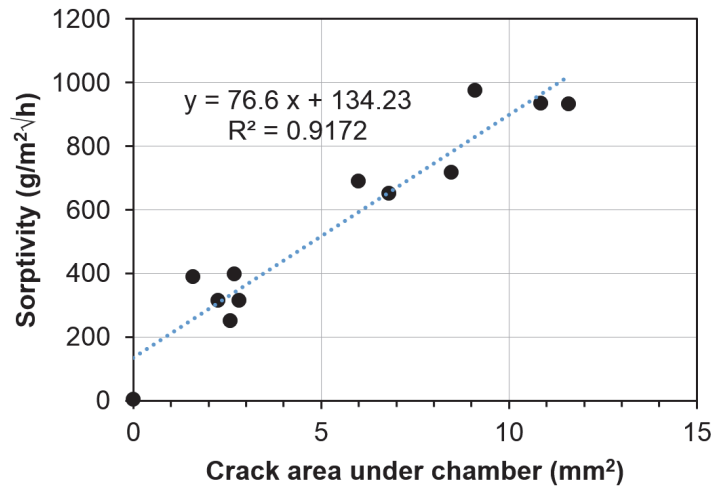
Fig. 14_ Capillary absorption as a function of the crack area until the strain level of 0.2%

In order to validate the averaging method used for reporting the capillary absorption at different strain levels, the average capillary absorption at strain levels of 0.2, 1, and 2% from Table 4 were plotted in Fig. 15 versus the crack area calculated based on Fig. 8 and were compared with the linear relationship calculated in Fig. 14. The results fitted well on the linear relationship which confirmed both the validity of the averaging method and the crack information provided in Fig. 8.
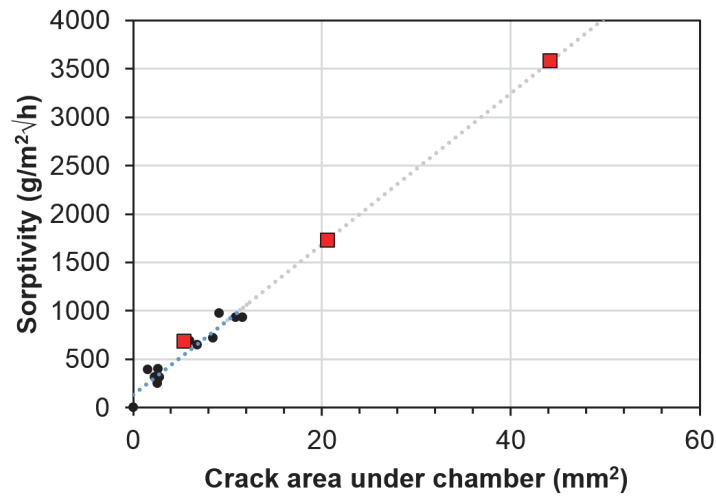
Fig. 15_ Validation of the averaging method

4.4 Capillary absorption test after unloading

Specimen for capillary absorption tests after unloading were cored out of the dumbbell specimens for strain levels of 0.05%, 0.1%, 0.15%, 0.2%, 1% and 2%. Fig. 16 shows the average absorption of three cores, which were taken from each specimen after unloading on the same locations as that of the respective chambers A, B, C. The capillary absorption increased gradually with increasing strain levels. Although there was a linear correlation between capillary absorption and the square root of time for the lower strain levels (0.05 and 0.1%), the relation deviated from linearity at the higher strain levels. This can be explained by the contrary effect of gravity on the capillary rise in the wider cracks which takes place for the configuration of the test after EN13057:2002 [45] (soaking from bottom face).
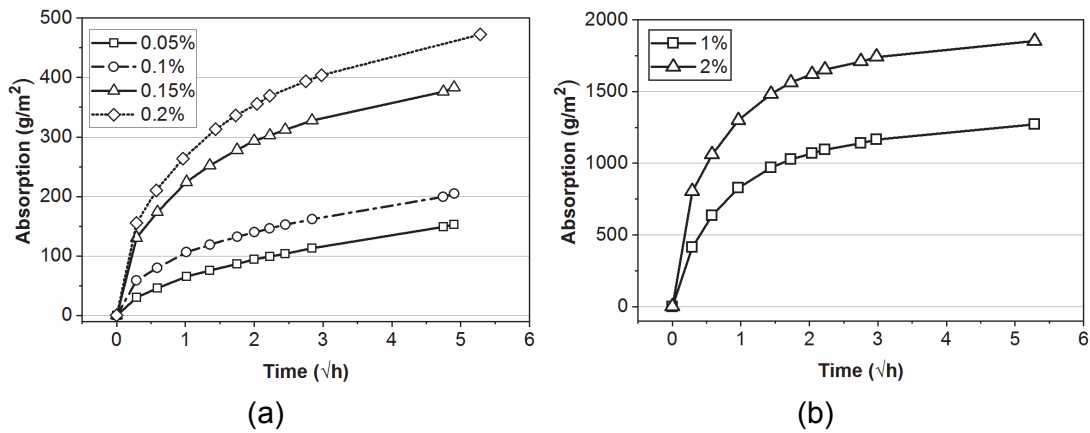
Fig. 16_ Average of water capillary absorption test results from three cores, for the strain levels of (a) 0.05 to 0.2%, and (b) 1 and 2%, after unloading

Table 5 presents the capillary absorption coefficient of the specimens that were tested after unloading (individual results and average), for the investigated strain levels.

Table 5_ Capillary absorption coefficients (g/m²√h) for tests after unloading, from each core and the average values for strain level of 0.05 to 2%

Strain level	0.05%	0.1%	0.15%	0.2%	1%	2%
Core A	25	46	87	57	203	142
Core B	24	18	53	48	186	211
Core C	25	22	5	77	75	224
Average	25	29	48	61	155	192

4.5 Discussion

Fig. 17 compares the capillary absorption of PE-UHPFRC with that of SHCC under various strain levels, taken from Mechtcherine et al. [36] and Wittmann et al. [43]. In this figure, the capillary absorption coefficient of PE-UHPFRC is the average of three values. In all the cases, the specimen is damaged under tension and the capillary absorption test is performed on the cores from the tensile specimen after unloading.
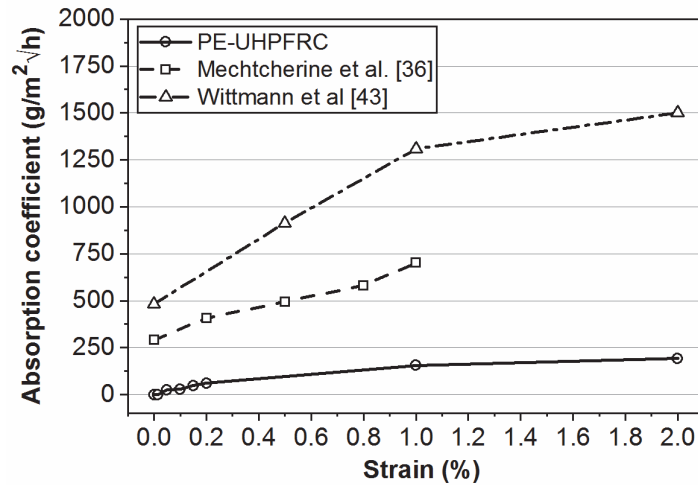
Fig. 17_ Comparison between capillary absorption coefficient of PE-UHPFRC, and SHCC at different strain level after unloading

It can be noticed from Fig. 17 that the water capillary absorption of PE-UHPFRC is at least one order of magnitude lower than that of SHCC. This highlights the fact that although crack width limitation criteria are a necessary condition for durability, the density of the microstructure plays an equally important role on transport properties and thereupon on the durability of the material. Moreover, as it can be seen in this figure, even after experiencing the strain level of 2%, after unloading, the absorption coefficient of PE-UHPFRC is lower than that of undamaged normal concrete, which is in the range of 300 $g/m^2\sqrt{h}$.

The influence of imposed tensile stresses on capillary absorption of UHPFRC with steel fibers under tensile loading has been investigated by Wittmann et al. [24]. Tensile test results for the same material are presented in [57]. On this basis and considering a typical range of strain levels corresponding to elastic limits of PE-UHPFRC from 0.015 to 0.02%, Fig. 18 shows a sudden increase in capillary absorption coefficients after the elastic limit. A similar trend was observed for the PE-UHPFRC.
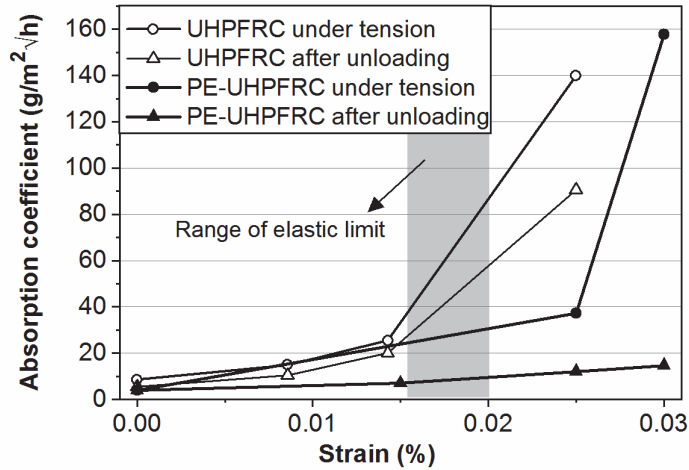
Fig. 18_ Capillary absorption of UHPFRC with steel fibers and PE-UHPFRC versus strain level

Moreover, the capillary absorption coefficient of steel fiber UHPFRC decreases by approximately 35% after unloading while according to Fig. 19, the capillary absorption of PE-UHPFRC decreases at least 10 times after unloading. This can be explained by different crack closure behaviors of these two materials after unloading. The stiffness of steel fibers hinders the closure of cracks, while synthetic fiber can hardly oppose to crack closure after unloading.
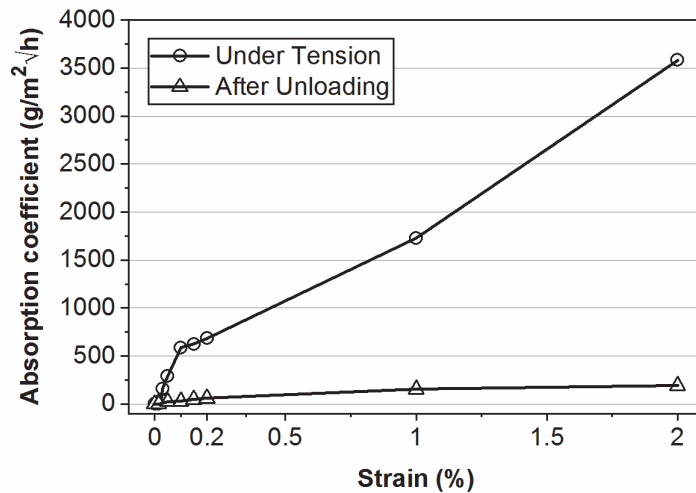
Fig. 19_ Average capillary absorption coefficient of the PE-UHPFRC versus strain level

The durability related requirements for the Serviceability Limit State (SLS) depend on both material properties and the expected service life of the structure. Considering that the expected service life for UHPFRC applications is the full service life of the structure without

107

any further rehabilitation, the UHPFRC layer should remain impermeable during the whole remaining service life of the structure after rehabilitation, to fulfill the SLS criteria. The French standard on UHPFRC [58] followed the normal and fiber-reinforced concrete codes [59] and recommended limitations on the maximum crack width for the durability related SLS. However, this approach is questionable according to the results of this study and other investigations reported in the literature [24,60]. As such, in order to provide proper protective function throughout the entire lifetime of the structure, the PE-UHPFRC layer should stay un-cracked. Thus, the sum of the tensile stresses in a PE-UHPFRC layer from internal and external action effects should remain below the tensile elastic limit of the material at SLS, from a purely local, deterministic point of view. However, further investigations should be carried out to generalize these findings to the determination of Serviceability Limit States for Strain Hardening UHPFRC in structural members considering the deterioration mechanisms followed by the ingress of liquids through microcracks in UHPFRC, with or without rebar.

5. Conclusions

The effect of the strain level on the capillary absorption of water in PE-UHPFRC was investigated in two ways: (I) under tension, using an original testing setup, and (II) after unloading, based on standards. According to the results,

- The cracking behavior of PE-UHPFRC was similar to that of other cementitious materials with high deformation capacity (ECC and SHCC), up to a strain level of 2%, and the cracks width similarly followed a lognormal distribution. The average crack width remained below 0.1 mm throughout the tensile behavior. However, for higher strain levels (3 and 4%), the crack width distribution changed towards a normal distribution.
- The capillary absorption of PE-UHPFRC after unloading was at least ten times less than that of SHCC, which is a comparable cementitious materials in terms of deformation capacity, at all the studied strain levels.
- There was a sudden significant increase in capillary absorption of UHPFRC (including literature) after the elastic limit under tensile loading.
- The capillary absorption of damaged PE-UHPFRC after unloading increased gradually with the strain level, and remained below 60.9 g/m^2√h even after experiencing a strain level of 0.2% before unloading.
- There was a considerable difference of approximately one order of magnitude in the rate of liquid ingress, when comparing the capillary absorption of same PE-

UHPFRC samples, under tension and after unloading. This highlights the necessity of developing more realistic test methods in order to define the durability properties and serviceability limit state of cementitious materials with high deformation capacity.

- Although crack width limitation is a necessary condition for durability, the density of the microstructure of the material plays an equally important role on transport properties and thereupon on its durability and protective properties.
- Fixing threshold values of crack width for durability must be done considering the relevant transport mechanisms.

Acknowledgments

References

1. Denarié, E., Kazemi Kamyab, M., Brühwiler, E., Haddad, B. G. & Nendaz, S. *Béton fibré ultra performant pour la maintenance, un nouvel élan. tracés n°12* 20–23 (2011).

2. Brühwiler, E. & Denarié, E. *Rehabilitation and strengthening of concrete structures using ultra-high performance fibre reinforced concrete*. Structural Engineering International: Journal of the International Association for Bridge and Structural Engineering (IABSE) 23, 450–457 (2013).

3. Denarié, E. & Brühwiler, E. *Cast-on site UHPFRC for improvement of existing structures–achievements over the last 10 years in practice and research*. 7th workshop on High Performance Fiber Reinforced Cement Composites, 1-3, June 2015, Stuttgart, Germany (2015).

4. Hajiesmaeili, A. & Denarie, E. *Next Generation UHPFRC for Sustainable Structural Applications*. ACI Special Publication 326, (2018).

5. Hall, C. *Water movement in porous building materials—I. Unsaturated flow theory and its applications*. Building and Environment 12, 117–125 (1977).

6. Lucas, R. *Rate of capillary ascension of liquids*. Kolloid Z 23, 15–22 (1918).

7. Washburn, E. W. *The dynamics of capillary flow*. Physical review 17, 273 (1921).

8. Bao, J. & Wang, L. *Capillary imbibition of water in discrete planar cracks*. Construction and Building Materials 146, 381–392 (2017).

9. Gardner, D., Jefferson, A. & Hoffman, A. *Investigation of capillary flow in discrete cracks in cementitious materials*. Cement and Concrete Research 42, 972–981 (2012).

10. Gardner, D., Jefferson, A., Hoffman, A. & Lark, R. *Simulation of the capillary flow of an autonomic healing agent in discrete cracks in cementitious materials*. Cement and Concrete Research 58, 35–44 (2014).

11. Zaccardi, Y. A. V., Alderete, N. M. & De Belie, N. *Improved model for capillary absorption in cementitious materials: Progress over the fourth root of time*. Cement and Concrete Research 100, 153–165 (2017).

12. Huang, H., Gao, X., Wang, H. & Ye, H. *Influence of rice husk ash on strength and permeability of ultra-high performance concrete*. Construction and Building Materials 149, 621–628 (2017).

13. Pyo, S. & Kim, H. K. *Fresh and hardened properties of ultra-high performance concrete incorporating coal bottom ash and slag powder*. Construction and Building Materials 131, 459–466 (2017).

14. Dobias, D., Pernicova, R. & Mandlik, T. *Water Transport Properties and Depth of Chloride Penetration in Ultra High Performance Concrete*. in *Key Engineering Materials* 711, 137–142 (Trans Tech Publ, 2016).

15. Wang, W. *et al. Durability of an Ultra High Performance Fiber Reinforced Concrete (UHPFRC) under progressive aging*. Cement and Concrete Research 55, 1–13 (2014).

16. Tam, C. M., Tam, V. W. Y. & Ng, K. M. *Assessing drying shrinkage and water permeability of reactive powder concrete produced in Hong Kong*. Construction and Building Materials 26, 79–89 (2012).

17. Mestrovic, D., Cizmar, D. & Stanilovic, V. *Reactive powder concrete: Material for the 21st century*. WIT Transactions on Engineering Sciences 57, 127–133 (2007).

18. Roux, N., Andrade, C. & Sanjuan M, A. *Experimental Study of Durability of Reactive Powder Concretes*. Journal of Materials in Civil Engineering 8, 1–6 (1996).

19. Toutlemonde, F. *et al. Long-term material performance checked on world's oldest UHPFRC road bridges at Bourg-Lès-Valence*. in *RILEM-fib-AFGC International symposium on UHPFRC* 265–274 (2013).

20. Toutlemonde, F. *et al. Field demonstration of UHPFRC durbility*. Concrete International 32, 39–45 (2010).

21. Sajna, A., Denarié, E. & Bras, V. *Assessment of UHPFRC based bridge rehabilitation in Slovenia, Two years after application*. in *Proceedings HIPERMAT 2012, 3rd International Symposium on Ultra-High Performance Concrete* (eds. Schmidt, M., Fehling, E., Glotzbach, C., Fröhlich, S. & Piotrowski, S.) 937–944 (Uni Kassel, 2012).

22. Kono, K. *et al. Durability study of the first PC bridge constructed with ultra high strength fiber reinforced concrete in Japan*. in *Proceedings of the RILEM-fib-AFGC International Symposium on Ultra-High Performance Fibre-Reinforced Concrete* 239–248 (2013).

23. Thomas, M. *et al. Marine performance of UHPC at Treat Island*. in *Proceedings of the 3rd International Symposium on UHPC and Nanotechnology for High Performance Construction Materials, Kassel, Germany* 365–370 (Uni Kassel, 2012).

24. Wittmann, F. H., Yao, X., Wang, P., Zhang, P. & Zhao, T. *Influence of an imposed tensile stress and subsequent self-healing on capillary absorption and chloride penetration into HPFRCC*. in *Seventh International RILEM Workshop on High Performance Fiber Reinforced Cement Composites (HPFRCC7)* 251–258 (2015).

25. Wang, R., Gao, X., Li, Q. & Yang, Y. *Influence of splitting load on transport properties of ultra-high performance concrete*. Construction and Building Materials 171, 708–718 (2018).

26. Wang, P., Yao, X., Wittmann, F. H., Zhang, P. & Zhao, T. *Influence of Imposed Compressive Stress and Subsequent Self-healing on Capillary Absorption and Chloride Penetration into UHPFRCC*. in *Seventh International RILEM Workshop on High Performance Fiber Reinforced Cement Composites (HPFRCC7)* 243–250 (2015).

27. Charron, J.-P., Denarié, E. & Brühwiler, E. *Transport properties of water and glycol in an ultra high performance fiber reinforced concrete (UHPFRC) under high tensile deformation*. Cement and Concrete Research 38, 689–698 (2008).

28. Ma, Z., Zhao, T. & Yao, X. *Influence of Applied Loads on the Permeability Behavior of Ultra High Performance Concrete with Steel Fibers*. Journal of Advanced Concrete Technology 14, 770–781 (2016).

29. Li, Y., Tan, K. H. & Yang, E.-H. *Influence of aggregate size and inclusion of polypropylene and steel fibers on the hot permeability of ultra-high performance concrete (UHPC) at elevated temperature*. Construction and Building Materials 169, 629–637 (2018).

30. Charron, J.-P., Denarié, E. & Brühwiler, E. *Permeability of ultra high performance fiber reinforced concretes (UHPFRC) under high stresses*. Materials and Structures 40, 269–277 (2007).

31. Li, V. C. *On engineered cementitious composites (ECC)*. Journal of advanced concrete technology 1, 215–230 (2003).

32. Curosu, I., Liebscher, M., Mechtcherine, V., Bellmann, C. & Michel, S. *Tensile behavior of high-strength strain-hardening cement-based composites (HS-SHCC) made with high-performance polyethylene, aramid and PBO fibers*. Cement and Concrete Research 98, 71–81 (2017).

33. Ranade, R., Li, V. C., Stults, M. D., Heard, W. F. & Rushing, T. S. *Composite Properties of High-Strength, High-Ductility Concrete*. ACI Materials Journal 110, (2013).

34. Wang, P. G., Wittmann, F. H., Zhang, P., Lehmann, E. H. & Zhao, T. J. *Observation of water penetration into cracked and water repellent SHCC after imposed strain by means of neutron radiography*. Restoration of Buildings and Monuments 20, 95–102 (2014).

35. Zhang, P., Wittmann, F. H., Villmann, B., Zhao, T. J. & Slowik, V. *Moisture diffusion in and capillary suction of integral water repellent cement based materials*. in *Proceedings of 5th International Conference on Water Repellent Treatment of Building Materials. Brussels, Belgium: Aedificatio Publishers* 273–286 (2008).

36. Mechtcherine, V. & Lieboldt, M. *Effect of cracking on air-permeability and water absorption of strain hardening cement-based composites*. in *Proceedings, Fifth International RILEM Workshop on High Performance Fiber Reinforced Cement Composites (HPFRCC 5)* 305–312 (2007).

37. Boshoff, W. P. & Adendorff, C. J. *Modelling SHCC cracking for durability*. Fracture and damage of advanced fibre-reinforced cement-based materials. Aedificatio Publishers, Dresden (2010).

38. Boshoff, W. P., Altmann, F., Adendorff, C. J. & Mechtcherine, V. *A new approach for modelling the ingress of deleterious materials in cracked strain hardening cement-based composites*. Materials and Structures 49, 2285–2295 (2016).

39. Şahmaran, M. & Li, V. C. *Influence of microcracking on water absorption and sorptivity of ECC*. Materials and structures 42, 593–603 (2009).

40. Lepech, M. & Li, V. C. *Water permeability of cracked cementitious composites*. Proceedings ICF11, 11th International Conference on Fracture (2002).

41. Lepech, M. D. & Li, V. C. *Water permeability of engineered cementitious composites*. Cement and Concrete Composites 31, 744–753 (2009).

42. Wittmann, F. H., Wang, P., Zhang, P., Zhao, T. & Beltzung, F. *Capillary absorption and chloride penetration into neat and water repellent SHCC under imposed strain*. in *2nd International RILEM Conference on Strain Hardening Cementitious Composites (SHCC2-Rio)* 165–172 (RILEM Publications SARL Rio de Janeiro, 2011).

43. Wittmann, F. H., Zhao, T., Tian, L., Wang, F. & Wang, L. *Aspects of durability of strain hardening cement-based composites under imposed strain*. in *Advances in Cement-Based Materials* (eds. Van Zijl, G. & Boshoff, W. P.) 173–179 (Taylor & Francis Group, 2010).

44. Zhang, P. *et al. Observation and quantification of water penetration into strain hardening cement-based composites (SHCC) with multiple cracks by means of neutron radiography*. Nuclear Instruments and Methods in Physics Research Section A: Accelerators, Spectrometers, Detectors and Associated Equipment 620, 414–420 (2010).

45. *BS EN 13057:2002, Determination of resistance of capillary absorption*. (British Standards Institution, 2002).

46. Fennis, S., Walraven, J. C. & Den Uijl, J. A. *Compaction-interaction packing model: regarding the effect of fillers in concrete mixture design*. Materials and structures 46, 463–478 (2013).

47. *ASTM C1437-15, Standard Test Method for Flow of Hydraulic Cement Mortar*. (ASTM International, 2015).

48. Neuber, H. *Der zugbeanspruchte Flachstab mit optimalem Querschnittsübergang*. Forschung im Ingenieurwesen A 35, 29–30 (1969).

49. Denarié, E., Maître, M., Conciatori, D. & Brühwiler, E. *Air permeability measurements for the assessment of the in situ permeability of cover concrete*. in *International Conference on Concrete Repair, Rehabilitation and Retrofitting, Cape Town, South Africa* 475–481 (2005).

50. Helbling, A. & Brühwiler, E. *Eine neue Halterung für Zugversuche mit Beton-Probekörper*. Material und Technik 15, 103–107 (1987).

51. Denarie, E. & Brühwiler, E. *Structural Rehabilitations with Ultra-High Performance Fibre Reinforced Concretes (UHPFRC)/Strukturelle Instandsetzung von Betonbrücken mit Ultra-hochleistungsfähigem Faserfeinkornbeton (UHFB)*. Restoration of Buildings and Monuments 12, 93–108 (2006).

52. Kamen, A., Denarie, E. & Brühwiler, E. *Thermal effects on physico-mechanical properties of ultra-high-performance fiber-reinforced concrete*. ACI materials journal 104, 415 (2007).

53. Loukili, A., Khelidj, A. & Richard, P. *Hydration kinetics, change of relative humidity, and autogenous shrinkage of ultra-high-strength concrete*. Cement and Concrete Research 29, 577–584 (1999).

54. Waller, V. *Relations entre composition des bétons, exothermie en cours de prise et résistance en compression*. in *Doctoral thesis* (Thèse de doctorat de L'école Nationale des Ponts et Chaussées, LCPC, 1999).

55. Jensen, O. M. & Hansen, P. F. *Water-entrained cement-based materials: I. Principles and theoretical background*. Cement and concrete research 31, 647–654 (2001).

56. Adendorff, C. J., Boshoff, W. P. & Van Zijl, G. *Characterisation of crack distribution of strain-hardening cement composites (SHCC) under imposed strain*. in *Advances in Cement-Based Materials* (2010).

57. Zhang, P., Ma, W., Wittmann, F., Wang, W. & Zhao, T. *Influence of Steel Fiber Content on Fracture Energy of HPFRCC*. in *High Performance Fiber Reinforced Cement Composites (HPFRCC7)* 119–125 (2015).

58. *NF P18-710: National addition to Eurocode 2–Design of concrete structures: Specific rules for ultra-high performance fiber-reinforced concrete (UHPFRC)*. AFNOR (2016).

59. *fib Model Code for Concrete Structures 2010. Ernst & Sohn* (2013).

60. Rafiee, A. *Computer modeling and investigation on the steel corrosion in cracked ultra high performance concrete*. Doctoral thesis 21, (2012).

Chapter 5

Paper 4

Life Cycle Analysis of Strengthening Existing RC Structures with R-PE-UHPFRC

1 – corresponding author - conducted all the calculations presented in the paper along with the writing of the full article

2 – thesis supervisor

3 – support for LCA tools and methods

Abstract

PE-UHPFRC, a novel Strain Hardening Ultra High-Performance Fiber Reinforced Concrete (UHPFRC) with low clinker content and synthetic fibers, was developed for structural applications of rehabilitation. A comprehensive Life Cycle Assessment (LCA) was carried out to study the environmental impact of interventions on an existing bridge using PE-UHPFRC compared with conventional UHPFRC and post-tensioned reinforced concrete methods in three categories of Global Warming Potential (GWP), Cumulative Energy Demand (CED), and Ecological Scarcity (UBP). The results showed 55% and 29% decrease in the environmental impact of the PE-UHPFRC method compared with reinforced concrete and conventional UHPFRC methods respectively, which highlighted the effectiveness of this material for rehabilitation/strengthening of structures from the viewpoint of environmental impact.

Keywords: UHPFRC; LCA; Sustainability; UHMW-PE fibers; Rehabilitation; Strengthening

1. Introduction

Over the last few decades, aging of transportation infrastructure systems became an acute societal issue and rehabilitation and strengthening of existing structures now prevail over new constructions. Considering Fig. 1 which shows the number of commissioned bridges per 5 years in Switzerland, it can be predicted that the need for rehabilitation of the bridges which were constructed in 1960-1980 with a planned service life of 50 years, will result in the near future in a much higher demand of resources and fundings. A similar scenario takes place in most of the developed countries, which have developed their infrastructures between the 60's and 80's. Material consumption and environmental issues of construction sites are heavy burdens for society in terms of economy and environment [1–3]. Thus, developing reliable and more efficient strategies and technologies of construction works are essential in order to *meet the needs of the present without compromising the ability of future generations to meet their own needs* [4] that is the concept of sustainable development.
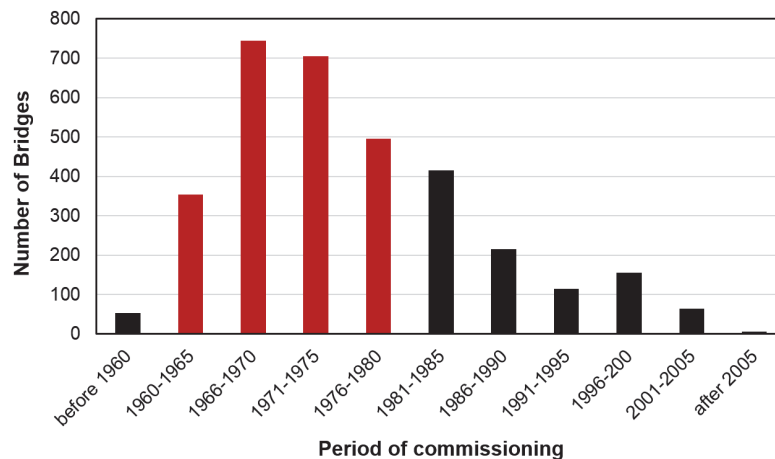
Fig. 1_ Number of commissioned bridges per 5 years in Switzerland [5]

The concept of rehabilitation and strengthening of existing bridges with UHPFRC for the whole service life was proposed by Brühwiler in 1999 after pioneering works of Bache et al. [6]. The basic idea was to use efficiently, as an "everlasting winter coat", a thin UHPFRC overlay in zones of severe mechanical and environmental exposure, where the outstanding UHPFRC properties in terms of durability and strength can be exploited effectively, with the UHPFRC alone or associated to rebar for strengthening applications. This idea was successfully implemented for rehabilitation and strengthening of road and railway infrastructures as well as buildings for over 15 years and extended to marine structures by Denarié [7–9].

Starting in 2007, Denarié et al. [10] developed for the first time Eco-UHPFRC mixes with massive use of limestone filler in replacement of clinker. These tensile strain hardening UHPFRC mixes were applied successfully at the industrial scale first to the rehabilitation of the Log Čezsoški bridge in Slovenia [11] (mix based mostly on local components) and later in Switzerland (also using mostly local components) for numerous rehabilitation sites, including thixotropic mixes applicable on slopes up to 12 % [12].

Habert et al. [13] performed a Life Cycle Analysis of the Log Čezsoški application in Slovenia, highlighting the significant improvements brought by low clinker mixes to the reduction of the Global Warming Potential (GWP). Rehabilitation methods using UHPFRC already decrease the environmental impact of construction sites by up to 50% [13] and considerably reduce the construction time compared to conventional methods. However, there is still a potential to improve this method even further and make it more sustainable focusing on the environmental cost of clinker and fibrous mixes used to achieve a robust strain hardening response. Considering that more than 95% of the environmental impact (GWP and Embodied Energy) of current UHPFRC is from the steel fibers and clinker contributions (48% and 47% respectively for GWP) [14,15], replacing the steel fibers with synthetic ones while also replacing clinker with SCM can reduce significantly the environmental costs of this material.

PE-UHPFRC is a newly developed UHPFRC mix in which the steel fibers are replaced with Ultra High Molecular Weight Polyethylene (UHMW-PE) ones and 50% of the clinker is replaced with limestone fillers [16]. The high tensile elastic limit above 7 MPa, the tensile strength of more than 10 MPa, and tensile deformation capacity of more than 3.5% make PE-UHPFRC well adapted for structural applications. This newly developed material has the potential to strongly decrease the environmental impact of UHPFRC rehabilitation/strengthening method. Additionally, the dead weight of PE fiber based UHPFRC mixes is significantly reduced compared to that of conventional UHPFRC with steel fibers (thanks to the 10 to 20 times reduction in the mass of the fibrous mix for comparable tensile properties).

The present study reports on the properties and advantages of a new Strain Hardening UHPFRC mix with synthetic PE fibers and reduced clinker content adapted for structural applications, in terms of consequences on reducing environmental burdens. In a first step, the properties of the material are presented. Secondly, the LCA method [17–20] is described, explaining the functional unit and the inventory data for this study. Finally, the environmental impact of three types of intervention on an existing bridge including (1)

demolition and reconstruction with post-tensioned reinforced concrete, (2) strengthening with steel fiber UHPFRC combined with rebar and (3) strengthening with PE-UHPFRC combined with rebar are evaluated in three categories of GWP, CED, and UBP.

2. Mix design and properties of PE-UHPFRC

In the newly developed *PE-UHPFRC* mix, the steel fibers were fully replaced by UHMW-PE ones and 50% volume of the clinker was replaced by two limestone fillers of different gradings (OMYA Betocarb®- HP SL and Betoflow®-D). The composition of the mix is given in Table 1. The fibrous mix consisted of 2% vol. 6 mm long, chopped UHMW-PE fiber type SK 99 from DSM Dyneema®. $Ca(NO_3)_2$ is added to improve the efficiency of the HRWRA in order to decrease its dosage.

Table 1_ Mix proportions of the PE-UHPFRC (Mix PE21)

Components	(kg/m^3)
Cement CEM I 52.5 HTS	508
Silica fume	178
Betocarb®- HP SL	170
Betoflow®-D	389
Fine sand (d_{50}=250 μm)	525
Quartz powder	223
Water	165
HRWRA	27
$Ca(NO_3)_2$	11
UHMW PE fibers (Dyneema® SK99)	19.6

Typical properties of PE-UHPFRC are presented in Table 2. The results are the average of fifteen dumbbell specimens based on [21] for the tensile properties, three cylinders based on [22] for compressive strength and six specimens based on [23] for capillary absorption coefficient, all at 28 days. Furthermore, at the fresh state, the air content and the specific weight of the material are 4.5 % and 2215 kg/m^3, respectively and the flow is 48% after ASTM C1437 [24], with a final diameter after 25 blows of 150 mm.

Table 2_ Properties of PE- UHPFRC (average values)

Properties	PE-UHPFRC
Tensile strength (MPa)	11.7
Tensile elastic limit (MPa)	7.7
Tensile strain at peak stress (‰)	35
Compressive strength (MPa)	120
Young's modulus (Gpa)	43
Sorptivity (g/m^2√h)	24
Specific weight (kg/m^3)	2215

3. Environmental evaluation method

3.1 Function unit and System boundaries

In this study, the LCA method based on ISO14040 [25] was chosen to perform an environmental evaluation and investigate the impact of the newly developed material with respect to other ones. As the alternative materials do not all have similar mechanical and durability properties compared with that of PE-UHPFRC, it was not sufficient to benchmark these materials per unit volume. Thus, different structural solutions with comparable performances in terms of protective function and load carrying capacity were compared and finally the opportunities to improve the environmental performance of the current techniques were identified. The *functional unit* was an intervention on the Guillermaux Bridge (restoration or replacement) that was built in 1920/21 in Payerne, Switzerland [26]. The original bridge structure was a massive reinforced concrete arch (span 34 m) with three hinges (at the arch crown and the two abutments) that carried a 6.5 m wide bi-directional roadway and sidewalks (10 m width in total). The Guillermaux Bridge, its arc and hinges before intervention are shown in Fig. 2.
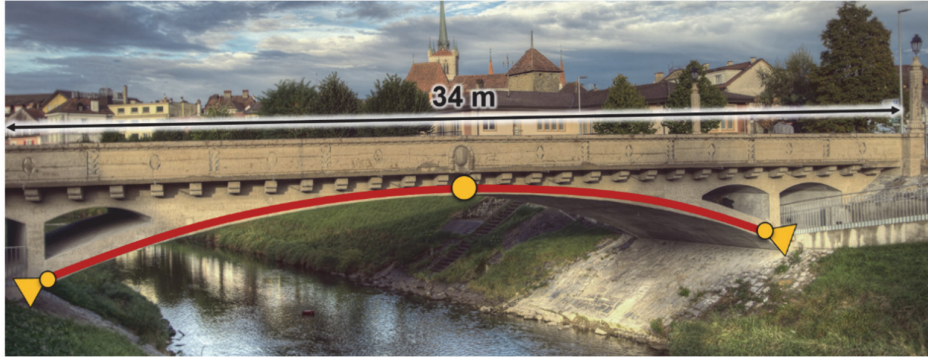
Fig. 2_ The Guillermaux Bridge, its arc and hinges before intervention

As the surface of the bridge was never protected with waterproofing, the concrete of the bridge structure showed signs of water infiltration, leachates, and corrosion. The requirement of utilization after the restoration was an unrestricted road traffic (after SIA 269/1 load models) including specially authorized exceptionally heavy vehicles. The environmental impact of three different methods that provide the same functions was compared:

1- Method 1 was demolition of the existing structure and construction of a new post-tensioned reinforced concrete (P-RC) bridge. For this scenario, the design from [27] of a new bridge with multiple T-section post-tensioned girders was used with the span and width corresponding to the existing structure in which the requirements for the clearance to the water level of river below was fulfilled. It was considered that the ready-mixed concrete was transported and placed on site for construction of the bridge. Fig. 3 shows the cross-section of the new structure [27].
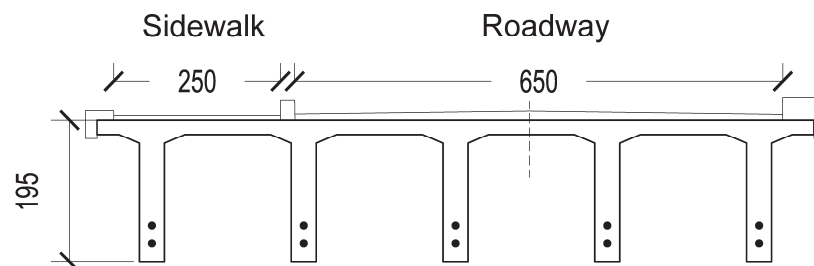
Fig. 3_ Cross section of post-tensioned girders (all dimensions in cm), method 1

2- Method 2 was strengthening the existing bridge with the help of steel fiber UHPFRC (S-UHPFRC) with rebar. In this method, a 50 mm thick layer of reinforced UHPFRC was cast over the entire length of the bridge's top surface, on the deck and internal faces of curbs, and was fixed at both extremities by new transition slabs anchored in the ground in order to

122

provide an R-UHPFRC tensile membrane. Furthermore, the hinge at the arch crown was locked using reinforced concrete such as to allow for bending resistance. Fig. 4 depicts the details of this method.

3- Method 3 was similar to method 2, but using PE-UHPFRC instead of S-UHPFRC.
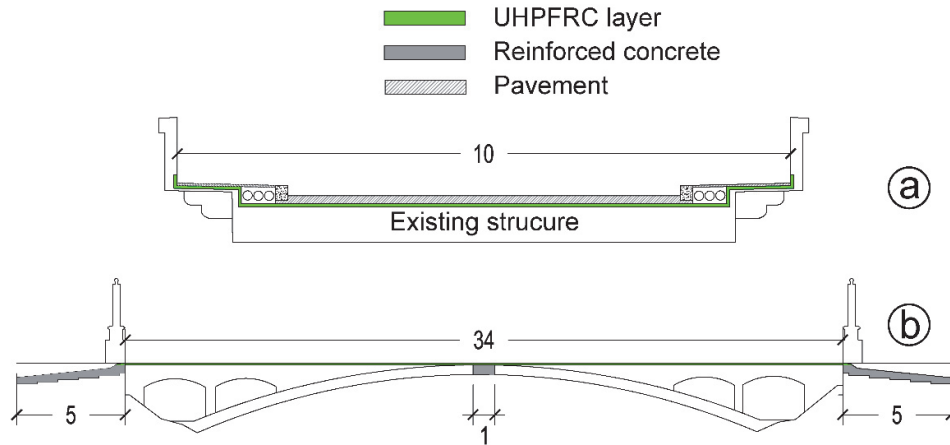
Fig. 4_ Cross section (a) and longitudinal cross-section (b) of the interventions using UHPFRC (all dimensions in m), methods 2 and 3.

The verification of the bridge after the interventions corresponding to a strengthening (methods 2 and 3) showed conformity factors with enough margin to accommodate traffic load models according to the standard applicable for new constructions (type II after SIA 261/1), corresponding to the verification in method 1 [28].

Fig. 5 presents the boundaries of the studied model, which take into account partial/full demolition and disposal of the existing structure as well as material production and transportation for renewal works. The same target service life of 100 years was considered for all methods. For the maintenance, the asphalt pavement has to be replaced every 25 years for all methods. Moreover, in case of method 1, the waterproofing membrane, deteriorated concrete underneath the waterproofing membrane, and the whole curbs have to be changed every 50 years. At the contrary, because of the very low water permeability of UHPFRC, it is possible to avoid the waterproofing membrane in method 1 and 2. Furthermore, considering the much higher durability of UHPFRC methods, no further concrete replacement is assumed to be needed. As the environmental impact of the daily traffic does not depend on the construction scenarios and is largely dominant during the service life of a bridge [29], this effect was not considered in order to be able to compare the impact of three different intervention methods.

123
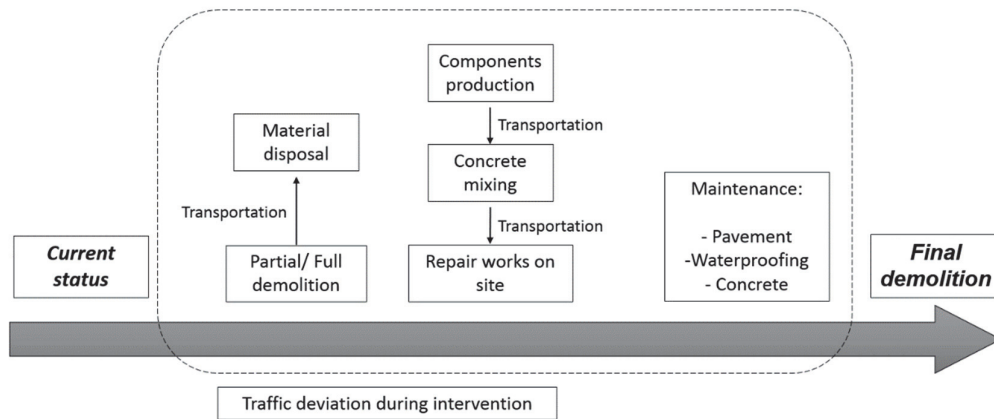
Fig. 5_ System boundaries for the restoration/renewal of the Guillermaux Bridge

The different steps for demolition and reconstruction with P-RC and strengthening with UHPFRC are presented in Table 3 and Table 4, respectively. The transport distances for disposal, formworks, steel rebars, post-tensioning cables, ready-mix concrete, waterproofing membrane, and hot mix asphalt, are also given in the same tables. It was assumed that the UHPFRC is prepared on site, using portable mixers.

Table 3_ Operations for demolition and reconstruction (method 1)

	Description	*Quantity*	*Distance*
Construction	Demolition and disposal of the existing bridge	360 m^3	50 km
	Formworks	8.2 t	30 km
	Reinforcing steel	34.5 t	83 km
	Post-tensioning cables	7.8 t	83 km
	Concrete for girders and slab	237.6 m^3	8 km
	waterproofing membrane	340 m^2	50 km
	Asphalt pavement	18.9 m^3	51.7 km
Maintenance	Removing and disposal of pavement	16 m^3	50 km
	New pavement	16 m^3	51.7 km
	Removing and disposal of pavement	18.9 m^3	50 km
	Removing and disposal of deteriorated concrete	10 m^3	50 km
	Removing and disposal of waterproofing	340 m^2	50 km
	New waterproofing	340 m^2	50 km
	New concrete	10 m^3	8 km
	New pavement	18.9 m^3	51.7 km
	Removing and disposal of pavement	16 m^3	50 km
	New pavement	16 m^3	51.7 km

124

Table 4_ Operations for strengthening with S/PE-UHPFRC and rebar (methods 2 and 3)

	Description	Quantity	Distance
Strengthening	Removing and disposal of pavement	18.9 m³	50 km
	Removing and disposal of deteriorated concrete	17 m³	50 km
	High-pressure water jetting	5 h	-
	Reinforcing steel	13.3 t	83 km
	Concrete	45 m³	8 km
	S/PE-UHPFRC	21.5 m³	Per component
	Gravel	46 m³	98 km
	Asphalt pavement	18.9 m³	51.7 km
Maintenance	Removing and disposal of pavement	16 m³	50 km
	New pavement	16 m³	51.7 km
	Removing and disposal of pavement	16 m³	50 km
	New pavement	16 m³	51.7 km
	Removing and disposal of pavement	16 m³	50 km
	New pavement	16 m³	51.7 km

The mix proportions and amounts of concrete and UHPFRC materials that are needed for different methods as well as the transport distance of the different components (to ready-mix plant for concrete and to site for UHPFRC) are shown in Table 5, Table 6, and Table 7 for P-RC, S-UHPFRC, and PE-UHPFRC methods, respectively. It should be noted that method 2 was applied on the bridge deck in 2016 [26] and the UHPFRC used was the proprietary mix HOLCIM 707 [30]. As an approximation, the recipe of a closely related material of know composition (HIFCOM 13s) was used in this study, with a fiber dosage corresponding to that of HOLCIM H707.

Table 5_ Material mix design for demolition and reconstruction with R-PC (method 1)

Material components	Distance (km)	Mix design (kg/m³)		Total (kg)
		C30/37	C20/25	
CEM I 42.5 R	41	350	280	80,010
Water	-	180	168	42,216
Sand	98	650	650	15,4375
Gravel	98	1,200	1,300	28,9450
HRWRA	30	5	1.5	1,032
Total volume (m³)		193	44.5	

Table 6_ Material mix design for S-UHPFRC (method 2)

Material components	Distance (km)	Mix design (kg/m³)		Total (kg)
		S-UHPFRC	Concrete	
CEM I 42.5 R	41		385	17,325
CEM III/B 32.5 N	41	1,277		27,455
Silica fume (I)	685	96		2,064
Fine quartz sand (I)	550	643		13,824
Sand	98		690	31,050
Gravel	98		1,030	46,350
Water	-	173	185	12,044
HRWRA	30	42	4.9	1,123
Steel fibers	20,780[1]	298		6,407
Total volume used	(m³)	21.5	45	

[1] 150 Truck + 2,630 Train + 18,000 Ship

Table 7_ Material mix design for PE-UHPFRC (method 3)

Material components	Distance (km)	Mix design (kg/m³)		Total (kg)
		PE-UHPFRC	Concrete	
CEM I 52.2 N	410	508		10,922
CEM I 42.5 R	41		385	17,325
Silica fume	482	178		3,827
Limestone filler	698[1]	559		12,018
Quartz powder	144	223		4,794
Fine quartz sand	336	525		11,287
Sand	98		690	31,050
Gravel	98		1,030	46,350
Water	-	165	185	11,872
HRWRA	30	27	4.9	801
PE fibers	25,950[2]	19.6		421.4
Total volume used	(m³)	21.5	45	

[1] 112 Truck + 586 Train
[2] 150 Truck + 1,060 Train + 24,740 Ship

Table 8 shows the production location, transport distance and the transport type of the different components.

Table 8_ Transport distances (km) of the different components

Component	Location	Truck	Train	Ship
CEM I 52.5 N	Le Teil, France	410		
CEM I 42.5 R	Eclépens, Switzerland	41		
CEM III/B 32.5 N	Untervaz, Switzerland	285		
Silica fume (I)	Pocking, Germany	685		
Silica fume (II)	Le Pontet, France	482		
Limestone fillers	Perpignan, France	112	586	
Quartz powder	Basel, Switzerland	144		
Fine quartz sand (I)	Baumbach, Germany	550		
Fine quartz sand (II)	Hostun, France	336		
Sand and Gravel	Marin, Switzerland	35		
HRWRA	Düdingen, Switzerland	30		
Steel fibers	China	150	2,630	18,000
PE fibers	Japan	150	1,060	24,740
Steel reinforcement	Gerlafingen, Switzerland	83		

3.2 Inventory data and Impact assessment

The environmental impact of the different methods was investigated considering three impact categories, with a time horizon of one hundred years: Global Warming Potential (GWP_{100}), which is expressed in kg CO_{2-eq}, Cumulative Energy Demand (CED), which is expressed in MJ, and Ecological Scarcity (UBP), which measures in a single weighted indicator by ecopoints, the contribution of the processes on the overall environmental impacts, including toxicity.

The assessment methods used in this study are harmonized with the methods adopted by Koordinationskonferenz der Bau- und Liegenschaftsorgane der öffentlichen Bauherren (KBOB) [31], a well-established LCA dataset for construction products in Switzerland. The GWP_{100} was assessed by using the IPCC 2013 method [32] while the Cumulative Energy Demand 1.09 Method was considered for CED calculation [33]. Finally, the UBP indicator was calculated according to the Ecological Scarcity 2013 Method [34], an indicator particularly suitable for Switzerland as it employs eco-factors based on Swiss environmental targets and legislation.

Secondary data from Ecoinvent 3 [35] -currently the most reliable database for Swiss unit processes- were assumed for material processes, freights transportation, energy and waste treatments, and SimaPro 8.5 was used as a software to model the processes [36]. The allocation at the point of substitution was considered as the most representative for process modeling, and data from the library "unit process" adopted.

The environmental burdens from production and transportation of components were considered and calculated with the original system boundaries of the Ecoinvent database. All the production processes not included in the Ecoinvent database, namely for silica fume, HRWRA, steel fibers, and PE fibers, were modeled using secondary data from literature [13,37–39]. As it was shown that the environmental loads from the transportation of the construction equipment to the site are negligible [27,40,41], this impact was not included in the investigation.

Two criteria were considered to define the system boundaries for products processing. The first one considers the 2nd order calculation depth, which includes materials used for processing, transport, and other operations. The second one considers the cut-off method, which defines when a flow is no longer relevant to the system. Thus, by-products, such as recycled materials or production residues, are outside the system boundaries. All benefits and loads beyond the system boundaries, e.g. recycling potential, energy recovering, etc., were not taken into account. In the end of life (EoL) model, a landfill scenario was assumed for demolished materials. A process for onsite demolition, crushing, and disposal in an inert landfill was assumed for disposing of concrete, while a specific process for a sanitary landfill was assumed for asphalt and waterproofing membrane.

4. Results and Discussion

Three different levels of evaluation were investigated. In the first level, only the impact of components production on environmental burdens of the bridge intervention was considered. The second level considered the effect of all the steps that are needed for the intervention on the bridge including the impact of demolition works, and transportation of the components and materials. Finally, the third level investigated the environmental impact of the bridge through its lifetime, considering the required maintenance works.

As a first step of the environmental analysis, a comparison based on the impacts of material processing for the interventions carried out and the results are shown in Fig. 6. In this figure, the results were normalized based on those for method 1 and 100% stands for 151.3 t CO_{2eq},

1505.8 GJ and 264.6 MPt in GWP, CED and UBP categories, respectively. The reinforcement (steel rebars and tendons), steel fibers, and cement accounted for the highest impact at this scale. In CED category, the production of asphalt pavement is responsible for approximately 7% of the overall impact.

In case of the PE-UHPFRC method, it would be possible to avoid the bituminous pavement and process the PE-UHPFRC surface to achieve an integral pavement with sufficient skid resistance, which can pave the way to additional reduction in the environmental impact. Furthermore, the rebars account for approximately 50% of the environmental impact in thr PE-UHPFRC method, which indicates the greater potential of this material to decrease even more the environmental impact for rehabilitation applications without reinforcement compared with that of methods using P-RC or S-UHPFRC.
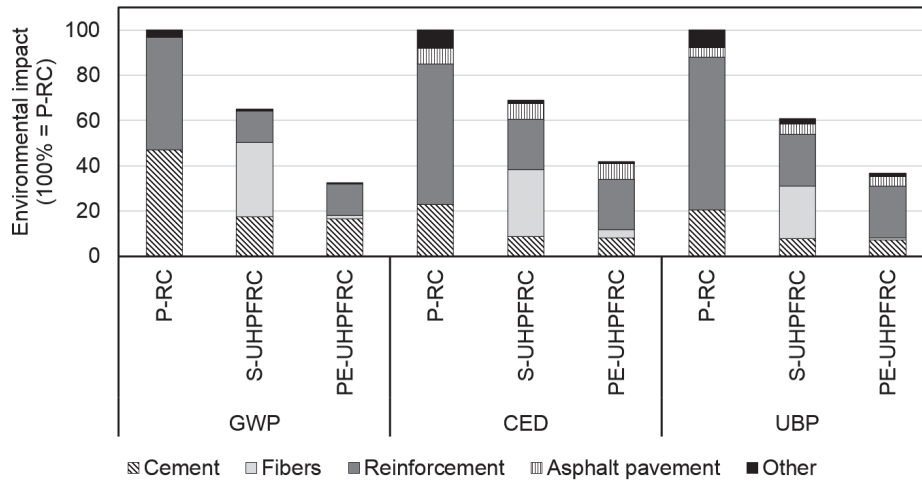
Fig. 6_ Normalized environmental impact at the structure scale (only materials)

Fig. 7 presents the LCA results of the restoration of the bridge, normalized based on those for method 1 with P-RC. Considering the whole process of restoration, production of the components has the largest influence on the environmental impact, while transportation is responsible for almost 10% of the total impact.
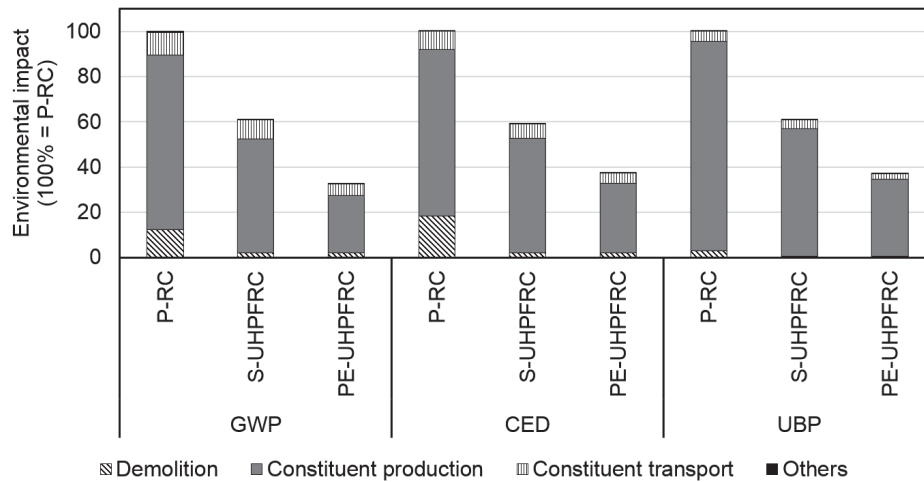
Fig. 7_ Normalized environmental impact at the scale of the structure (without maintenance)

Fig. 8 shows the total environmental impact of the different methods over the lifetime of the bridge (100 years), according to the three different categories of environmental indices. The use of UHPFRC resulted in a reduced environmental impact of the bridge intervention in all the cases. The GWP decreased by 40% and 70% by using S-UHPFRC and PE-UHPFRC, respectively. Furthermore, a similar trend was achieved for CED and UBP.
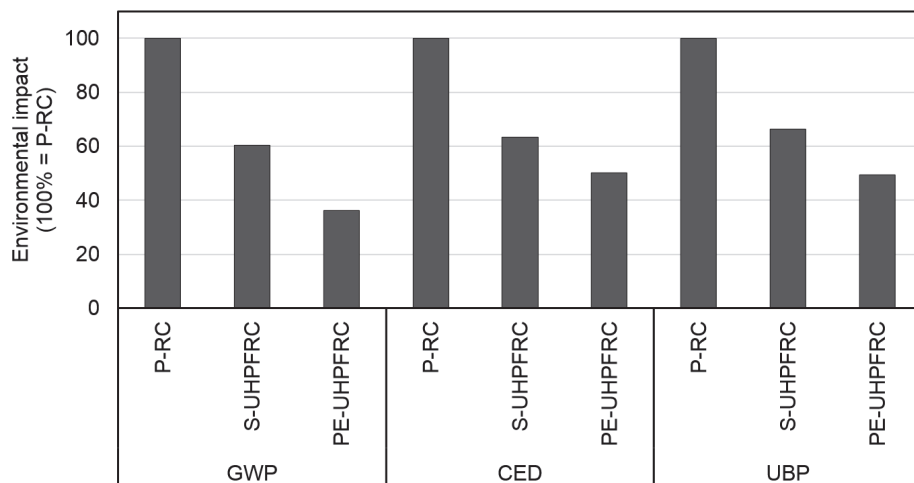
Fig. 8_ Normalized environmental impact over the life cycle of 100 years

It should be noted that the environmental effect of traffic deviation during the site works was not accounted for in this study. However, Habert et al. [13] showed that taking traffic deviation into account is beneficial for UHPFRC methods as the duration of site works for a P-RC method is almost three times more than that for a method using UHPFRC.

5. Conclusions

- A novel structural UHPFRC with synthetic fibers was introduced for rehabilitation and strengthening of existing structures.
- The LCA showed 55% and 29% decrease in the environmental impact of the strengthening method using PE-UHPFRC compared with that of the replacement with a new bridge, and of conventional UHPFRC methods for restoration a 34 m span road bridge, respectively. This highlights the strong potential of PE-UHPFRC in reducing the environmental impact of construction sites.
- This reduction will be even more pronounced for rehabilitation applications without rebar (pure protective function of the UHPFRC overlay).
- The reinforcement (steel rebars and tendons), steel fibers, and cement accounted for the highest environmental impact among the material components.
- The production and casting of the asphalt pavement are responsible for approximately 7% of the cumulative energy demand of all methods. The possibility of avoiding the asphalt pavement in the PE-UHPFRC method opens up the possibility of additional reductions in the environmental impact of rehabilitation/strengthening sites and simplifications of the associated construction works.

Acknowledgments

References

1. Solomon, S., Qin, D., Manning, M., Averyt, K. & Marquis, M. *Climate change 2007-the physical science basis: Working group I contribution to the fourth assessment report of the IPCC*. 4, (Cambridge university press, 2007).

2. Corvalan, C., Hales, S. & McMichael, A. *Ecosystems and human well-being*. in *Millennium Ecosystem Assessment* (Island press, 2005).

3. Stern, N. *The economics of climate change: the Stern review*. (cambridge University press, 2007).

4. Brundtland, G. H., Khalid, M., Agnelli, S. & Al-Athel, S. *Our common future*. in *Report of the World Commission on Environment and Development* (1987).

5. Cuche, A. *et al. Rapport sur l'état du réseau des routes nationales 2016. OFROU* 14 (2016).

6. Buitelaar, P. *Ultra high performance concrete: developments and applications during 25 years*. in *Plenary session International Symposium on Ultra High Performance Concrete. Kassel* (2004).

7. Denarié, E. & Brühwiler, E. *Cast-on site UHPFRC for improvement of existing structures–achievements over the last 10 years in practice and research*. 7th workshop on High Performance Fiber Reinforced Cement Composites, 1-3, June 2015, Stuttgart, Germany (2015).

8. Brühwiler, E. & Denarié, E. *Rehabilitation and strengthening of concrete structures using ultra-high performance fibre reinforced concrete*. Structural Engineering International 23, 450–457 (2013).

9. Brühwiler, E. & Bastien Masse, M. *Strengthening the Chillon viaducts deck slabs with reinforced UHPFRC. IABSE Conference Geneva 2015 'Structural Engineering: Providing Solutions to Global Challenges'* 1171–1178 (2015).

10. Denarié, E. *ARCHES D06: Recommendations for the tailoring of UHPFRC recipes for rehabilitation*. in *European project 6th FWP / ARCHES Assessment and Rehabilitation of Central European Highway Structures, WP 5 – 'Harden Structures to last with UHPFRC'* (2009).

11. Denarié, E., Habert, G. & Šajna, A. *ARCHES D14 - Recommendations for the use of UHPFRC in composite structural members – rehabilitation Log Čezsoški bridge*. in *European project 6th FWP / ARCHES Assessment and Rehabilitation of Central European Highway Structures, WP 5 – 'Harden Structures to last with UHPFRC'* (MCS/EU PP - Lausanne/Brussels, 2009).

12. Denarié, E. & Brühwiler, E. *Strain-hardening ultra-high performance fibre reinforced concrete: deformability versus strength optimization*. Restoration of Buildings and Monuments 17, 397–410 (2011).

13. Habert, G., Denarié, E., Šajna, A. & Rossi, P. *Lowering the global warming impact of bridge rehabilitations by using Ultra High Performance Fibre Reinforced Concretes*. Cement and Concrete Composites 38, 1–11 (2013).

14. Stengel, T. & Schießl, P. *Life cycle assessment (LCA) of ultra high performance concrete (UHPC) structures*. in *Eco-efficient construction and building materials* (eds. Pacheco-Torgal, F., Cabeza, L. F., Labrincha, J. & de Magalhães, A. B. T.-E. C. and B. M.) 528–564 (Woodhead Publishing, 2014). doi:https://doi.org/10.1533/9780857097729.3.528

15. Stengel, T. & Schießl, P. *Sustainable construction with UHPC–from life cycle inventory data collection to environmental impact assessment*. in *Proceedings of the 2nd international symposium on ultra high performance concrete. Kassel University Press, Kassel* 461–468 (2008).

16. Hajiesmaeili, A. & Denarie, E. *Next Generation UHPFRC for Sustainable Structural Applications*. ACI Special Publication 326, (2018).

17. Fava, J. A. *Will the next 10 years be as productive in advancing life cycle approaches as the last 15 years?* The International Journal of Life Cycle Assessment 11, 6–8 (2006).

18. Asif, M., Muneer, T. & Kelley, R. *Life cycle assessment: A case study of a dwelling home in Scotland*. Building and environment 42, 1391–1394 (2007).

19. Bouhaya, L., Le Roy, R. & Feraille-Fresnet, A. *Simplified environmental study on innovative bridge structure*. Environmental science & technology 43, 2066–2071 (2009).

20. Ortiz, O., Castells, F. & Sonnemann, G. *Sustainability in the construction industry: A review of recent developments based on LCA*. Construction and building materials 23, 28–39 (2009).

21. Hajiesmaeili, A. & Denarié, E. *Capillary flow in UHPFRC with synthetic fibers, under high tensile stresses*. Construction and Building Materials (2019).

22. *SIA 2052, "Béton fibré ultra-performant (BFUP): Matériaux, dimensionnement et exécution"*. (Cahier Technique, 2017).

23. *BS EN 13057:2002, Determination of resistance of capillary absorption*. (British Standards Institution, 2002).

24. *ASTM C1437-15, Standard Test Method for Flow of Hydraulic Cement Mortar*. (ASTM International, 2015).

25. *ISO 14040 - Environmental Management: Life Cycle Assessment; Principles and Framework*. in *International Organization for Standardization* (2006).

26. Brühwiler, E. & Schiltz, P. *Le BFUP pour ajouter de la plus-value aux ouvrages en béton armé*. TRACÉS 02, 6–10 (2018).

27. Kawai, K., Sugiyama, T., Kobayashi, K. & Sano, S. *Inventory data and case studies for environmental performance evaluation of concrete structure construction*. Journal of Advanced Concrete Technology 3, 435–456 (2005).

28. Loraux, C. & Denarié, E. *Vérification de la sécurité structurale du Pont de Guillermaux à l'état actuel et après la rénovation*. in *Rapport n° MCS 23.13.07-1* (2014).

29. Beuving, E., De Jonghe, T., Goos, D., Lindahl, T. & Stawiarski, A. *Environmental impacts and fuel efficiency of road pavements*. European Roads Review (2004).

30. HOLCIM. *Béton fibré à ultra haute performances – produits et applications*. Holcim (Suisse) SA (2011).

31. KBOB. *Betonsortenrechner*. (2019).

32. Krey, V. *et al. Annex II: metrics & methodology ed O Edenhofer et al*. in *Climate Change 2014: Mitigation of Climate Change, Contribution of Working Group III to the Fifth Assessment Report of the Intergovernmental Panel on Climate Change* 1281–1328 (Cambridge: Cambridge University Press, 2014).

33. Hischier, R. *et al. Implementation of Life Cycle Impact Assessment Methods*. Swiss Centre for Life Cycle Inventories, Dubendorf, Switzerland 176 (2010).

34. Frischknecht, R. & Knöpfel, S. B. *Ecological scarcity 2013—new features and its application in industry and administration—54th LCA forum, Ittigen/Berne, Switzerland, December 5, 2013*. The International Journal of Life Cycle Assessment 19, 1361–1366 (2014).

35. Wernet, G. *et al. The ecoinvent database version 3 (part I): overview and methodology*. The International Journal of Life Cycle Assessment 21, 1218–1230 (2016).

36. *PRé Consultants, What's New in SimaPro 8.3*. (2016).

37. Häner, A., Schluep, M. & Gälli, R. *MASS FLOW AND RISK ANALYSIS OF MODERN SUPERPLASTICISERS*. in *ORGAGEC Symposium* 6–7 (Citeseer, 2005).

38. Chen, C. *Une étude des bétons de construction classiques et alternatifs par la méthode d'analyse du cycle de vie*. Composite structures (2009).

39. Cicala, G. & Lo Faro, C. *Material Selection: Polymeric Composites Matrix*. Wiley Encyclopedia of Composites 1–38 (2011).

40. Ventura, A., Mazri, C., Monéron, P., Jullien, A. & Schemid, M. *Environmental comparison of pavement binding courses recycled at varying rates by means of the Life Cycle Analysis method*. Bulletin des laboratoires des ponts et chaussées 250, 251 (2004).

41. Xing, S., Xu, Z. & Jun, G. *Inventory analysis of LCA on steel-and concrete-construction office buildings*. Energy and Buildings 40, 1188–1193 (2008).

Chapter 6

Conclusions and Outlook

1. Overview

With respect to the objectives set in the introduction of this document, the main findings of the thesis are summarized in this chapter under the following five headings and will be described briefly in the upcoming section.

1. Development of PE-UHPFRC
2. Delayed response of PE-UHPFRC under full restraint condition
3. Crack characteristics of PE-UPFRC at different strain levels
4. Capillary absorption of PE-UPFRC at different strain levels
5. Environmental impact of PE-UHPFRC at the structural level

2. Synthesis of main findings

2.1 Development of PE-UHPFRC

I. The generalized Compaction-Interaction Packing Model (CIPM), which considers multiple grain classes with arbitrary PSD as well as interaction functions for the particles smaller than 125 μm, was developed as a tool to optimize cementitious matrices.

II. A structural UHPFRC with synthetic fibers was developed with 120 MPa compressive strength, 43 GPa elastic modulus, above 7.7 MPa tensile elastic limit, 11.7 MPa tensile strength, and more than 3.5% tensile deformation capacity on average.

III. The PE-UHPFRC mix showed a robust strain hardening and the amplitude of the stress fluctuations in the hardening zone were much lower compared with that in other results from literature [1]. The scatter of the tensile elastic limit was very low with a standard deviation of only 0.7 MPa (over 15 specimens tested).

IV. The PE-UHPFRC mix is optimal from the structural viewpoint, for use with rebar, considering its extremely high deformation capacity. Reinforced PE-UHPFRC structures can be designed with full structural ductility.

V. The setting time of PE-UHPFRC was significantly reduced (from 14 to 4 h) compared with that of conventional UHPFRC, which can be beneficial both for cast-in-situ and precast applications.

VI. Use of quartz sand in the mixture, with less paste, improved the tensile elastic limit of the mix, which was in accordance with the packing density values of the mixes. However, the tensile strength of the mix with sand was lower than that of the mix without sand. Considering the PE fibers diameter of 12 μm, quartz sand had a negligible role in the bond between matrix and fibers. Therefore, the reduction of the tensile strength in the mixes with sand can be explained considering that adding sand decreased by 25% the volume of the other finer powders that could contribute positively to the bond of the fibers.

VII. Using quartz powder in the mix design considerably improved both the tensile elastic limit and the tensile strength of the mixes. This can be explained by a lower water/fines ratio of the mixes with quartz powder and by the very high form factor of this powder, which improved the interlocking of the grains and enhanced the bond between matrix and fibers.

VIII. The elastic modulus of the fibers affected both the tensile elastic limit and the tensile strength of the mixes. The average elastic limit of the composite increased from 6 to 7.7 MPa by a 37% increase in the elastic modulus of the fibers.

2.2 Delayed response of PE-UHPFRC under full restraint conditions

I.   The autogenous shrinkage was 2 to 3 times higher in PE-UHPFRC compared with that of conventional UHPFRC in the first days; however, this difference was reduced to 25% at 28 days. The stiff steel fibers skeleton resisted against the autogenous deformations and reduced the autogenous shrinkage at early ages while the flexible PE fibers could not hinder those autogenous deformations.

II.   PE-UHPFRC showed 70% and 50% lower eigenstresses under full restraint conditions compared with that of conventional UHPFRC with steel fibers with no clinker replacement, and with 50% reduced clinker, respectively. The lower value of eigenstresses in PE-UHPFRC can be explained by two reasons. First, Hafiz et al. [2] showed a higher viscoelastic response for the mixes with a higher dosage of limestone filler (S-LF-UHPFRC) which results in a higher relaxation potential and helps in relaxing the developed eigenstresses. Second, concerning the fibrous mix, it was shown that using fibers with a smaller diameter increases creep in tension [3]. Thus, the smaller diameter of the PE fibers compared to the steel fibers can lead to that of higher tensile creep in PE-UHPFRC mixes and consequently provide greater stress relaxation.

2.3 Crack characteristics of PE-UPFRC at different strain levels

I.   The tensile test specimens exhibited a dense multiple cracking behavior and the average crack width remained below 20 µm up to a strain level of 0.2%, which is approximately the yield strain of conventional steel reinforcement bars. Furthermore, the average crack widths did not exceed 0.1 mm even up to a very high strain level of 4.5%.

II.   The cracking behavior of PE-UHPFRC was similar to that of other cementitious materials with high deformation capacity (ECC and SHCC) [4–6], up to strain level of 2%, and the cracks width similarly followed a lognormal distribution.

III.   The crack width distribution changed towards a normal distribution for higher strain levels (3 and 4%).

2.4 Capillary absorption of PE-UPFRC at different strain levels

I. The influence of the tensile strain level on the capillary absorption of PE-UHPFRC under loading was negligible before the elastic limit; however, there was a sudden significant increase in capillary absorption of PE-UHPFRC after the elastic limit under tensile loading, reaching immediately values above 100 $g/m^2\sqrt{h}$, whereas the value was 24 $g/m^2\sqrt{h}$ before cracking.

II. The capillary absorption of damaged PE-UHPFRC specimens after unloading was at least ten times less than that of SHCC, which is a comparable cementitious material in terms of deformation capacity, at all the studied strain levels.

III. The capillary absorption of damaged PE-UHPFRC specimens after unloading increased gradually with the maximum experienced strain level and remained below 60.9 $g/m^2\sqrt{h}$ after experiencing a strain level of 0.2%.

IV. There was a considerable difference of approximately one order of magnitude, in the rate of liquid ingress, when comparing the capillary absorption of the same PE-UHPFRC samples, under tension and after unloading. However, there are only a few studies, which considered the effect of tensile stresses on transport properties of cementitious materials under loading [7,8]. The reported capillary absorption and permeability of the damaged cementitious material are mostly based on the methods prescribed by standards. This highlights the necessity of developing more realistic test methods in order to define the durability properties and serviceability limit states of cementitious materials with high deformation capacity, under loading.

V. Although crack width limitation is a necessary condition for durability, the density of the microstructure of the material plays an equally important role in transport properties and thereupon on its durability and protective properties. As such, limiting crack width or using a self-healing potential [9] cannot compensate for an intrinsically poor matrix with respect to transport properties.

2.5 Environmental impact of PE-UHPFRC

I.   The environmental impact of the PE-UHPFRC mix in terms of embodied energy was reduced by 70% compared to that of a typical UHPFRC mix with steel fibers with similar properties, by replacing steel fibers with UHMW-PE fibers and replacing 50% vol. of clinker with limestone filler.

II.   A LCA showed 55% and 34% decrease on average in the environmental impact (CO_2 emission, embodied energy and toxicity) of the interventions using PE-UHPFRC (strengthening, with rebar) compared to that for interventions with normal concrete (replacement of the bridge) respectively, and conventional UHPFRC (strengthening, with rebar) for the restoration of a 34 m span road bridge.

3.   Perspectives and future works

In the framework of future research, works motivated by the conclusions of this thesis could be undertaken in the following domains:

3.1 Development of sprayable PE-UHPFRC mixes

The use of flexible synthetic fibers and the thixotropic properties of PE-UHPFRC at fresh state make it a good candidate for the tailoring to shotcrete applications. Sprayable mixes will not only be suitable for protecting vertical surfaces like bridge piers and walls but also for tunnels construction and maintenance. In order to develop a sprayable material, the rheology of the mix should be modified to have shear thinning properties at fresh state to facilitate pumping, combined with a sufficient yield stress. The mechanical and protective properties of the sprayed mix should be investigated on representative specimens cut out of larger plates cast using the spraying technology.

3.2 Investigation of the mechanical behavior of R-PE-UHPFRC

Oesterlee [10], Noshiravani [11], Makita [12], and Bastien Masse [13] have studied the structural response of Reinforced conventional UHPFRC with steel fibers. The combination of high deformation capacity of PE-UHPFRC with that of reinforcement bars in direct tension and bending (R-PE-UHPFRC) opens up a new field of study, especially to investigate the deformation compatibility and composite integrity of PE-UHPFRC and steel reinforcement in R-PE-UHPFRC at higher strain levels. Furthermore, the behavior of R-PE-

UHPFRC under cyclic loading needs to be investigated in order to confirm their efficiency in terms of energy dissipation for example for seismic retrofitting [14]. Fischer et al. [15,16] investigated the tensile and bending behavior of reinforced ECC elements and confirmed deformation compatibility between ECC and steel rebars.

3.3 Investigation of the protective function of PE-UHPFRC using a probabilistic approach

Although a detailed investigation on the effect of damage on capillary absorption at different strain levels had been realized in this study, another comprehensive experimental campaign should be carried out on the deterioration mechanisms followed by the ingress of catalysts of corrosion like water and aggressive agents in the material. A probabilistic model needs to be developed in order to define appropriate Serviceability Limit States for the material regarding durability issues.

3.4 Investigation and modeling of the creep at meso and macro-level

In order to appropriately use PE-UHPFRC in the construction industry, it is essential to understand and characterize its time-dependent properties. To identify the time-dependent behavior, creep tests are needed on the meso-level (a level where the pull-out of a fiber and their mechanical response are prominent) and at the macro-level. As such, an experimental campaign is needed to investigate the fiber and pull-out creep in meso-level and tensile and compressive creep of the material in macro-level at different ages and stress levels. The results should be used to develop a creep and shrinkage model in order to fully characterize the time-dependent properties of PE-UHPFRC.

3.5 Modeling the bending response

On account of challenges for characterization of UHPFRC tensile response with the direct uniaxial tensile tests, unnotched bending tests associated to inverse analysis methods [17–20] are suggested for determination of tensile properties of this material by Swiss recommendations for UHPFRC [21] and French standard on UHPFRC [22]. However, the accuracy of this method to predict the ultimate tensile strength in the case of cementitious materials with a very high tensile deformation capacity (several %) decreases due to the large deflections under loading which are not considered in the analytic base of the models. Although a simplified inverse analysis method for SHCC was introduced by [23], further study of the bending response of PE-UHPFRC is needed for the development of suitable inverse analysis methods for this material.

3.6 Investigation of the fatigue behavior

Considering the rehabilitation of bridge deck slabs as one of the most important applications of PE-UHPFRC, fatigue loading is potentially one of the most detrimental actions for this material. Therefore, an experimental campaign is needed in order to study the fatigue behavior of PE-UHPFRC and reinforced PE-UHPFRC, both under tension and under compression. Taking into account the fact that the tensile elastic limit is a significant property to describe the fatigue strength of UHPFRC [24], similar fatigue behavior to conventional UHPFRC can be expected for PE-UHPFRC. Furthermore, the performance of the PE-UHPFRC under fatigue loading is expected to be better than that of ECC/SHCC materials [25] considering the higher tensile elastic limit of PE-UHPFRC.

3.7 Investigation of the fire safety

The vulnerability of UHMW-PE fibers to temperature higher than 160 °C underlines the necessity of further investigation of the fire resistance of the PE-UHPFRC material in order to increase its range of applications to buildings. An experimental campaign is needed to investigate the spalling resistance and the residual mechanical performance of this material after exposure to high temperature. Preliminary investigations on this subject showed that the spalling resistance of PE-UHPFRC highly depends on the fiber type (e.g. PE-UHPFRC with SK99 fibers had a higher resistance to spalling compared with SK78 and SK62 fibers that have a significantly lower elastic modulus). It can be expected that combination of PE-UHPFRC with rebar or using hybrid fibrous mixes of steel and PE fibers could increase the fire safety of this material.

References

1. Ranade, R., Li, V. C., Stults, M. D., Heard, W. F. & Rushing, T. S. *Composite Properties of High-Strength, High-Ductility Concrete.* ACI Materials Journal 110, (2013).

2. Hafiz, M. A., Hajiesmaeili, A. & Denarié, E. *Tensile response of low clinker UHPFRC subjected to fully restrained shrinkage*. Cement and Concrete Research (2019).

3. Bissonnette, B. & Pigeon, M. *Tensile creep at early ages of ordinary, silica fume and fiber reinforced concretes*. Cement and Concrete Research 25, 1075–1085 (1995).

4. Boshoff, W. P., Altmann, F., Adendorff, C. J. & Mechtcherine, V. *A new approach for modelling the ingress of deleterious materials in cracked strain hardening*

cement-based composites. Materials and Structures 49, 2285–2295 (2016).

5.   Boshoff, W. P. & Adendorff, C. J. *Modelling SHCC cracking for durability*. Fracture and damage of advanced fibre-reinforced cement-based materials. Aedificatio Publishers, Dresden (2010).

6.   Adendorff, C. J., Boshoff, W. P. & Van Zijl, G. *Characterisation of crack distribution of strain-hardening cement composites (SHCC) under imposed strain*. in *Advances in Cement-Based Materials* (2010).

7.   Rafiee, A. *Computer modeling and investigation on the steel corrosion in cracked ultra high performance concrete*. Doctoral thesis 21, (2012).

8.   Wittmann, F. H., Yao, X., Wang, P., Zhang, P. & Zhao, T. *Influence of an imposed tensile stress and subsequent self-healing on capillary absorption and chloride penetration into HPFRCC*. in *Seventh International RILEM Workshop on High Performance Fiber Reinforced Cement Composites (HPFRCC7)* 251–258 (2015).

9.   Van den Heede, P., De Belie, N., Pittau, F., Habert, G. & Mignon, A. *Life cycle assessment of self-healiing engineerd cementitious composite (SH-ECC) used for the rehabilitation of bridges*. in *Life-Cycle Analysis and Assessment in Civil Engineering: Towards an Integrated Vision (IALCCE2018)* 2269–2275 (Taylor and Francis, 2018).

10.   Oesterlee, C. *Structural Response of Reinforced UHPFRC and RC Composite Members*. Doctoral thesis (2010).

11.   Noshiravani, T. *Structural Response of R-UHPFRC - RC Composite Members Subjected to Combined Bending and Shear*. Doctoral thesis (2012).

12.   Makita, T. *Fatigue behaviour of UHPFRC and R-UHPFRC - RC composite members*. Doctoral thesis (2014).

13.   Bastien Masse, M. *Structural Behavior of R-UHPFRC - RC Composite Slabs*. Doctoral thesis (2015). doi:10.5075/epfl-thesis-6841

14.   Kunieda, M. & Rokugo, K. *Recent progress on HPFRCC in Japan*. Journal of Advanced Concrete Technology 4, 19–33 (2006).

15.   Fischer, G. & Li, V. C. *Influence of matrix ductility on tension-stiffening behavior of steel reinforced engineered cementitious composites (ECC)*. Structural Journal 99, 104–111 (2002).

16.   Li, V. C. & Fischer, G. *Reinforced ECC-An evolution from materials to structures*. Composite structures (2002).

17.   Chanvillard, G. & Corvez, D. *Explicit back analysis method for quick determination of direct tensile strength of plate structural members*. in *RILEM-fib-AFGC Int. Symposium on Ultra-High Performance Fibre-Reinforced Concrete, UHPFRC 2013* (2013).

18. Baby, F., Graybeal, B., Marchand, P. & Toutlemonde, F. *UHPFRC tensile behavior characterization: inverse analysis of four-point bending test results*. Materials and structures 46, 1337–1354 (2013).

19. López, J. Á., Serna, P., Navarro-Gregori, J. & Camacho, E. *An inverse analysis method based on deflection to curvature transformation to determine the tensile properties of UHPFRC*. Materials and Structures 48, 3703–3718 (2015).

20. Denarié, E., Sofia, L. & Brühwiler, E. *Characterization of the tensile response of strain hardening UHPFRC-Chillon viaducts*. in *AFGC-ACI-fib-RILEM Int. Symposium on Ultra-High Performance Fibre-Reinforced Concrete, UHPFRC 2017* 242–250 (2017).

21. *SIA 2052, "Béton fibré ultra-performant (BFUP): Matériaux, dimensionnement et exécution"*. (Cahier Technique, 2017).

22. *NF P18-470: Bétons fibrés à ultra-hautes performances – Spécification, performance, production et conformité*. AFNOR (2016).

23. Qian, S. & Li, V. C. *Simplified inverse method for determining the tensile strain capacity of strain hardening cementitious composites*. Journal of Advanced Concrete Technology 5, 235–246 (2007).

24. Makita, T. & Brühwiler, E. *Tensile fatigue behaviour of ultra-high performance fibre reinforced concrete (UHPFRC)*. Materials and Structures 47, 475–491 (2014).

25. Müller, S. & Mechtcherine, V. *Fatigue behaviour of strain-hardening cement-based composites (SHCC)*. Cement and Concrete Research 92, 75–83 (2017).

Curriculum vitae

Amir Hajiesmaeili
27.01.1991

Contact information

Rue Saint-Laurent 36, 1003 Lausanne, Switzerland

amir.hajiesmaeili@gmail.com
https://www.linkedin.com/in/amir-hajiesmaeili-94821258/

Experience

August. 2015 - present	Ph.D. student / Research engineer
	MCS | EPFL, Switzerland

Next generation Ultra High Performance Fiber Reinforced concrete (UHPFRC): *Investigation and development of the next generation of UHPFRC materials with synthetic fibers and 50% reduction in clinker amount, towards a sustainable building environment.*

Detailed achievements

- Development of Structural UHPFRC with synthetic fibers.
- Improving and facilitating the rehabilitation of structures.
- 75% reduction in environmental impact.
- 12% reduction in deadweight.

September 2013 – July 2015	Master Student
	University of Tehran

Experimental and Numerical Investigation of Structural Behavior of UHPFRC Beam Elements: *Developing a numerical method to analyze structural members with complex shapes in order to be able to optimize cross sections and maximize use of the capacity of UHPFRC materials.*

Detailed achievements

- Development of a numerical model for analysis of non-prismatic beams based on Basic Displacement Functions (BDFs) method.
- Development of UHPFRC with steel fibers.
- Validating the developed FEM model by experimental results.

June 2010 – July 2015   **Research Assistant**

                                        Construction Material Institute (CMI), Iran

Selected projects

- Condition assessment of *Persian Gulf Mining & Metal Industries Special Zone (PGSEZ)* jetty and providing solutions for rehabilitation.
- Publish a Book titled "Guideline for Ready Mixed Concrete".

Education

Ecole Polytechnique Fédérale de Lausanne	**Ph.D. Structural Engineering**

August 2015 – present

University of Tehran	**M.Sc. Civil Engineering, Structure**

September 2013 – July 2015   Weighted grade avg. **18.32/20**

Skills

- Industry Knowledge:
  o Structural Engineering
  o UHPFRC technology
  o Concrete Technology
  o Design of Steel Structures
  o Design of Reinforced Concrete Structures
  o Infrastructure management
  o Earthquake Engineering
  o FEM Modelling
  o Rehabilitation planning
  o Structural Health Monitoring

- Tools and Technologies:
  o Engineering software packages: ETABS, SAP200, STAAD Pro, AutoCAD 2D & 3D
  o Programing languages: MATLAB, C++, VB, Fortran
  o Miscellaneous software: MS Office, Photoshop

Languages

English	Full professional proficiency
French	Working proficiency (B2)
German	Elementary proficiency (A2)
Persian	Native

Awards and honors

− Directly admitted to the Master program as an excellent student award, 2013.
− Ranked 1st among 124 civil engineering undergraduate students, 2012.
− Being an exceptional talent student in University of Tehran for 6 years (B.Sc. and M.Sc.).
− Ranked 517st among more than 600,000 participants in the national wide university entrance exam (2009).

List of publications

- 2019, **A. Hajiesmaeili**, E. Denarié "Development of Next Generation UHPFRC with synthetic fibers, for structural applications" to be submitted to Cement and Concrete Composites

- 2019, **A. Hajiesmaeili**, M. A. Hafiz, E. Denarié "Tensile response of PE-UHPFRC under imposed shrinkage deformations" to be submitted to Materials and Structures

- 2019, **A. Hajiesmaeili**, E. Denarié, "Capillary flow in UHPFRC with synthetic fibers, under high tensile stresses" to be submitted to Cement and Concrete Research

- 2019, **A. Hajiesmaeili**, E. Denarié, Francisco Pittau, Guillaume Habert "Life Cycle Analysis of Strengthening Existing RC Structures with R-PE-UHPFRC" to be submitted to Cement and Concrete Composites, https://doi.org/10.1016/j.cemconres.2019.105804.

- 2019, M. A. Hafiz, **A. Hajiesmaeili**, E. Denarié "Tensile response of low clinker UHPFRC subjected to fully restrained shrinkage" Cement and Concrete Research

- 2018, **A. Hajiesmaeil**i and E. Denarié "*Next generation UHPFRC for sustainable structural applications.*" ACI Special Publication (2018) 326.

- 2017, **A. Hajiesmaeili** and E. Denarié. "*Effect of fiber orientation and specimen thickness on the tensile response of strain hardening UHPFRC mixes with reduced Embodied Energy.*" 4th International Conference on Strain-Hardening Cement-Based Composites (SHCC 4), Dresden, September 18-20, 2017.

- 2016, Z. Sharon, G. Habert, P. Lura, E. Denarié, and **A. Hajiesmaeili**. "*Environmental assessment of radical innovation in concrete structures.*" Sustainable Built Environment (SBE) Regional Conference, Zurich, June 15-17, 2016, 682-687. DOI: 10.3218/3774-6_110

- 2013, M. Shekarchi, M. Eftekhar, **A. Hajiesmaeili** "*Guideline for Ready Mixed Concrete*", Elm va Adab Publication

- 2012, **A. Hajiesmaeili**, M. Moradian,M .Eftekhar, P. Hosseini, M. Shekarchi "*Evaluation of Deterioration of Damaged Structures in Aggressive Environment*", The 2nd International Conference on Microstructure Related Durability of Cementitious Composites, Delft University of Technology